



Analytical and Numerical Buckling analysis for Cruise Vessel specific Structures

submitted on 22nd July 2019 by

GARCIA HUMIA, Alejandro

Concili Egarenc, 88, Bajos.

08224 Terrassa, Spain

garcialex.h@gmail.com

Student ID No.: 218205301

First Reviewer:

Prof. Dr.Eng./Hiroshima Univ. Patrick Kaeding

Chair of Ship Structures

University of Rostock

Albert-Einstein-Str. 2

18059 Rostock

Germany

Second Reviewer:

Dipl.-Ing. Stefan, Griesch

Senior Project Engineer

MV WERFTEN Wismar GmbH

Wertfallee, 10

18119 Rostock

Germany

Declaration of authorship

I, *Alejandro Garcia Humia*, declare that this thesis and the work presented in it are my own and have been generated by me as the result of my own original research.

Where I have consulted the published work of others, this is always clearly attributed.

Where I have quoted from the work of others, the source is always given. With the exception of such quotations, this thesis is entirely my own work.

I have acknowledged all main sources of help.

Where the thesis is based on work done by myself jointly with others, I have made clear exactly what was done by others and what I have contributed myself.

This thesis contains no material that has been submitted previously, in whole or in part, for the award of any other academic degree or diploma.

I cede copyright of the thesis in favour of the University of Rostock.

Date:

Signature

22nd of July, 2019

A handwritten signature in blue ink, consisting of a series of loops and a long vertical stroke at the end.

Contents

Acknowledgements	iv
Abstract	v
List of abbreviations	vi
List of figures	vi
List of Tables	viii
1. INTRODUCTION	1
1.1 Background and motivation	1
1.2 Problem formulation and approach	3
1.3 Short historical review	6
2. FUNDAMENTAL THEORY OF BUCKLING	8
2.1 Introduction	8
2.2 Types of Buckling analysis	11
2.2.1 Linear Eigenvalue Buckling Analysis	11
2.2.2 Non-linear Buckling Analysis	13
2.3 Boundary conditions	14
2.4 Initial imperfections	15
2.4.1 Welding residual stresses	16
2.4.2 Initial deflections	17
2.5 Modes of buckling deformation	19
3. FUNDAMENTAL THEORY OF PLATES BUCKLING	21
3.1 Basic configuration	21
3.2 Failure mechanism and behaviour	22
3.3 Elastic buckling of a simply supported plate	24
3.3.1 Under single compressive load	24
3.3.2 Under Biaxial compressive load	25
3.4 Non-linear governing differential equation	26
4. FUNDAMENTAL THEORY OF STIFFENED PANELS BUCKLING	27
4.1 Basic configuration	27
4.2 Failure mechanism and behaviour	29
4.3 Overall Buckling	30
4.4 Local Buckling	32
4.4.1 Buckling of plating between stiffeners	32
4.4.2 Buckling of stiffener web	32
4.4.3 Lateral-torsional Buckling of stiffeners	34
4.5 Non-linear governing differential equations	35

5. INVESTIGATION OF TYPICAL STRUCTURES IN LARGE CRUISE VESSELS	37
5.1 Plating	38
5.2 Stiffened Panel	39
5.3 Selected configurations for the analysis	40
6. TYPICAL CLASS METHODS OF UNSTIFFENED AND STIFFENED STRUCTURES	42
6.1 Closed form method (CFM)	43
6.2 PULS method	45
6.2.1 Theory fundamentals	47
6.2.2 Buckling modes for stiffened panels	52
6.2.3 Boundary conditions	53
6.2.4 Initial imperfections	54
6.2.5 Design Principles.....	54
6.3 Non-linear Finite Element Method	56
6.3.1 Non-linear geometrical behaviour	56
6.3.2 Non-linear material behaviour	57
6.4 Comparison between presented methods.....	58
7. NUMERICAL ANALYSIS.....	59
7.1 Material properties and behaviour	60
7.2 Boundary conditions	61
7.3 Convergence study	63
7.3.1 Elastic buckling stress and buckling factor	63
7.3.2 Eigenmodes	68
7.4 Mesh	71
7.5 Linear Eigenvalue Buckling Analysis	73
7.6 Non-Linear Analysis	78
7.6.1 Initial imperfections	79
7.6.2 Unstiffened plates	81
7.6.3 Stiffened panels.....	86
7.6.4 Enhanced models	91
7.7 Verification	99
7.7.1 Unstiffened Plates	99
7.7.2 Stiffened Panel	100
8.CONCLUSION	102
9. FURTHER WORK	106
10. REFERENCES	107
11. ANNEXES.....	108
11.1 Convergence study	108

Acknowledgements

I would like to express my gratitude to MV Werften shipyards for the opportunity of performing this Master Thesis with them and the invaluable field experience gained through it. Especially, to Dipl.-Ing. Stefan Griesch for the close supervision, guidance and contributions throughout the whole thesis.

A particular acknowledgement is due to Dr.-Ing. Thomas Lindemann and Prof. Dr.Eng./Hiroshima Univ. Patrick Kaeding from University of Rostock for their continuous support and willing to help.

Last but not least, I would like to thank to all my relatives and friends for transmitting me the love, motivation and strength to carry on.

Abstract

Buckling is one of the main failure modes in ship structures subjected to compressive loading and it is of crucial importance for the overall structural strength. This Thesis is based in the buckling analysis of unstiffened plates and stiffened panels which form the basic building block and load bearing element in ship structure.

Different structural arrangements based on a global cruise vessel of 342 m long are derived. The analysis considers unstiffened plates, stiffened panels and an enhanced model for the stiffened panel including surrounding heavy members such as girders and frames. A comparison between analytical, semi-analytical (PULS) and numerical methods (Non-linear Finite Element Method) is performed for longitudinal and transverse loading conditions.

The increase in structural capacity due to the influence of surrounding structures and their influence in the boundary conditions is derived through the numerical method. Initial imperfections introduced by scaling the buckling eigenmode according to production standards as well as non-linear large deflection and material effects are considered.

Moreover, the agreement between the semi-analytical and numerical method is analysed. A trend is observed, PULS tends to underestimate the ultimate capacity for thin structures while for thick structures tends to overestimate it. This trend arises from PULS assumption of neglecting the effect of bending stress in the limit state yield criteria, which tends to become significant as the thickness increase.

Finally, given that PULS is a code for rules checking purposes according to DNV and IACS, the increase in strength by applying an Ultimate Limit State design is derived with results provided by the numerical enhanced model.

List of abbreviations

FEM	<i>Finite Element Method</i>
NFEM	<i>Non-linear Finite Element Method</i>
PULS	<i>Panel Ultimate Limit State</i>
DNV-GL	<i>Det Norske Veritas - Germanischer Lloyd</i>
IACS	<i>International Association of Classification Societies</i>
ISUM	<i>Idealized Structural Unit Method</i>
CSR	<i>Common Structural Rules</i>
H-CSR	<i>Harmonized Structural Rules</i>
CFM	<i>Closed Form Method</i>
CFF	<i>Closed Cell Formulas</i>
UC	<i>Ultimate Capacity</i>
BS	<i>Buckling Strength</i>
LEB	<i>Local Elastic Buckling</i>
GEB	<i>Global Elastic Buckling</i>
ULS	<i>Ultimate Limit State</i>
SLS	<i>Serviceability Limit State</i>

List of Figures

FIGURE 1:STIFFENED PANEL INTEGRATED IN SHIP STRUCTURE	1
FIGURE 2:STIFFENED PANEL SURROUNDED BY HEAVY MEMBERS [2]	4
FIGURE 3:LOCAL STRUCTURAL COLLAPSE/PLASTIC BUCKLING IN SHIP STRUCTURE [6]	8
FIGURE 4:BUCKLING DESIGN CURVES AS FUNCTION OF SLENDERNESS, SCHEMATICALLY [6].....	9
FIGURE 5: BUCKLING REGIONS ACCORDING TO PLASTICITY [4].....	9
FIGURE 6: ELASTIC STABILITY CATEGORIZATION [6]	10
FIGURE 7: BIFURCATION POINT FOR LINEAR EIGENVALUE ANALYSIS [7]	11
FIGURE 8: COMPARISON BETWEEN LINEAR AND NON-LINEAR EIGENVALUE BUCKLING ANALYSIS [7]	13
FIGURE 9: EFFECT OF BOUNDARY CONDITIONS ON THE BUCKLING COEFFICIENT FOR RECTANGULAR PLATES [4]	14
FIGURE 10: INITIAL DEFLECTION IN STIFFENED PANEL DUE TO WELDING [5].....	15
FIGURE 11: INITIAL DEFLECTION AND WELDING RESIDUAL STRESSES PRODUCED ON PLATE AND STIFFENER BY FILLET WELD [5].....	16
FIGURE 12: WELDING RESIDUAL STRESSES PRODUCED ON A PLATE BY FILLET WELD [5].....	16
FIGURE 13: WELDING INDUCED DISTORTIONS [5].....	17
FIGURE 14: WELDING INDUCED DISTORTIONS IN PLATE-STIFFENER CONNECTION [5]	18
FIGURE 15: BUCKLING MODE DEFORMATION ILLUSTRATION FOR LONGITUDINAL LOADING [4].....	19
FIGURE 16: BUCKLING COEFFICIENT FOR SIMPLY SUPPORTED PLATE UNDER LONGITUDINAL LOADING AS FUNCTION OF ASPECT RATIO	20
FIGURE 17: RECTANGULAR PLATE UNDER COMBINED IN-PLANE LOADING [4]	21
FIGURE 18: AVERAGE STRESS-AVERAGE STRAIN RELATION FOR UNSTIFFENED PLATE UNDER COMPRESSIVE LOADING [4]	22
FIGURE 19: AXIAL MEMBRANE STRESS DISTRIBUTION IN A PLATE UNDER LONGITUDINAL COMPRESSIVE LOADING [2].....	23
FIGURE 20: TYPICAL STIFFENED PANEL CONFIGURATION IN SHIP STRUCTURE [5]	27
FIGURE 21: TYPICAL STIFFENERS USED IN STIFFENED PANELS [5].....	28
FIGURE 22: CROSS-STIFFENED PANEL UNDER COMBINED IN-PLANE LOADS AND LATERAL PRESSURE [5].....	28
FIGURE 23: AVERAGE STRESS-AVERAGE STRAIN RELATION FOR A TYPICAL STIFFENED PANEL UNDER COMPRESSIVE LOADING [4]	29
FIGURE 24: OVERALL BUCKLING OF STIFFENED PANEL [5]	30
FIGURE 25: PLATE-STIFFENER COMBINATION [5].....	30
FIGURE 26: LOCAL BUCKLING OF PLATING BETWEEN STIFFENERS [5]	32
FIGURE 27: LOCAL BUCKLING OF STIFFENER WEB [5]	33
FIGURE 28: LATERAL-TORSIONAL BUCKLING OF STIFFENERS.....	34

FIGURE 29: LATERAL-TORSIONAL BUCKLING IDEALIZATION OF DEFORMATIONS: ACTUAL DEFORMATION (LEFT), IDEALIZED (RIGHT) .	34
FIGURE 30: IDEALIZATION OF STIFFENED PANEL INTO ANISOTROPIC PLATE [4]	35
FIGURE 31: SECTION VIEW OF CONSIDERED CRUISE VESSEL	37
FIGURE 32: LONGITUDINAL CUT THROUGH AMIDSHIPS OF VESSEL CONSIDERED.....	37
FIGURE 33: PLATE THICKNESSES ALONG HEIGHT OF THE VESSEL	38
FIGURE 34: REPRESENTATIVE STIFFENED PANEL FOR THE VESSEL.....	40
FIGURE 35: SCHEMATIC COMBINED LOADING FOR UNSTIFFENED PLATE (LEFT) AND STIFFENED PANEL (RIGHT) [1]	45
FIGURE 36: PULS AVAILABLE ELEMENTS [6]	46
FIGURE 37: INCREMENTAL SOLUTION ALGORITHM STEPPING A NON-LINEAR EQUILIBRIUM PATH [6]	49
FIGURE 38: STRESS CONTROL POINTS FOR ULTIMATE CAPACITY ASSESSMENT [1]	50
FIGURE 39: ULTIMATE CAPACITY SURFACE IN LOAD SPACE [6].....	51
FIGURE 40: DEFINITION OF GEOMETRICAL IMPERFECTIONS [1].....	54
FIGURE 41: BI-LINEAR IDEALIZATION OF NON-LINEAR MATERIAL BEHAVIOUR [6]	57
FIGURE 42: NON-LINEAR MATERIAL BEHAVIOUR USED IN THE ANALYSIS	60
FIGURE 43: BOUNDARY CONDITIONS AND COUPLING APPLIED IN UNSTIFFENED PLATE MODEL.....	61
FIGURE 44: BOUNDARY CONDITIONS AND COUPLING APPLIED IN STIFFENED PANEL MODEL	62
FIGURE 45: BOUNDARY CONDITIONS AND COUPLING APPLIED IN ENHANCED MODEL.....	62
FIGURE 46: ELASTIC BUCKLING STRESS CONVERGENCE UNSTIFFENED PLATE OF 6 MM THICKNESS UNDER LONGITUDINAL LOADING	65
FIGURE 47: ELASTIC BUCKLING STRESS CONVERGENCE 6 MM UNSTIFFENED PLATE OF UNDER TRANSVERSAL AND BIAxIAL LOADING ...	65
FIGURE 48: ELASTIC BUCKLING STRESS CONVERGENCE FOR STIFFENED PANEL OF 6 MM PLATE THICKNESS UNDER LONGITUDINAL LOADING.....	66
FIGURE 49: ELASTIC BUCKLING STRESS CONVERGENCE FOR STIFFENED PANEL OF 6MM PLATE THICKNESS UNDER TRANSVERSAL AND BIAxIAL LOADING	67
FIGURE 50: BUCKLING MODES ACCORDING TO ANALYTICAL FORMULATION FOR THE CONSIDERED UNSTIFFENED PLATE	68
FIGURE 51: THRESHOLD MESH SIZE FOR A CONSISTENT REPRESENTATION OF EIGENMODE UNDER LONGITUDINAL LOADING FOR UNSTIFFENED PLATE OF 6 MM THICKNESS	69
FIGURE 52: THRESHOLD MESH SIZE FOR A CONSISTENT REPRESENTATION OF EIGENMODE UNDER LONGITUDINAL LOADING FOR STIFFENED PLATE OF 6MM PLATE THICKNESS	69
FIGURE 53: LONGITUDINAL EIGENMODES FOR UNSTIFFENED PLATE OF 6 MM THICKNESS (UP) AND STIFFENED PANEL OF 6 MM PLATE THICKNESS (DOWN)	70
FIGURE 54: UNSTIFFENED PLATE MESH	71
FIGURE 55: STIFFENED PANEL MESH	72
FIGURE 56: ENHANCED MODEL MESH	72
FIGURE 57: COMPARISON OF EIGENMODES BETWEEN FEM AND PULS FOR UNSTIFFENED PLATE OF 12 MM THICKNESS.....	74
FIGURE 58: COMPARISON OF EIGENMODES BETWEEN FEM AND PULS FOR STIFFENED PANEL OF 6 MM PLATE THICKNESS.....	75
FIGURE 59: COMPARISON OF EIGENMODES BETWEEN FEM AND PULS FOR STIFFENED PANEL OF 12 MM PLATE THICKNESS.....	75
FIGURE 60: COMPARISON OF EIGENMODES BETWEEN FEM AND PULS FOR STIFFENED PANEL OF 15.5 MM PLATE THICKNESS	76
FIGURE 61: EIGENMODE VARIATION UNDER LONGITUDINAL LOADING FOR DIFFERENT STIFFENED PANELS.....	77
FIGURE 62: ASYMMETRICAL BUCKLING PATTERN OF PLATING BETWEEN STIFFENERS OBTAINED BY FEM	77
FIGURE 63: NEWTON-RAPHSON SCHEME FOR NON-LINEAR SOLUTION APPROACH [10]	78
FIGURE 64: IMPLEMENTATION OF INITIAL IMPERFECTIONS FOR UNSTIFFENED PLATES.....	79
FIGURE 65: INITIAL IMPERFECTIONS FOR STIFFENED PANEL UNDER LONGITUDINAL LOADING. MID-STIFFENED PANEL SECTION.....	80
FIGURE 66: ULTIMATE CAPACITY CURVES FOR UNSTIFFENED PLATES UNDER LONGITUDINAL LOADING.....	82
FIGURE 67: VON MISES COMPARISON BETWEEN NFEM AND PULS FOR UNSTIFFENED PLATE OF 6 MM THICKNESS UNDER LONGITUDINAL LOADING	83
FIGURE 68: ULTIMATE CAPACITY CURVES FOR UNSTIFFENED PLATES UNDER TRANSVERSE LOADING.....	84
FIGURE 69: VON MISES COMPARISON BETWEEN NFEM AND PULS FOR UNSTIFFENED PLATE OF 6 MM THICKNESS UNDER TRANSVERSE LOADING.....	85
FIGURE 70: ULTIMATE CAPACITY CURVES FOR STIFFENED PANELS UNDER LONGITUDINAL LOADING	87

FIGURE 71: VON MISES COMPARISON BETWEEN NFEM AND PULS FOR STIFFENED PANEL WITH PLATING OF 6 MM UNDER LONGITUDINAL LOADING	88
FIGURE 72: ULTIMATE CAPACITY CURVES FOR STIFFENED PANELS UNDER TRANSVERSE LOADING	89
FIGURE 73: VON MISES COMPARISON BETWEEN NFEM AND PULS FOR STIFFENED PANEL OF 6 MM UNDER TRANSVERSE LOADING ..	90
FIGURE 74: UC CURVES COMPARISON FOR SINGLE STIFFENED PANEL AND ENHANCED MODEL UNDER LONGITUDINAL LOADING	92
FIGURE 75: UC CURVES COMPARISON FOR SINGLE STIFFENED PANEL AND ENHANCED MODEL UNDER TRANSVERSE LOADING	92
FIGURE 76: ROTATIONAL CONSTRAINT INTRODUCED BY HEAVY MEMBERS IN STIFFENED PANEL	94
FIGURE 77: NFEM STRESS DISTRIBUTION COMPARISON BETWEEN SINGLE STIFFENED PANEL AND ENHANCED MODEL	95
FIGURE 78: NFEM STRESS DISTRIBUTION COMPARISON BETWEEN SINGLE STIFFENED PANEL AND ENHANCED MODEL	96
FIGURE 79: UC CURVE FOR THIN UNSTIFFENED PLATE UNDER LONGITUDINAL LOADING AS FUNCTION OF IMPERFECTION SIZE [6]	99
FIGURE 80: UC CURVE FOR THIN UNSTIFFENED PLATE UNDER TRANSVERSE LOADING AS FUNCTION OF IMPERFECTIONS SIZE [6]	100
FIGURE 81: COMPARISON OF UC BETWEEN PULS AND NFEM FOR STIFFENED PANELS AS FUNCTION OF SLENDERNESS [11]	101
FIGURE 82: FIRST YIELDING AT MIDPLANE UNDER LONGITUDINAL FOR THE CONFIGURATIONS CONSIDERED	102
FIGURE 83: FIRST YIELDING AT MIDPLANE UNDER TRANSVERSE LOADING FOR THE CONFIGURATIONS CONSIDERED	103
FIGURE 84: BUCKLING COEFFICIENT CONVERGENCE FOR 6 MM UNSTIFFENED PLATE UNDER LONGITUDINAL LOADING	109
FIGURE 85: ELASTIC BUCKLING STRESS CONVERGENCE OF 6MM UNSTIFFENED PLATE UNDER LONGITUDINAL LOADING	109
FIGURE 86: BUCKLING COEFFICIENT CONVERGENCE OF 6 MM UNSTIFFENED PLATE UNDER TRANSVERSAL AND BIAXIAL LOADING	110
FIGURE 87: ELASTIC BUCKLING STRESS CONVERGENCE OF 6 MM UNSTIFFENED PLATE UNDER TRANSVERSAL AND BIAXIAL LOADING ..	110
FIGURE 88: ELASTIC BUCKLING STRESS CONVERGENCE OF 6 MM STIFFENED PANEL UNDER LONGITUDINAL LOADING	111
FIGURE 89: ELASTIC BUCKLING STRESS CONVERGENCE OF 6 MM STIFFENED PANEL UNDER TRANSVERSAL AND BIAXIAL LOADING	112

List of Tables

TABLE 1: SELECTED UNSTIFFENED PLATES FOR THE ANALYSIS	41
TABLE 2: SELECTED STIFFENED PANELS FOR THE ANALYSIS	41
TABLE 3: SUMMARY OF UNSTIFFENED PLATE CONFIGURATIONS	59
TABLE 4: SUMMARY OF STIFFENED PANEL CONFIGURATIONS	59
TABLE 5: ANALYTICAL SOLUTIONS FOR ELASTIC BUCKLING STRESS AND BUCKLING FACTOR FOR UNSTIFFENED PLATES	63
TABLE 6: RESULTS SUMMARY FOR UNSTIFFENED PLATE OF 6 MM PLATE THICKNESS WITH 50 MM MESH SIZE	64
TABLE 7: RESULTS SUMMARY FOR STIFFENED PANEL OF 6 MM PLATE THICKNESS WITH 50 MM MESH SIZE	66
TABLE 8: UNSTIFFENED PLATES MESH DESCRIPTION	71
TABLE 9: STIFFENED PANELS MESH DESCRIPTION	72
TABLE 10: ENHANCED MODELS MESH DESCRIPTION	72
TABLE 11: COMPARISON BETWEEN RESULTS OBTAINED FOR UNSTIFFENED PLATES	73
TABLE 12: COMPARISON BETWEEN RESULTS OBTAINED FOR STIFFENED PANELS	74
TABLE 13: NFEM RESULTS FOR UNSTIFFENED PLATES	81
TABLE 14: NFEM RESULTS FOR STIFFENED PANELS	86
TABLE 15: NFEM RESULTS FOR ENHANCED MODELS	91
TABLE 16: INCREASE IN STRENGTH FOR TRANSVERSE LOADING	93
TABLE 17: NFEM RESULTS FOR THE INNER STIFFENED PANEL WITHIN THE ENHANCED MODELS	94
TABLE 18: RESULTS FOR THE STIFFENED PANELS BASED IN AN ULS APPROACH	97
TABLE 19: CONVERGENCE STUDY RESULTS FOR UNSTIFFENED PLATE OF 6 MM THICKNESS	108
TABLE 20: CONVERGENCE STUDY FOR STIFFENED PANEL OF 6MM THICKNESS	111

1. INTRODUCTION

1.1 Background and motivation

The scope of this work is focused on the buckling phenomena of plates and stiffened panels which form the fundamental structural unit in ship and offshore structures. These elements form the basic building block and so the main load bearing element. They are typically located in the ship sides, bottom, decks and bulkheads as illustrated in Fig.1.

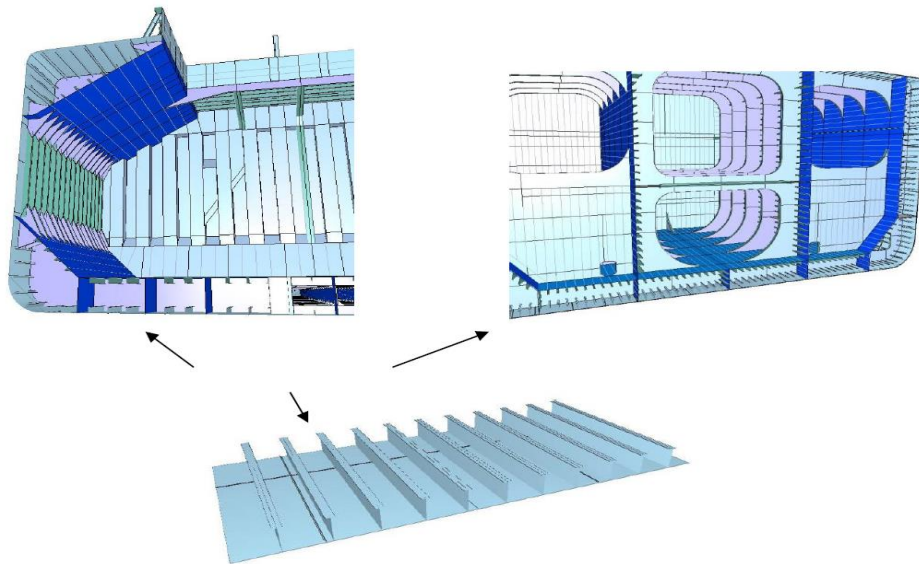


Figure 1: Stiffened panel integrated in ship structure [1]

It is important to consider and study both structures because the overall structural capacity depends on them. Moreover, their individual behaviours are correlated and influence each other. In a stiffened panel, the plating between the stiffeners will behave and deform much like an unstiffened plate.

Stiffened panels are especially sensitive to buckling due to the predominantly in-plane loads and thin thickness plating. Therefore, it is of main concern to determine the buckling strength of this kind of structures as well as their failure mechanism to ensure a safe and efficient performance of the structure.

Traditionally, the buckling strength has been assessed by rule formulas which are based in linear buckling theory in combination with some corrections to account for residual stresses, imperfections and plasticity. Although they provide quick strength estimations, they are very limited when dealing with complicated geometries, different load combinations, initial imperfections or geometric and material non-linearities. Thus, inaccurate results may be obtained due to the large influence that previous phenomenon can have in the structural response when considered altogether.

However, the rise in computational resources and tools has changed this trade providing a more consistent and accurate alternative approach than rule formulas. Current state of the art analysis procedures considers Non-linear Finite Element Methods (NFEM) to account for the phenomena that rule formulas cannot. This powerful tool has one main drawback, which is a large modelling and computation cost especially for large structures. Consequently, it is not practical in terms of design and when a large number of structures are to be analysed as is the case of a shipyard.

A current applied method for performing a fast buckling and ultimate strength assessment is PULS. It is a computerized code developed by DNV-GL and IACS which pretends to be an analysis tool in the mid-way between rule formulas and NFEM calculations. It provides more accurate results than simplified formulations with more efficient and cheaper computation cost than NFEM. However, this fast assessment has a price in accuracy as may be expected. Some of PULS considerations and assumption, discussed further in the thesis, tend to lead in most cases to conservative results.

Therefore, the aim of this work is to investigate and identify possible improvement margins and allowances with respect to PULS by performing a non-linear analysis with different structural configurations. This could lead to weight savings and a higher performance of the vessel in structural terms. As well known in the maritime field, weight savings in one area allows to increase the capability in another are such as increasing payload capacity, fuel capacity, improved speed or more facilities that can be introduced for the passengers in the specific case of cruise vessels.

1.2 Problem formulation and approach

The buckling analysis is carried out considering two main structural elements:

- Unstiffened plate
- Stiffened panel

Different configurations, 3 unstiffened plates and 3 stiffened panels, are derived according to a 3D model of a global class cruise vessel of 342 meters long and capacity for up to 9500 passengers. The selection aims to represent in a consistent way different arrangements observed in the vessel within a certain range of thicknesses.

Depending on the part of the structure the stiffened panel will be subjected to a different set of loads. Typically, main load components acting on a local stiffened panel/plate are:

- i) In-plane load in the direction of the stiffener
- ii) In-plane load in the direction perpendicular to the stiffener
- iii) In-plane shear
- iv) Lateral pressure
- v) In-plane bending

The in-plane loads arise from the overall hull girder bending moment. In sagging, bottom plates are under tension and deck plates are under compression, hence buckling will be triggered in the deck structure. In the same direction, in hogging conditions buckling will be triggered in the bottom structure. Shear stress is induced by the hull girder shear force or torsion and lateral pressure by internal cargo or external water level.

For a cruise vessel, the main and most influential load with respect to buckling arises from longitudinal bending. Therefore, to perform the analysis shear loading is disregarded. For other types of vessels such as open profile structures, shear and torsional loading can become critical and should be taken into account. In addition, lateral pressure is disregarded to account for a general stiffened panel and not constrain the analysis into bottom or side panels.

In the current analysis, the main load components considered are the following:

- In-plane compressive load in the direction of the stiffener
- In-plane compressive load in the direction perpendicular to the stiffener
- Biaxial in-plane compressive loading with a loading ratio of 1 (same load in both edges)

One of PULS considerations that tend to lead in most cases to conservative results is considering an isolated stiffened panel. In such a model, the redistribution of forces into surrounding panels as illustrated in Fig. 2 is not accounted for. Therefore, in order to account for this effect enhanced models including surrounding structures are needed. In addition, with an enhanced model it is possible to determine how realistic the boundary conditions assumed in the isolated structure are.

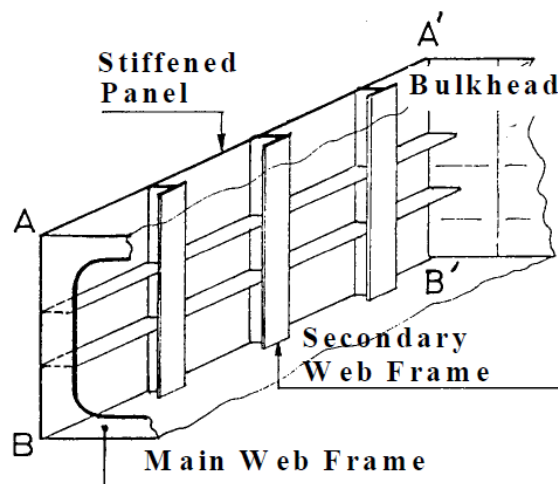


Figure 2: Stiffened panel surrounded by heavy members [2]

Another consideration from PULS which may lead to conservative results is the estimation of ultimate strength by using first yielding in the structure as collapse criteria [1]. When yielding takes place, the structure may be able to sustain further additional loading until it collapses due to the loss in strength.

Given the previous considerations, the approach to perform the analysis is presented below:

1. Derivation of structural configurations and assessment of elastic buckling stress and ultimate capacity (UC) according to PULS. Three loading conditions are considered:
 - *Longitudinal*: In-plane compressive load along stiffeners direction
 - *Transversal*: In-plane compressive load perpendicular to stiffeners direction
 - *Biaxial*: in-plane compressive loading with a loading ratio of 1 (same load along edges)
2. Mesh convergence study to ensure adequate and consistent results in terms of stresses and representation of buckling modes.
3. Linear eigenvalue FEM analysis for elastic buckling stress and buckling eigenmodes assessment. Comparison with respect to the values derived by PULS and analytical formulation.
4. NFEM analysis taking into account material and geometrical non-linearities. Initial imperfections implemented by eigenmodes scaled by production standards defined by PULS. Assessment of buckling, first yielding and Ultimate capacity is performed.
5. Enhancement of the model to study load redistribution into surrounding panels and assess the influence of heavy members in the rotational restraint of the stiffened panel edges.
6. Comparison of obtained results and conclusion.

1.3 Short historical review

The first work regarding buckling was performed by Euler (1759), who calculated the critical load for which an ideal column under compressive loads starts to deflect laterally and become unstable. This approach is still in use to perform quick estimations.

Afterwards, the Perry-Robertson approach (Perry 1886 and Robertson 1925) is based on a column with initial imperfections and uses the first yield as the elastic limit load. This method has been largely implemented in design codes and rule formulas such as DNV-GL.

Regarding large deflection, Kirchhoff (1850) discovered the importance of non-linear terms for large deflection problems. The plate differential equation for large deflections was derived by von Karman (1910) and extended to plates with initial curvature by Marguerre (1937) [3].

In past times, performing progressive analysis to assess the ultimate strength of members taking into account the influences of yielding and buckling was not possible. In contrast, tensile strength was considered as a parameter to control the capacity and prevent structural failure. Bryan (1881) was the first in considering buckling as a criterion to determine thickness in ship structures by solving the buckling problem of panels theoretically and deriving formulas to evaluate the buckling load of a rectangular plate under thrust. [4]

The introduction of Finite Element Method (FEM) by Turner et al. (1956) and the continuous developments of computer performance and computational environments have allowed performing analysis of complex structures including non-linear effects. Nowadays, FEM is a tool used daily in design and assessment of marine structures. In contrast, use of non-linear FEM is more focused into research given that is more time-consuming and computation costly specially for large structures.

In addition, an alternative method to simulate collapse behaviour is given by the Idealized Structural Unit Method (ISUM) developed by Ueda and Rashed (1974). The structure is divided into larger structural units for which geometric and material non-linear behaviour is idealized, although its formulation is in the framework of FEM.

Previous methods have helped in the understanding of buckling and ultimate strength behaviour of structural member in ship structures. Typically, buckling assessment has been performed by rule formulas based in linear theory corrected by empirical corrections. These formulas imply simplifying assumptions that are valid only within certain limits. Outside of this range they may be inaccurate. In addition, they do not include the interaction between the numerous structural failure modes, which are numerous and complex. For these reasons there is a general trend towards a rational-based structural design and analysis which allows a better performance in terms of reliability, efficiency and economy [2].

Classification societies are working nowadays in this direction and they include the possibility of submitting a direct analysis as way of approval. In this direction was the development of PULS by DNV-GL and IACS, aiming to provide improved buckling formulations with a compromise between rule design formulas and NFEM.

2. FUNDAMENTAL THEORY OF BUCKLING

This chapter deals with the fundamentals of Buckling to provide a theoretical basis to understand the phenomena and perform the analysis. The theory presented in this chapter is available and further developed in Rigo (2003) [2], Yao and Fukujibo (2016) [4] and Paik and Thayambaili (2003) [5].

2.1 Introduction

Buckling is a phenomenon where a structural member under compression loading deflect in an out-of-plane direction when the load reaches a critical value. After buckling, the deflection begins to increase in addition to the in-plane displacement, which leads to a reduction of in-plane or axial stiffness. Therefore, the load-carrying capacity of the structural member is decreased. This causes redistribution (increase) of internal forces in unbuckled members, which may lead to progressive occurrence of buckling failure. If the load increases further, progressive buckling may result in the collapse of the whole structure.

In general, ship structures are designed in a way that buckling collapse will occur in the secondary structural members (plating and secondary stiffeners) as illustrated in Fig. 3, rather than in primary structural members (frames, girders and bulkheads).



Figure 3: Local structural collapse/Plastic buckling in ship structure [6]

The critical load at which buckling will take place is function of a great variety of factors such geometry, material properties, loading characteristics, boundary conditions and initial imperfections. However, one of the most influencing factors is slenderness. This will influence which failure mechanism the structure will fail by. As presented in Fig. 4, slender designs tend to fail by buckling while stocky designs tend to fail by UC.

The graph is based in slenderness λ , and the relation between the critical buckling strength σ_{cr} and yielding strength, defined in the rules [8] as R_{eH} .

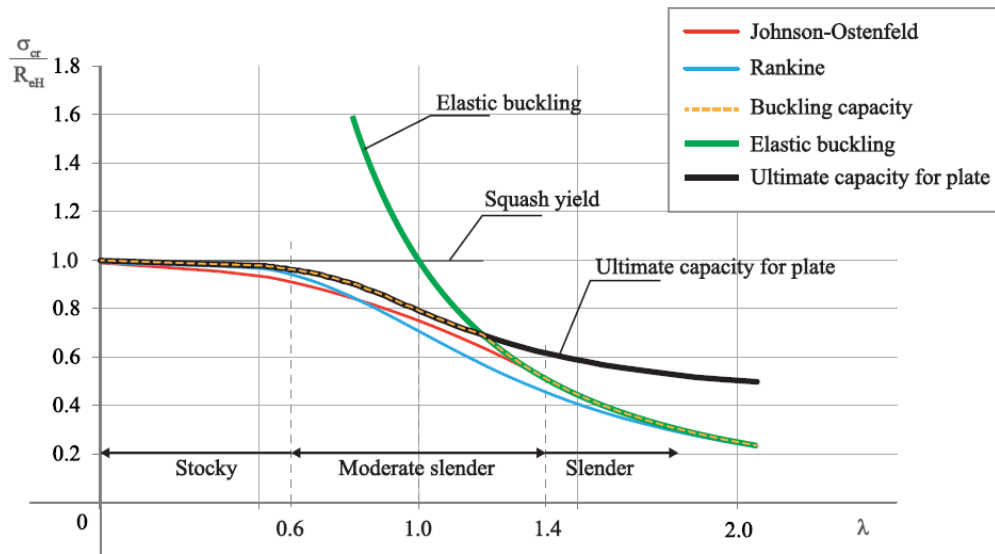


Figure 4: Buckling design curves as function of slenderness, schematically [6]

The phenomenon of buckling is normally categorized by plasticity in three regions as illustrated in Fig. 5:

- Elastic Buckling
- Elastic-Plastic Buckling
- Plastic Buckling

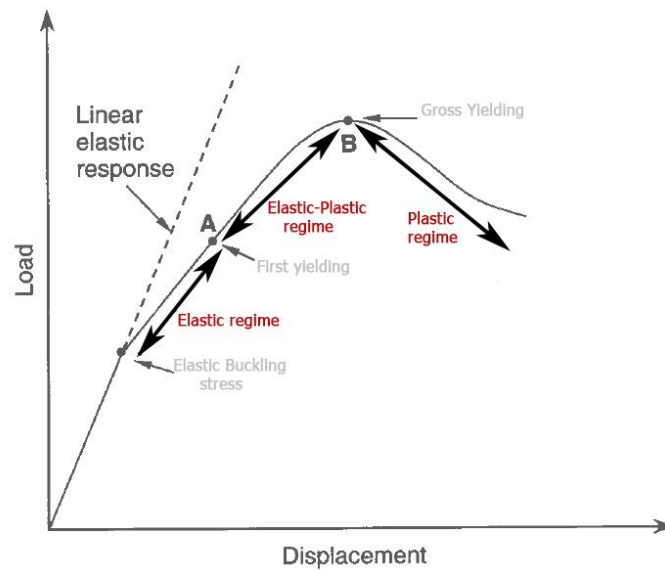


Figure 5: Buckling regions according to plasticity [4]

Elastic Buckling is the state where the structure loses its stability and large out-of-plane deflections start to develop. The elastic buckling stress or limit refers to the load that will trigger this behaviour and it is normally associated to the minimum eigenvalue of the structure. In this regime the induced stresses are below the yielding strength, hence when the structural element is unloaded the deflections are recovered and the element takes its initial shape.

This elastic buckling limit can be stable, unstable or neutral according to the load bearing capacity of the element as shown in Fig. 6. A stable limit allows the structure to carry higher loads than the eigenvalue even though large deflection appears. In contrast, an unstable limit does not allow the structure to carry further loads and its capacity drops below the eigenvalue with a fast deflection growth. For a neutral limit the load carrying capacity does neither increase or decrease. [6]

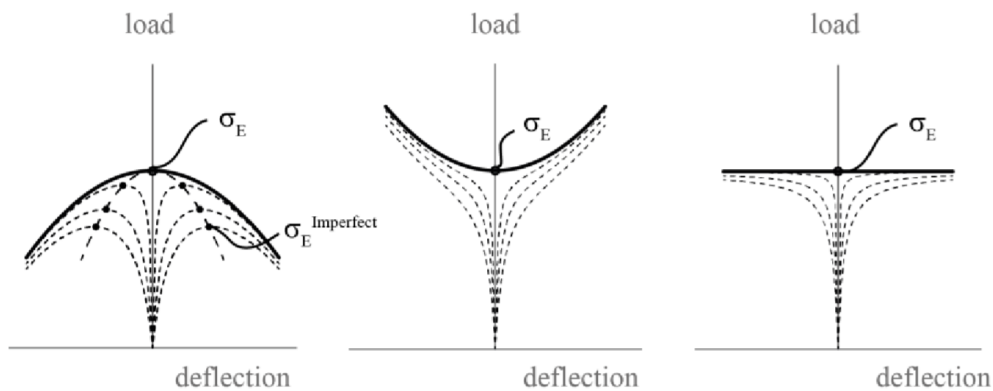


Figure 6: Elastic stability categorization [6]

The elastic buckling stress may be taken as a limit state depending on the type of structure. For instance, when buckling takes place in a column, the element starts to undergo yielding due to bending and capacity starts to decrease with a deflection increase. Thus, the buckling strength is considered the maximum load-carrying capacity and can be considered as the ultimate strength for columns.

However, in ship structures elastic buckling of plate elements is not a critical issue due to their redundancy and large deflections can be accepted as long as a controlled behaviour of the structure is ensured. Allowing so to sustain further loads than its buckling strength even if the stiffness of the element decreases considerably after undergoing buckling.

Elastic-plastic buckling takes place when a local region in the structural element undergoes yielding and so a plastic deformation. From this point, yielding starts to develop over the element until gross yielding takes place.

Finally, once gross yielding has taken place, the *plastic buckling* regime is reached. It is characterized by a non-linear material behaviour and due to the large deformations also to a non-linear geometric behaviour. Due to the previous facts, the in-plane stiffness starts to decrease until it becomes zero and the structure cannot sustain further load, attaining thus its UC.

In terms of safety and performance assessment, it is important to know the extreme loads the structure may be exposed to and how will react to them. Therefore, it is needed to understand the plastic buckling and collapse behaviour of the structural member including the capacity beyond the ultimate strength. To do so, it is needed to introduce in the analysis both material and geometrical non-linearities to reproduce a consistent and realistic behaviour. [4]

2.2 Types of Buckling analysis

In buckling analysis, two types of techniques/approaches are considered:

- Linear or bifurcation
- Non-linear or non-bifurcation

2.2.1 Linear Eigenvalue Buckling Analysis

This analysis is based on an ideal perfect structure to predict the theoretical buckling strength under a linear elastic assumption. Under this condition, there is an equilibrium position at a critical load for which the structure suddenly buckles as illustrated in Fig. 7. This load is also known as bifurcation point.

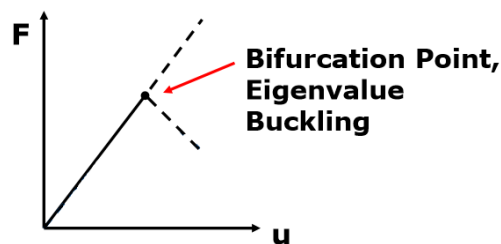


Figure 7: Bifurcation point for Linear Eigenvalue Analysis [7]

The critical load is calculated based on the eigenvalue problem considering the load-displacement relationship under a linear elastic state:

$$K q = G \quad (1)$$

where:

K : Stiffness matrix

G : Load vector

q : Displacement vector

Assuming the displacements are small and the behaviour is linear function of the applied load, a lambda factor is introduced and the incremental equilibrium can be expressed as:

$$(K + \lambda K_s) q = G \quad (2)$$

where:

K_s : Small displacement stiffness matrix

At the beginning of the instability, the structure will have a change in deformation for no additional loading ($G = 0$), which leads to the following equilibrium equation:

$$(K + \lambda K_s) q = 0 \quad (3)$$

In order to satisfy the previous equation is needed to have:

$$\det (K + \lambda K_s) = 0 \quad (4)$$

The displacement matrix q represents the eigenvectors or deformations of the buckling mode. The critical load or bifurcation point is given for the minimum value of λ satisfying the previous equation [7].

Given that the initial imperfections and non-linear behaviours are not considered, for real structures this value will happen at an earlier stage. The element will start to deform immediately when loading is applied with a non-linear response. Thus, this type of analysis lead to non-conservative results and to gain a deeper understanding of buckling phenomena a non-linear analysis should be performed.

However, this type of analysis present two main advantages:

- It is relatively fast to perform, in terms of computation resources
- The buckling eigenmodes can be used as initial imperfections for further analysis in order to provide more realistic results.

2.2.2 Non-linear Buckling Analysis

This approach is based on a non-linear static analysis in order to determine the critical load for which the structure becomes unstable. With this approach, initial imperfections and other non-linear effects such as plasticity, large deformation or contact can be included in the analysis.

In this case there is no bifurcation given that bending and lateral deflections are induced from the beginning of the loading, although the increasing rate is low. When the critical load is reached the out-of-plane deflections starts to increase as rapidly as the bifurcation case. Therefore, in this case an obvious sudden buckling point does not appear until the member collapses [5].

As mentioned in the previous section, Fig.8 illustrates how the critical load takes places at a lower level than the linear eigenvalue approach given the additional features considered by this analysis.

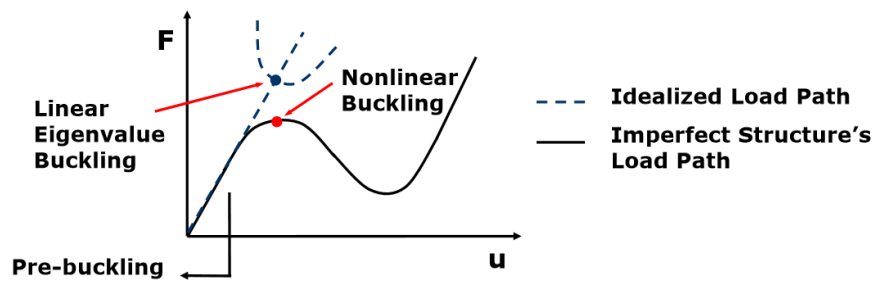


Figure 8: Comparison between Linear and Non-Linear Eigenvalue Buckling Analysis [7]

The initial imperfections to initiate buckling are typically introduced from the buckling eigenmodes obtained from the linear eigenvalue analysis. The imperfections amplitude can be estimated according to manufacturing tolerances and production standards.

In summary, the non-linear buckling analysis provides a more accurate and realistic results than the linear eigenvalue analysis since it considers the effects of initial imperfections and non-linearities. Thus, it is recommended for the design and evaluation of actual structures. Moreover, the gradual application of the load allows to trace the post-buckling behaviour which can be useful for stable buckling configuration where the structure can sustain further loading after undergoing buckling.

2.3 Boundary conditions

The boundary conditions are constraints applied into the structure that represent their interaction with the environment in terms of forces and displacements. They have a direct influence in the buckling, post-buckling and ultimate strength characteristics of the structure. For structural analysis and design the support conditions are commonly idealized as simply support or clamped, which represent a zero and infinite torsional rigidity respectively.

Regarding buckling and ultimate strength assessment, two sets of boundary conditions are of particular importance:

- **Out-of-plane or rotational boundary condition**

This boundary condition relates to the rotational constraint of the structure around the edges. Typically spans from simply supported where the rotation is free to clamped support where the rotation is fully constrained.

It influences significantly the elastic buckling stress (eigenvalue) as illustrated in Fig. 9. The clamped boundary condition (Curve D) provide a higher buckling coefficient given that the rotation will be more constrained, hence a higher elastic buckling stress in comparison with simply supported boundary condition (Curve A).

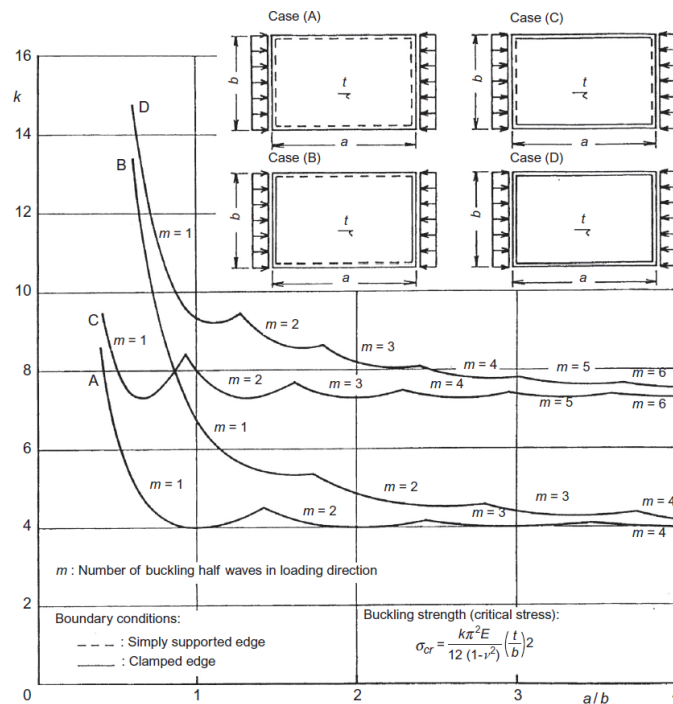


Figure 9: Effect of boundary conditions on the Buckling coefficient for rectangular plates [4]

In general, according to rule procedures the out-of-plane boundary condition is taken as simply supported for all four edges. This leads to a conservative set of boundary conditions given that in actual structures there will be a finite value of torsional rigidity along the edge and the rotation will be restrained in some extent.

- **In-plane or membrane boundary condition**

This boundary condition accounts for the in-plane behaviour of the edges, representing the restraints introduced from surrounding structures. They are important with respect to the elastic post-buckling behaviour. They define the available strength beyond the elastic buckling limit and so the ultimate capacity of the element.

In a continuous structure such an integrated plate or stiffened panel, the edges of the element are supported by stronger beam members. This implies that the relative lateral deflections of the support members to the structure are very small, even up to collapse. Therefore, in general it is assumed that the support members along the four edges remain in the same plain. In other words, the edges are forced to remain straight but movable in-plane.

2.4 Initial imperfections

During fabrication of a stiffened panel, the stiffeners in both directions are fitted into the plate by welding. Due to thermal effects, this process introduces initial imperfections and residual stresses into the structure as shown schematically in Fig. 10. They tend to reduce the buckling and ultimate capacity of the element, hence it is important to know which is their shape and magnitude to include them as an influencing parameter in design or analysis processes.

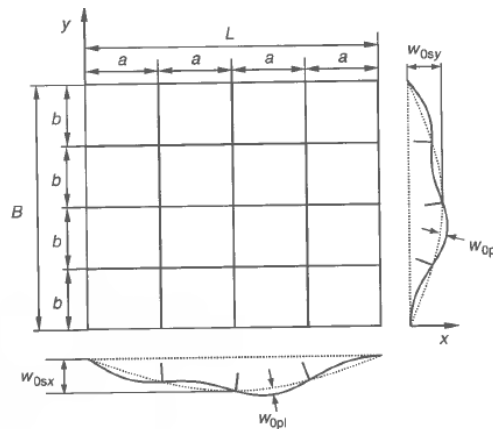


Figure 10: Initial deflection in stiffened panel due to welding [5]

Different efforts have been made to study and predict the initial imperfections in a theoretical and numerical basis such as Masabuchi (1980) or Ueda (1999). However, due to the complexity of the phenomena and that the effect produced is normally of secondary interest approximate methods based from measurements are usually applied.

These imperfections related to fabrication procedures should be minimized by the election of proper welding procedures and fabrication methods.

2.4.1 Welding residual stresses

The heat input due to the welding process melts the material producing the joint and then solidifies again. During the cooling process, because of the adjacent cold parts tensile stresses are produced in the welding while compressive stresses are produced in the neighbouring region as illustrated in Fig. 11.

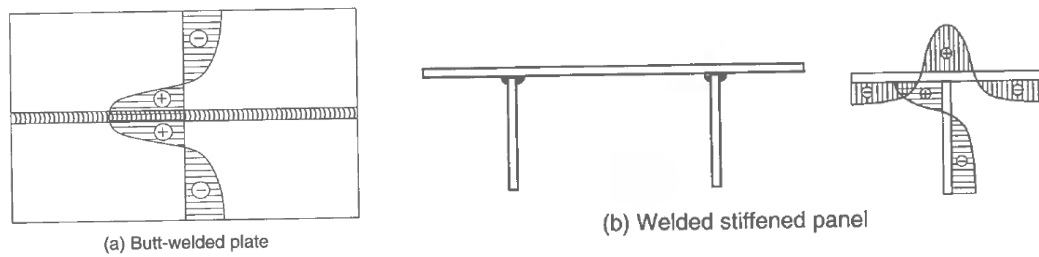
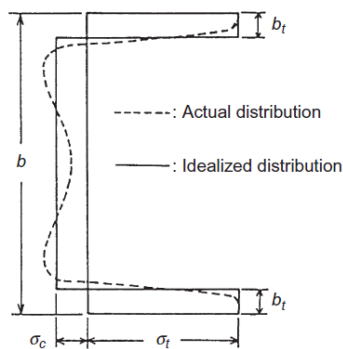


Figure 11: Initial deflection and welding residual stresses produced on plate and stiffener by fillet weld [5]

Generally, the residual stresses are idealized by tensile and compressive blocks as shown in Fig. 12. Given that there no action from external loads, equilibrium of the residual stresses is reached providing the following equation:



$$2 b_t \sigma_t = (b - 2 b_t) \sigma_c \quad (5)$$

where:

b : Structure width

b_t : Tensile stress width

σ_t : Tensile stress

σ_c : Compressive stress

Figure 12: Welding residual stresses produced on a plate by fillet weld [5]

The residual stresses can be estimated based on:

b_t , which is function of the weld heat input, plate thickness and length of the weld

σ_t , which depends in the material. For ordinary steels is equal to the yield stress. For higher strength steels, it is considered to be between 0.5 and 0.8 times the yielding stress.[4]

2.4.2 Initial deflections

In addition to the residual stresses, initial deflections are introduced in the plating and stiffeners due to the welding process as illustrated in Fig. 13. In terms of buckling and ultimate strength, the deflections of greater influence are the angular change and the bending distortion since they lead to lower in-plane stiffness.

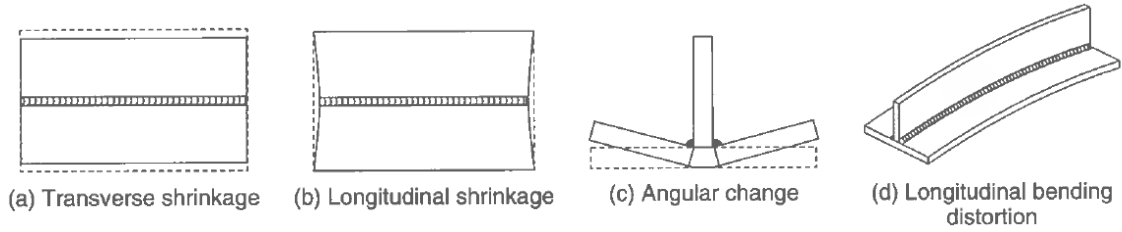


Figure 13: Welding induced distortions [5]

The geometrical configuration of such initial deflections is quite complex since it includes the interaction of different deformation modes. For unstiffened plate the initial deflection can be expressed as:

$$w_0 = \sum_i^m \sum_j^n A_{0ij} \sin\left(\frac{i\pi x}{a}\right) \sin\left(\frac{j\pi y}{b}\right) \quad (6)$$

where:

A_{0ij} : Welding – induced deflection amplitude

a, b : Plate length and width respectively

m, n : Half – wave number in x and y direction respectively

The deflection amplitudes may be estimated from initial deflection measurements. However, if they are not available the amplitudes may be estimated based on empirical formulations provided by different authors such as Faulkner (1975), Smith (1988) or class societies.

For practical design purposes, a typical rectangular plate element loaded along x-direction (its long side) will show a multi-wave pattern in this direction ($m > 1$) and a single half-wave in the transversal direction ($n = 1$). Therefore, the previous expression can be simplified as:

$$w_0 = \sum_i^m A_{0ij} \sin\left(\frac{i\pi x}{a}\right) \sin\left(\frac{\pi y}{b}\right) \quad (7)$$

On the other hand, when the plate is loaded along its y-direction the deflection patterns shows one half-wave in both directions ($m = 1, n = 1$). This phenomenon is explained with further details in the section 2.5.

With regarding to stiffeners deflections, initial deflections in a vertical and horizontal direction are also produced as shown in Fig. 14. For practical purposes, the way to estimate their magnitude and shape follow the same reasoning than for the plating.

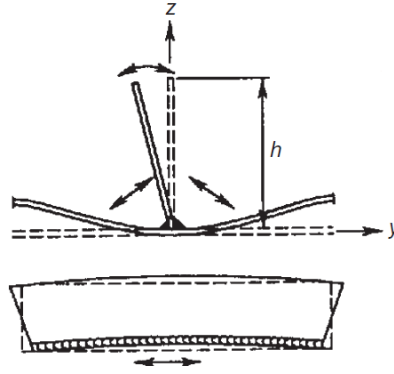


Figure 14: Welding induced distortions in plate-stiffener connection [5]

In order to perform a non-linear buckling analysis applying FEM, it is necessary to introduce initial imperfections in the structure. Otherwise, if there is no imperfection, only in-plane displacements are produced by in-plane loading and buckling will not be triggered.

In practice, the imperfection patterns are rather random and there is a lack of exact information regarding shape and amplitudes. Therefore, a widespread method to introduce initial imperfections is to consider the first buckling eigenmode of the perfect structure. This approximation provides a consistent and realistic approach to consider the imperfections in comparison with the measurements.

The model imperfection amplitudes are to be set in relation with typical production and fabrication standards. In fact, this is the approach followed by PULS to perform buckling and ultimate strength assessments.

2.5 Modes of buckling deformation

This section presents the fundamentals of buckling modes when a plate undergoes buckling which form the basis for understanding buckling modes of stiffened panels. The deformation pattern of a plate subjected to in-plane loading is function of mainly three factors:

- Type of loading
- Boundary conditions
- Aspect ratio of plate

The buckling deformation mode can be expressed as:

$$w = A_m \sin\left(\frac{m \pi x}{a}\right) \sin\left(\frac{n \pi y}{b}\right) \quad (8)$$

where:

m: buckling half – wave number for the plate in *x* direction

n: buckling half – wave number for the plate in *y* direction

The half-wave numbers *m* and *n* in both directions are mainly function of the aspect ratio *a/b* and have a direct influence in the buckling strength through the buckling factor *k*, which is presented in chapter 3 for the elastic buckling of simply supported plates.

One half-wave is normally produced in either the short edge or the direction in which the axial compressive loads are predominant as presented in Fig.15. Thus, for long plates as considered in this work *n* = 1 is typically taken.

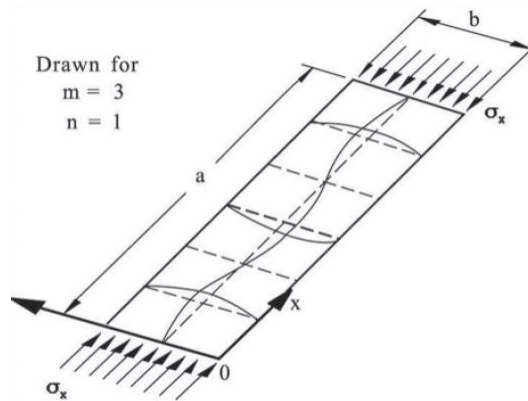


Figure 15: Buckling mode deformation illustration for longitudinal loading [4]

For *longitudinal loading*, the buckling mode or buckling half-wave number is function of the aspect ratio as illustrated in Figure. 16. It is defined as the minimum integer satisfying the following condition:

$$a/b \leq \sqrt{m(m+1)} \quad (9)$$

Thus, for an aspect ratio of $\sqrt{m(m+1)}$ the buckling mode will change from m to $m+1$.

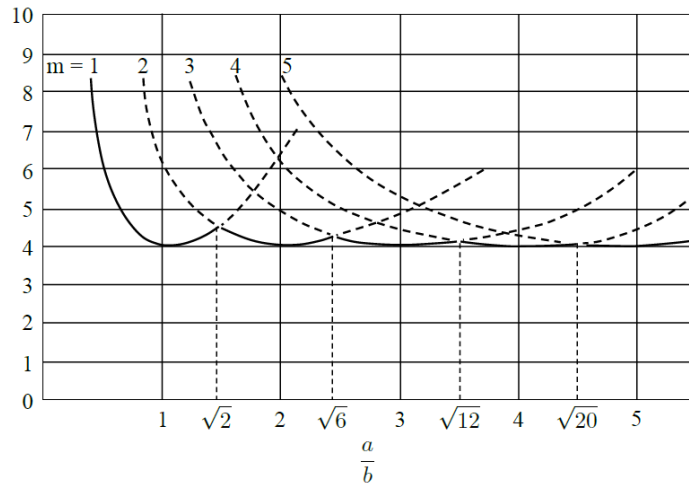


Figure 16: Buckling coefficient for simply supported plate under longitudinal loading as function of aspect ratio [4]

For *biaxial loading*, the buckling half-wave number m in the x direction can be predicted as the minimum integer satisfying the following condition:

$$\frac{\left(\frac{m^2}{a^2} + \frac{1}{b^2}\right)^2}{\left(\frac{m^2}{a^2} + \frac{c}{b^2}\right)} \leq \frac{\left(\frac{(m+1)^2}{a^2} + \frac{1}{b^2}\right)^2}{\left(\frac{(m+1)^2}{a^2} + \frac{c}{b^2}\right)} \quad (10)$$

This is derived from the analytical solution for the elastic buckling of a plate under biaxial loading given by Eq. 17 which is presented in the following chapter, section 3.3.2. It can be noted the dependence of the half-wave number on the applied loading ratio c and the plate aspect ratio. If the loading ratio is 0, the previous condition given by Eq. 9 is recovered.

3. FUNDAMENTAL THEORY OF PLATES BUCKLING

An unstiffened plate can be considered as the minimal structural unit in a stiffened panel partitioned by longitudinal and transverse stiffeners. It is important to study the behaviour of an isolated unstiffened plate in order to know how will interact with the stiffeners within the stiffened panel. When the plate undergoes buckling and out-of-plane deflection develops, the stiffeners restrict the rotation of the plate with a certain degree. However, the boundary condition is typically idealized to be simply supported along its four edges.

Therefore, this section presents fundamental ideas and methods for buckling strength assessment as well as main considerations regarding buckling modes.

3.1 Basic configuration

The typical geometrical configuration and coordinate system for an unstiffened plate is presented in Fig. 17. The coordinate system takes the x-direction along the long side of the plate and the y-direction along the short side. By this configuration the aspect ratio of the element a/b is always bigger than 1.

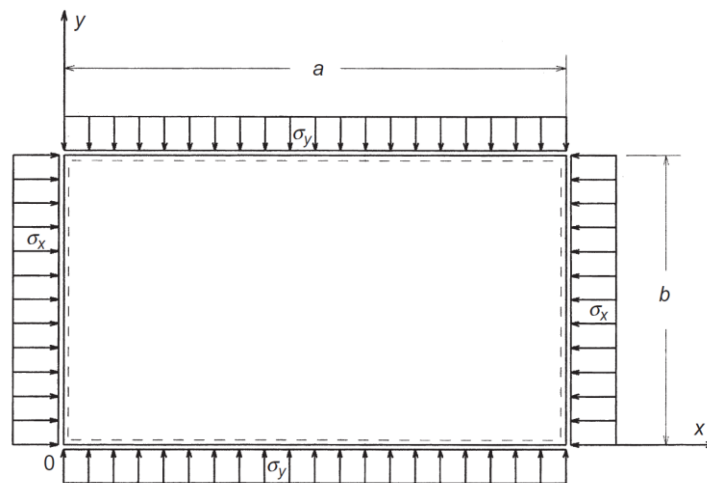


Figure 17: Rectangular plate under combined in-plane loading [4]

In the Figure, just the in-plane loads considered in the analysis are represented. The shear and lateral pressure are disregarded. Due to convenience, the compressive in-plane loads are taken as a positive sign while the tensile stresses are taken as negative.

3.2 Failure mechanism and behaviour

In this section is described the failure mechanism and behaviour of a simply supported unstiffened plate when undergoes buckling. The basic types of structural failure are driven by one of the following non-linear behaviour:

- Non-linearity associated with buckling or large deflection.
- Material non-linearity due to yielding or plastic deformation.

As slenderness is one of the main factors affecting the buckling of a structure, it is appropriate to make the distinction between thin and thick plates since they will have different behaviours.

- **Thin plate**

Beyond the buckling point, the capacity increases further with the increase of deflection, but the in-plane stiffness (slope of average stress – average strain curve) decreases to around 0.5 times the Young's modulus, depending on the aspect ratio. When yielding is reached, the in-plane stiffness starts to decrease gradually until it becomes zero and the ultimate strength is reached. Then, the capacity starts to decrease beyond the ultimate strength characterized by a high degree of instability [4].

- **Thick plate:**

Yielding starts to take place before buckling. The maximum load-carrying capacity, that is the ultimate strength, is nearly equal to the fully plastic strength. This capacity is kept until buckling takes place where the capacity starts to decrease with the increase of the out-of-plane deflection [4].

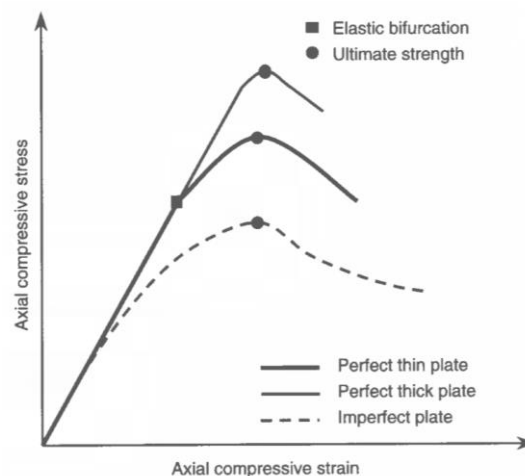


Figure 18: Average stress-average strain relation for unstiffened plate under compressive loading [4]

In addition, the membrane stress distribution along the plate can become non-uniform as the plate undergoes buckling. Figure 19 shows a typical example of axial membrane stress distribution inside a plate element under longitudinal compressive loading before and after buckling occurs.

Before buckling is triggered (case a), the stress distribution is uniform. As the plate undergoes buckling (case b and c), the stress distribution along x direction become non-uniform. With respect to the y direction, the stress distribution may also become non-uniform if unloaded plate edges remaining straight (case c). In contrast, no membrane stresses will develop if the unloaded edges are free to deform (case b).

With increase in the deflection and keeping the edges straight, the upper and/or lower fibres inside the middle of the plate element will yield initially by the action of bending. However, as long as it is possible to redistribute the applied loads to the straight plate boundaries, the plate element will not collapse. Collapse will occur when the most stressed boundary locations yield, since the plate element cannot keep the boundaries straight any further, resulting in a rapid increase of lateral plate deflection.

The maximum membrane stresses are developed around the edges that remain straight while the minimum stresses occur in the mid-plate. The possible yield locations are longitudinal mid-edges for longitudinal uni-axial compressive loads and transverse mid-edges for transverse uni-axial compressive loads.[2]

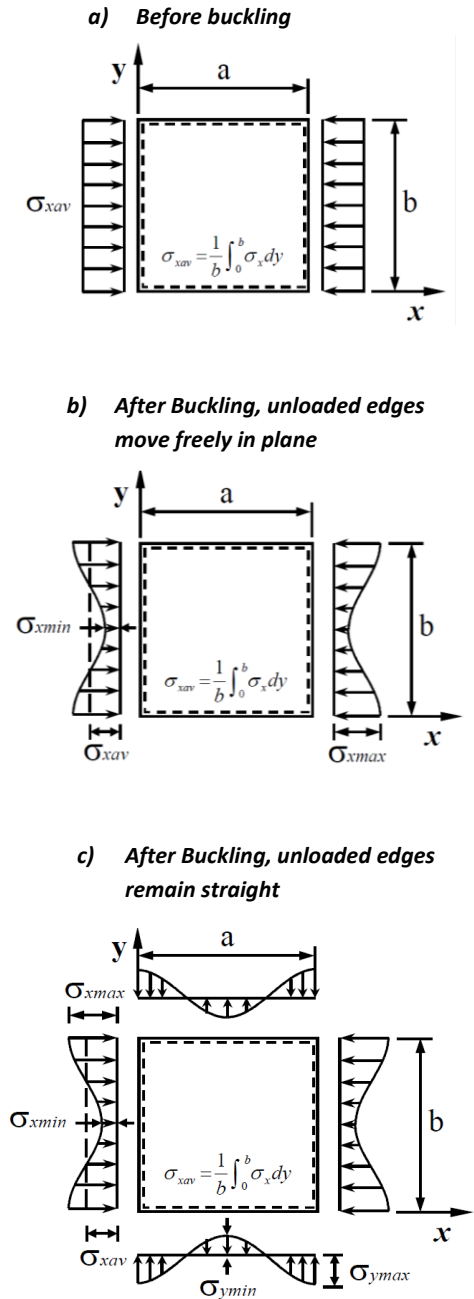


Figure 19: Axial membrane stress distribution in a plate under longitudinal compressive loading [2]

3.3 Elastic buckling of a simply supported plate

In this section the elastic buckling limit for which the plate will undergo buckling are provided. It should be considered that these values are obtained for a perfect ideal structure with the assumption of simply supported boundary conditions. Thus, by introducing initial imperfections in the structures and performing non-linear analysis lower values of elastic buckling limit are expected.

3.3.1 Under single compressive load

The elastic buckling stress solution for a plate under in-plane loading and simply supported boundary conditions is available from classical theory of elasticity derived from Timoshenko & Gere. The elastic buckling strength is given as follows:

$$\sigma_E = k \frac{\pi^2 E}{12(1-\nu^2)} \left(\frac{t}{b}\right)^2 \quad (11)$$

where:

σ_E : Plate buckling strength

k : Buckling coefficient for the corresponding load

t : Thickness of the plate

E : Young's Modulus

ν : Poisson's ratio

For *uniform longitudinal compressive loading* σ_x , the buckling coefficient is given by:

$$k_x = \left[\frac{a}{(m b)} + \frac{(m b)}{a} \right]^2 \quad (12)$$

For *uniform transverse compressive loading* σ_y , the buckling coefficient is given by:

$$k_y = \left[1 + \left(\frac{b}{a}\right)^2 \right]^2 \quad (13)$$

3.3.2 Under Biaxial compressive load

An analytical solution for the elastic buckling of a plate under biaxial loading and simply supported boundary conditions is given by [Hughes 1988, Paik 1991] as follows:

$$\frac{m^2}{a^2} \sigma_x + \frac{n^2}{b^2} \sigma_y - \frac{\pi^2 D}{t} \left(\frac{m^2}{a^2} + \frac{n^2}{b^2} \right)^2 = 0 \quad (14)$$

where:

D: Plate flexural rigidity:

$$D = \frac{E t^3}{12 (1-\nu^2)} \quad (15)$$

One half-wave number is normally taken in either the short edge or the direction in which the axial load is predominant. For a long plate ($a/b \geq 1$), $n = 1$ is typically taken. Then, considering the applied loading ratio is constant ($\frac{\sigma_y}{\sigma_x} = c$), the previous Eq. 14 can be expressed as:

$$\sigma_x \left(\frac{m^2}{a^2} + \frac{c}{b^2} \right) - \frac{\pi^2 D}{t} \left(\frac{m^2}{a^2} + \frac{1}{b^2} \right)^2 = 0 \quad (16)$$

Buckling will take place when Eq. 16 is satisfied. Thus, the elastic buckling stress is obtained by replacing σ_x to σ_{xE} :

$$\sigma_{xE} = \frac{\pi^2 D}{t} \frac{\left(\frac{m^2}{a^2} + \frac{1}{b^2} \right)^2}{\left(\frac{m^2}{a^2} + \frac{c}{b^2} \right)} \quad (17)$$

Where σ_{xE} indicates the elastic longitudinal buckling stress component. Given the previous definition of c , the elastic transverse buckling stress in is given by:

$$\sigma_{yE} = c \sigma_{xE} \quad (18)$$

3.4 Non-linear governing differential equation

The large-deflection behaviour of a plate in post-buckling regime can be analysed by the non-linear differential equations derived by Marguerre (1938), based on an equilibrium (Eq. 19) and a compatibility (Eq. 20) equations:

$$D \left(\frac{\partial^4 w}{\partial x^4} + 2 \frac{\partial^4 w}{\partial x^2 \partial y^2} + \frac{\partial^4 w}{\partial y^4} \right) - t \left[\frac{\partial^2 F}{\partial x^2} \frac{\partial^2 (w+w_0)}{\partial x^2} - 2 \frac{\partial^2 F}{\partial x \partial y} \frac{\partial^2 (w+w_0)}{\partial x \partial y} + \frac{\partial^2 F}{\partial y^2} \frac{\partial^2 (w+w_0)}{\partial y^2} + \frac{p}{t} \right] = 0 \quad (19)$$

$$\frac{\partial^4 F}{\partial x^4} + 2 \frac{\partial^4 F}{\partial x^2 \partial y^2} + \frac{\partial^4 F}{\partial y^4} - E \left[\left(\frac{\partial^2 w}{\partial x \partial y} \right)^2 - \frac{\partial^2 w}{\partial x^2} \frac{\partial^2 w}{\partial y^2} + 2 \frac{\partial^2 w_0}{\partial x \partial y} \frac{\partial^2 w}{\partial x \partial y} - \frac{\partial^2 w_0}{\partial x^2} \frac{\partial^2 w}{\partial y^2} - \frac{\partial^2 w}{\partial x^2} \frac{\partial^2 w_0}{\partial y^2} \right] = 0 \quad (20)$$

where:

w_0 : initial deflection,
 w : added deflection
 F : Airy's stress function

To solve the previous equations, it is necessary first to assume the added and initial deflections w_0 and w which are typically taken as:

$$w_0 = A_{0m} \sin \left(\frac{m \pi x}{a} \right) \sin \left(\frac{\pi y}{b} \right) \quad (21)$$

$$w = A_m \sin \left(\frac{m \pi x}{a} \right) \sin \left(\frac{\pi y}{b} \right) \quad (22)$$

where:

A_{0m} : amplitud of the initial deflection
 A_m : amplitude of the added deflection

Then, Galerkin method is applied to obtain a third order equation with respect to the unknown variable A_m . Considering the loading and boundary conditions, the amplitude of the added deflection A_m and Airy's stress function F can be calculated.

Once the previous parameters are known the membrane stress distribution within the plate stresses can be derived as follows:

$$\sigma_x = \frac{\partial^2 F}{\partial y^2} - \frac{E z}{1-\nu^2} \left(\frac{\partial^2 w}{\partial x^2} + \nu \frac{\partial^2 w}{\partial y^2} \right)^2 = 0 \quad (23)$$

$$\sigma_y = \frac{\partial^2 F}{\partial x^2} - \frac{E z}{1-\nu^2} \left(\frac{\partial^2 w}{\partial y^2} + \nu \frac{\partial^2 w}{\partial x^2} \right)^2 = 0 \quad (24)$$

4. FUNDAMENTAL THEORY OF STIFFENED PANELS BUCKLING

The stiffened panel is an assembly of plating and stiffener which act as support members and represents the main load bearing element in a ship hull. Unlike columns, this structure can sustain further loads after buckling occurs in the elastic or even inelastic regime until the ultimate capacity is reached. This section presents fundamental theory and methods with respect to buckling strength and collapse behaviour as well as main considerations regarding buckling patterns.

4.1 Basic configuration

The stiffened panel represent the main structural unit used in ship structure. There are different arrangements and configurations depending on the location where they operate and the loads they have to sustain. In general terms, its geometrical configuration is illustrated in Fig. 20.

The principal structural members composing a stiffened panel are:

- **Plate panels:** plating
- **Small support members:** stiffeners
- **Strong support members:** Frames, girders, bulkheads, box girders

Plating is primarily sustaining in-plane loads while the support members resist out-of-plane loads and bending. Small support members or stiffeners are supported by the strong heavy members which are spaced at bigger distances and ensuring that the plate panels have an adequate strength when loaded.

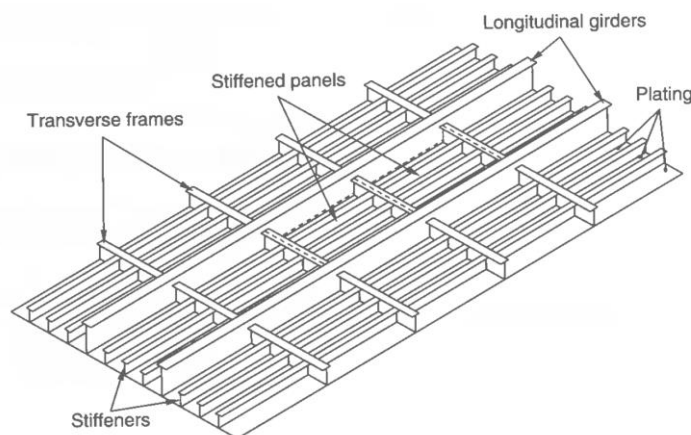


Figure 20: Typical stiffened panel configuration in ship structure [5]

In ship structures, heavy members are composed of deep webs and wide flanges. They are oriented in the primary loading condition (longitudinal direction for ship hulls of a certain size). When they are placed orthogonally to the primary load direction, they are usually called frames.

To improve the stiffness and strength of stiffened panels, increasing the stiffener dimensions is usually more efficient than simply increasing the plate thickness. Figure. 21 shows typical stiffener profiles used for stiffening the plating.

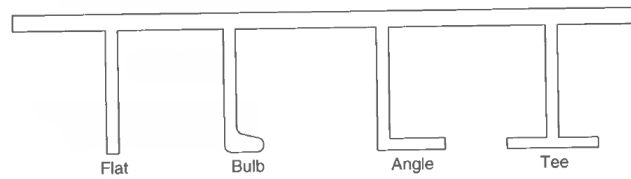


Figure 21: Typical stiffeners used in stiffened panels [5]

In general, ship structures are designed so that buckling collapse does not occur in the primary structural members for loads below the design load. In addition, the stiffeners are sized so that plating will buckle before the overall buckling mode of the whole structure which would lead to a significant instability.

A typical arrangement for a stiffened panel under combined in-plane loads and typical coordinates system is shown in Fig. 22.

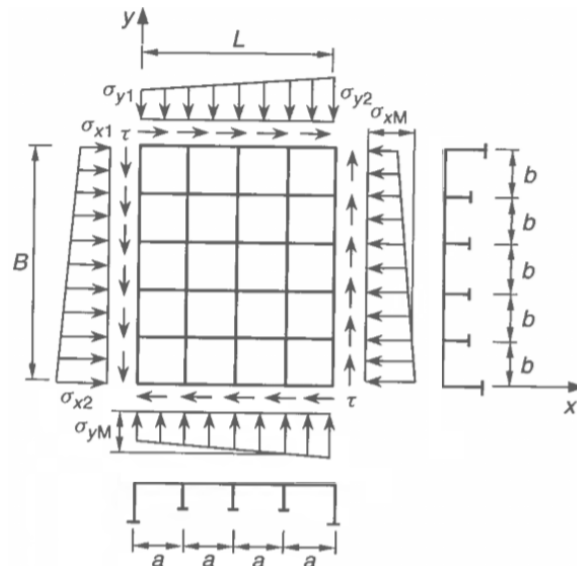


Figure 22: Cross-stiffened panel under combined in-plane loads and lateral pressure [5]

4.2 Failure mechanism and behaviour

In this section is described the failure mechanism and behaviour of a simply supported stiffened panel when undergoes buckling. In the same way than for unstiffened plates, the structural failure is driven by one of the following non-linear behaviour:

- Non-linearity associated with buckling or large deflection.
- Material non-linearity due to yielding or plastic deformation.

The compressive load is considered to act along the direction of the stiffeners. As slenderness is one of the main factors affecting the buckling behaviour of a structure, it is appropriate to make the distinction between different slenderness degrees as illustrated in Fig. 23.

- **High slenderness ratio (Curve A):** Elastic plate buckling (just at the panel) takes place locally at the point 1 and the stiffness decreases due to the inferred out-of-plane deflections. At point 3, yielding starts to take place and stiffness keeps decreasing gradually until it reaches Point 2 where it is zero and the overall buckling of the stiffened panel occurs. After this point the capacity starts to decrease.
- **Low slenderness ratio (Curve B):** Yielding starts to take place at Point 3 and as in the previous case, the ultimate strength is attained at point 4 by overall buckling of the stiffened panel.
- **Very low slenderness ratio (Curve C):** Yielding starts at point 5 and soon the general yielding takes place all over the stiffened panel. However, no out-of-plane deflection is produced yet. At Point 6, either the panel or the stiffener undergoes buckling and the capacity decreases with the increase inn deflection in the panel or in the stiffener. [4].

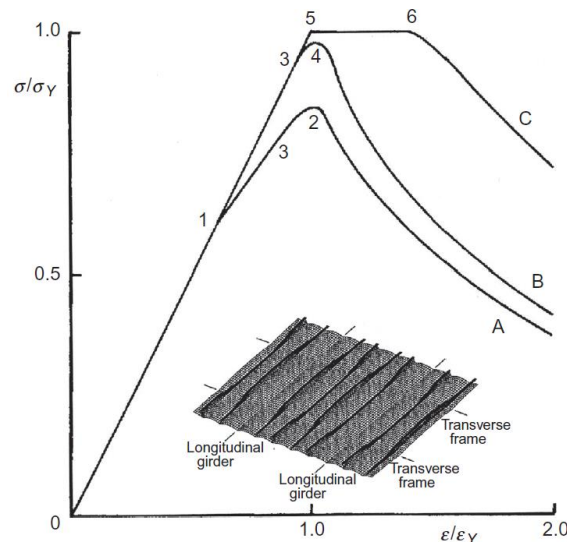


Figure 23: Average stress-average strain relation for a typical stiffened panel under compressive loading [4]

4.3 Overall Buckling

This mode is associated to the buckling pattern of the whole stiffened panel as a single plate. When the stiffeners are small, the stiffened panel can buckle together with the plating as illustrated in Fig. 24. This buckling pattern is called overall buckling and presents one half-wave in both directions longitudinal and transversal. It can be expressed as:

$$w_{overall} = A_{11} \sin \frac{\pi x}{a} \sin \frac{\pi y}{b} \quad (25)$$

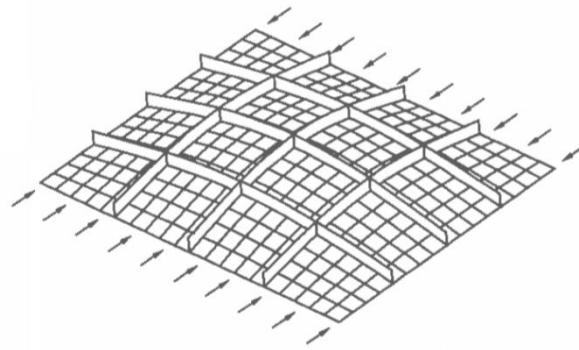


Figure 24: Overall Buckling of stiffened panel [5]

Even though if the stiffened panel can sustain further loads after the inception of buckling, the occurrence of overall buckling is considered a significant instability in the structure. Therefore, the structure is designed so overall buckling is prevented prior to local buckling of plating between stiffeners.

Elastic overall buckling formulations for a stiffened panel under single and combined loading are presented below:

- **Longitudinal axial compression**

The overall buckling of the panel under longitudinal loading can be approximated by the column buckling of a plate-stiffener combination representative of the panel as presented in Fig. 25. The boundary conditions are considered as simply supported.

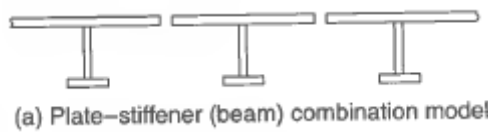


Figure 25: Plate-stiffener combination [5]

The elastic overall buckling stress σ_{xEO} is based on the Euler buckling load P_E and is derived as follows:

$$\sigma_{xEO} = \frac{P_E}{A} \quad (26)$$

Where:

$$P_E: \text{Euler Buckling Load given by} \quad P_E = \frac{\pi^2 E I_e}{L^2} \quad (27)$$

I_e : Moment of Inertia of the plate – stiffener combination taking the effective breadth

L : Length of the plate – stiffener combination

- **Transverse axial compression**

The overall buckling of the panel under transverse loading can be predicted from the plate buckling strength formula (Eq. 11) as presented in section 3.2.1 by neglecting the stiffeners.

*Given that this formulation is available for aspect ratios bigger than one, the coordinate system is to be rotated.

- **Combined Biaxial Compression**

The overall buckling strength of the panel under combined biaxial loading can be calculated analytically by solving the non-linear differential equation of large-deflection orthotropic plate theory presented in section 4.5. Immediately before buckling occurs, the panel lateral deflection must be zero. This results in an overall panel buckling strength under combined axial loading as follows:

$$\frac{m^2 B}{L} \sigma_x + \frac{n^2 L}{B} \sigma_y + \frac{\pi^2}{t} \left(D_x \frac{m^4 B}{L^3} + 2H \frac{m^2 n^2}{LB} + D_y \frac{n^4 L}{B^3} \right) = 0 \quad (28)$$

Which provides the elastic overall buckling stress as:

$$\sigma_{xEO} = - \frac{\pi^2}{t \left(m^2 \frac{B}{L} + cn^2 \frac{L}{B} \right)} \left(D_x \frac{m^4 B^2}{n^2 L^4} + 2H \frac{m^2}{L^2} + D_y \frac{n^2}{B^2} \right) \quad (29)$$

Where:

c : Loading ratio, $c = \sigma_x / \sigma_y$

D : Flexural rigidity of the orthotropic plate

H : Effective torsional rigidity

4.4 Local Buckling

When stiffeners are strong enough so the overall buckling mode is prevented, the stiffened panel will buckle in local modes. These buckling patterns refer to the mode where either plating or stiffeners buckle separately. In addition, they can occur simultaneously at the same time and interact with each other.

With respect to the scope of this work the main local buckling modes are the following:

- Buckling of plating between stiffeners
- Buckling of stiffener web
- Lateral-torsional buckling of stiffeners

4.4.1 Buckling of plating between stiffeners

This mode takes place when the stiffeners are strong enough remaining straight until the plating between them undergo buckling as illustrated in Fig. 26.

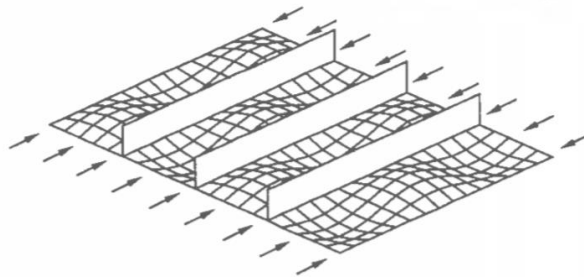


Figure 26: Local Buckling of plating between stiffeners [5]

The buckling strength of this mode can be derived by considering the bare plate element and applying formulation provided in section 3.3.

4.4.2 Buckling of stiffener web

This mode refers to the local buckle of the stiffener web as illustrated in Fig. 27. It generally takes place when the stiffener web is tall or the thickness is small.

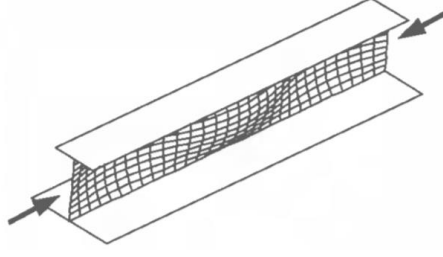


Figure 27: Local Buckling of stiffener web [5]

This buckling mode can sometimes be a sudden phenomenon which results in the unloading of the stiffened panel. It is mainly influenced by the torsional rigidities of adjacent members. When the stiffener undergoes buckling the plating is left with no stiffening, hence this situation to the stiffened panel collapse. To deal with this interaction, the structure is to be designed so buckling of stiffener web does not take place until plating between stiffeners buckles.

The buckling strength of stiffener web can be derived from the differential equation for the out-of-plane deflection with zero initial deflection and simply supported edges:

$$D_w \left(\frac{\partial^4 v}{\partial x^4} + 2 \frac{\partial^4 v}{\partial^2 x \partial^2 z} + \frac{\partial^4 v}{\partial z^4} \right) + t_w \sigma_x \frac{\partial^4 v}{\partial z^4} = 0 \quad (30)$$

Where:

v : lateral deflection of stiffener web

D_w : Bending rigidity of stiffener web

Which leads to:

$$\sigma_E^W = -k_w \frac{\pi^2 E}{12 (1-\nu^2)} \left(\frac{t_w}{h_w} \right)^2 \quad (31)$$

Where:

σ_E^W : Elastic buckling strength of stiffener web

k_w : Buckling strength coefficient of stiffener web

The theoretical development to obtain the elastic buckling strength expression is further developed in [5]. Solving Eq. 30 is not always straightforward, so for design and fast assessment stages a closed form method is usually used to derive k_w , for flat bar stiffeners:

$$k_w = \begin{cases} 0.303 \zeta_p + 0.427 & \text{for } 0 \leq \zeta_p \leq 1 \\ 1.277 - \frac{1}{(1.40 \zeta_p + 0.428)} & \text{for } 1 < \zeta_p \leq 6 \\ 1.2652 & \text{for } 60 < \zeta_p \end{cases} \quad (32)$$

Where:

ζ_p : Torsional rigidity of the plating

4.4.3 Lateral-torsional Buckling of stiffeners

This mode, also known as tripping, consists in the rotation of the stiffeners around the plate-stiffener connection as illustrated in Fig. 28. It takes place when the torsional rigidity of the stiffener is not strong enough so it twists sideways

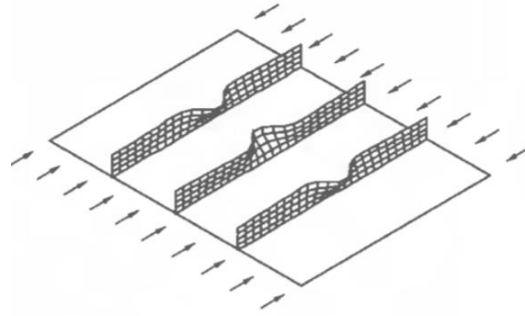


Figure 28: Lateral-torsional Buckling of stiffeners

In the same way than the buckling of stiffener web, it is produced suddenly reducing considerably the stiffness of the plating and thus overall collapse may be triggered afterwards.

There are some available theoretical approaches with respect to this buckling mode such as Smith (1975) or Hughes & Ma (1996). The derivation of theoretical solutions it is not straightforward considering the section deformations as illustrated in Fig. 29. That is why for practical and design purposes a closed -form expressions as provided by Paik are used [5].

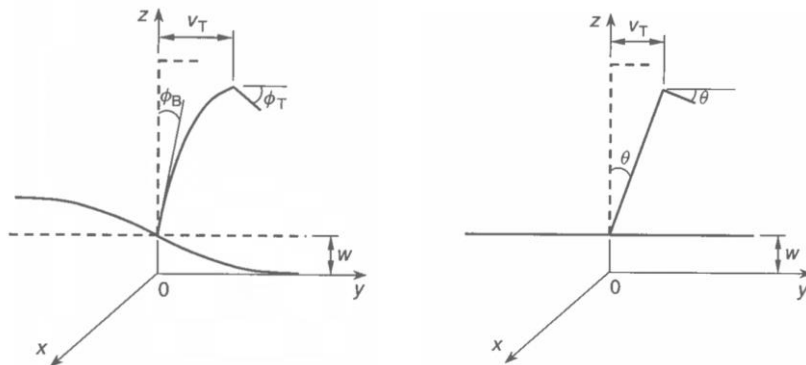


Figure 29: Lateral-torsional Buckling idealization of deformations: Actual deformation (left), idealized (right) [4]

4.5 Non-linear governing differential equations

The non-linear governing differential equations for stiffened panels are usually divided into two groups according to buckling modes as follows:

- *Overall panel buckling*, analysed by large-deflection orthotropic plate theory.

Orthotropic plate theory applies to plates having different flexural rigidities in two perpendicular directions. The structure is idealized assuming that the properties of the stiffeners are distributed uniformly over the plate as illustrated in Fig. 30.

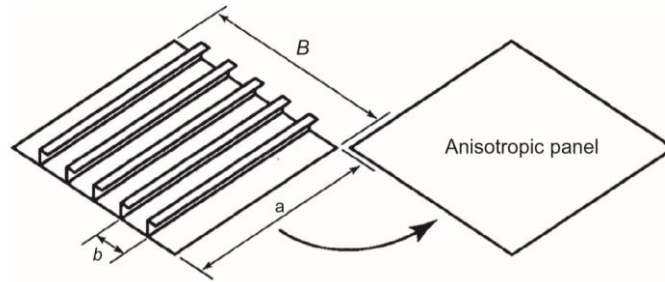


Figure 30: Idealization of stiffened panel into anisotropic plate [4]

The buckling behaviour of this mode can be analysed by solving non-linear governing differential equations which consist in the equilibrium (Eq. 33) and compatibility equation (Eq. 34) equations:

$$D_x \frac{\partial^4 w}{\partial x^4} + 2H \frac{\partial^4 w}{\partial x^2 \partial y^2} + D_y \frac{\partial^4 w}{\partial y^4} - t \left[\frac{\partial^2 F}{\partial y^2} \frac{\partial^2 (w+w_0)}{\partial x^2} - 2 \frac{\partial^2 F}{\partial x \partial y} \frac{\partial^2 (w+w_0)}{\partial x \partial y} + \frac{\partial^2 F}{\partial x^2} \frac{\partial^2 (w+w_0)}{\partial y^2} + \frac{p}{t} \right] = 0 \quad (33)$$

$$\frac{1}{E_y} \frac{\partial^4 F}{\partial x^4} + \left(\frac{1}{G_{xy}} + 2 \frac{\nu_x}{E_x} \right) \frac{\partial^4 F}{\partial x^2 \partial y^2} + \frac{1}{E_x} \frac{\partial^4 F}{\partial y^4} - \left[\left(\frac{\partial^2 w}{\partial x \partial y} \right)^2 - \frac{\partial^2 w}{\partial x^2} \frac{\partial^2 w}{\partial y^2} + 2 \frac{\partial^2 w_0}{\partial x \partial y} \frac{\partial^2 w}{\partial x \partial y} - \frac{\partial^2 w_0}{\partial x^2} \frac{\partial^2 w}{\partial y^2} - \frac{\partial^2 w}{\partial x^2} \frac{\partial^2 w_0}{\partial y^2} \right] = 0 \quad (34)$$

where:

w_0 : initial deflection,

w : added deflection

F : Airy's stress function

E_x, E_y : Elastic modulus in x and y directions

ν_x, ν_y : Poisson's ratio in x and y direction

D_x, D_y : Flexural rigidity in x and y directions

G_{xy} : Elastic shear modulus

H : Effective torsional rigidity

The solving procedure is similar as described in section 3.4 for an unstiffened plate but accounting for the anisotropy in the two perpendicular directions x and y arising from the arrangement of the stiffeners. Once the added deflection w and Airy's stress function are calculated, the stresses within the panel can be derived as:

$$\sigma_x = \frac{\partial^2 F}{\partial y^2} - \frac{E_x z}{1 - \nu_x \nu_y} \left(\frac{\partial^2 w}{\partial x^2} + \nu_y \frac{\partial^2 w}{\partial y^2} \right) = 0 \quad (35)$$

$$\sigma_y = \frac{\partial^2 F}{\partial x^2} - \frac{E_y z}{1 - \nu_x \nu_y} \left(\frac{\partial^2 w}{\partial y^2} + \nu_x \frac{\partial^2 w}{\partial x^2} \right) = 0 \quad (36)$$

- *Local panel buckling*, analysed by large-deflection isotropic plate theory. This case applies when stiffeners are strong enough so overall buckling is prevented. For analysing this buckling mode, the non-linear governing differential equation is described in the previous section 3.4.

5. INVESTIGATION OF TYPICAL STRUCTURES IN LARGE CRUISE VESSELS

In this section common structural features in terms of plating and stiffened panels are presented according to a global class cruise vessel of 342 m long, 46.4 m wide and a capacity for up to 9500 passengers [8]. Then, different configurations are selected in order to perform the further analysis.

Modern cruise vessels are very complex structures not only in terms of logistics and integration of systems but also in structural terms. Designs can vary widely from each other but they are often characterized by having multiple decks and long superstructures with many openings as shown in Fig. 31, which shows a cut section from within the vessel towards outside. The largest number of openings is due to the cabins having an outdoor view and often a balcony.

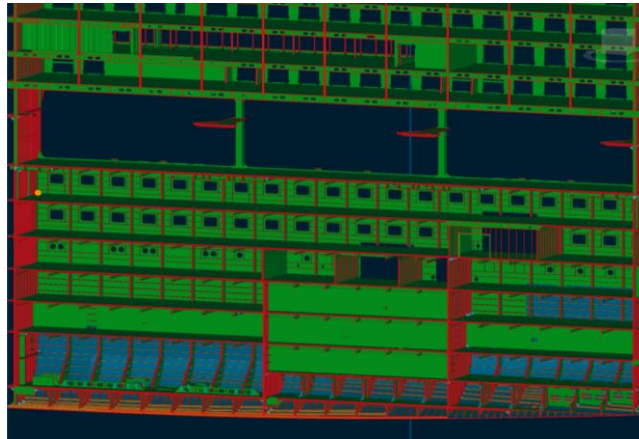


Figure 31: Section view of considered cruise vessel

In addition, they can be characterized in comparison with other type of vessels such as bulk carriers, tankers or containerships by having a large structural redundancy as illustrated in Fig. 32 through a section cut by amidships.

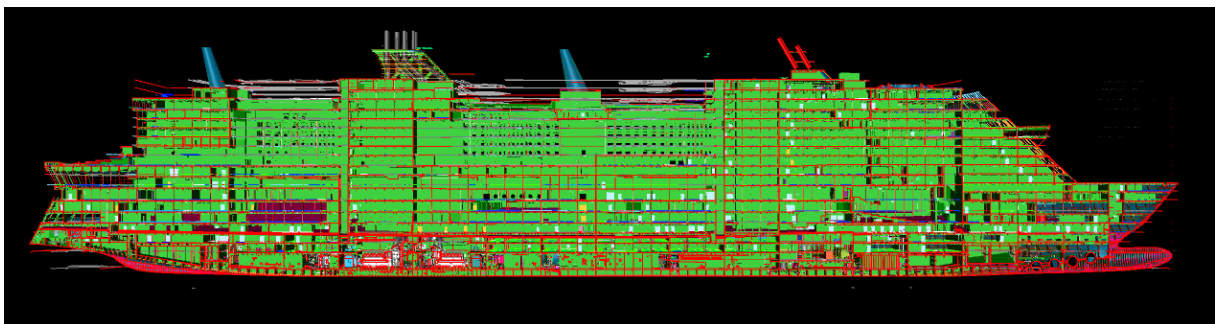


Figure 32: Longitudinal cut through amidships of vessel considered

Due to this complexity, the assessment of the design according to conventional rule formulas is difficult since they have been developed for similar structural arrangements. Thus, the assessment of modern cruise vessels tends to combine rule formulas with an extension by direct calculations to account for the particularities in the design.

5.1 Plating

There are different plate thicknesses depending on the location of the vessel and structural purpose of the section where they are placed. A representative range of thicknesses in the vessel vary from 10 to 18 mm approximately as illustrated in Fig. 33.

In the lower panels, up to the fourth deck from the baseline, the plating thickness is 15.5 mm. From fourth deck up to weather deck the thickness lies between 12 and 13.5 mm. For upper decks, characterized by large openings due to the cabin outdoor views and spaces, the plating has a thickness of 18 mm.

It can be seen that lower plating is characterized for being surrounded by stiffened panels and thus the thicknesses are lower than for the upper decks. In addition, lower values from 6 to 10 mm may be found in rather localized areas with a non-high demanding load bearing

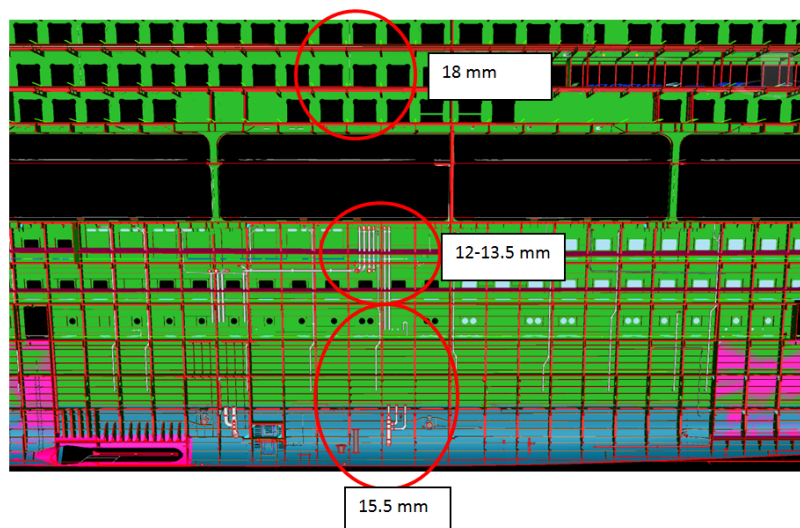


Figure 33: Plate thicknesses along height of the vessel

The most representative plating configuration in the vessel can be considered by taking the most representative stiffened panel as illustrated in Fig. 33. Thus, the unstiffened plate that is considered for the further analysis is defined by the stiffened panel configuration, that is the frame and stiffener spacing.

Length:	2.7 m	<i>(frame spacing)</i>
Width:	0.6 m	<i>(stiffeners spacing)</i>
Material:	A36	
Yielding strength:	355 MPa	

5.2 Stiffened Panel

Stiffened panel represent the main structural unit within the vessel and they are placed all along the sides, bottom, decks and also inner spaces. In the same way than the plating, the stiffeners size and thickness vary depending on the place they are located and its structural purpose.

Regarding the configuration, there is a wide variety of stiffener dimensions and thicknesses which vary according to the plate thicknesses described in previous sections and can be summarized as follows:

- *Stiffeners (L-Type):*
 - Height: From 100 to 240 mm
 - Width: From 21 to 60 mm
 - Thickness: From 100 to 240 mm
- *Heavy support members (T-Type):*
 - Web Height: From 235 to 640 mm
 - Web Thickness: From 7 to 10 mm
 - Flange width: From 100 to 150 mm
 - Flange Thickness: From 12 to 15 mm

Stiffener spacing is typically taken as 600 mm although in some locations irregular stiffening spacing is implemented due to practical issues in design and production.

In general terms, the most representative stiffened panel configuration in the vessel is presented in Fig. 34 with the following characteristics:

Length:	2.7 m	(frame spacing)
Width:	3 m	(girder spacing)
N° of stiffeners:	4-5	
Stiffeners spacing:	600 mm	
Material:	A36	
Yielding strength:	355 MPa	

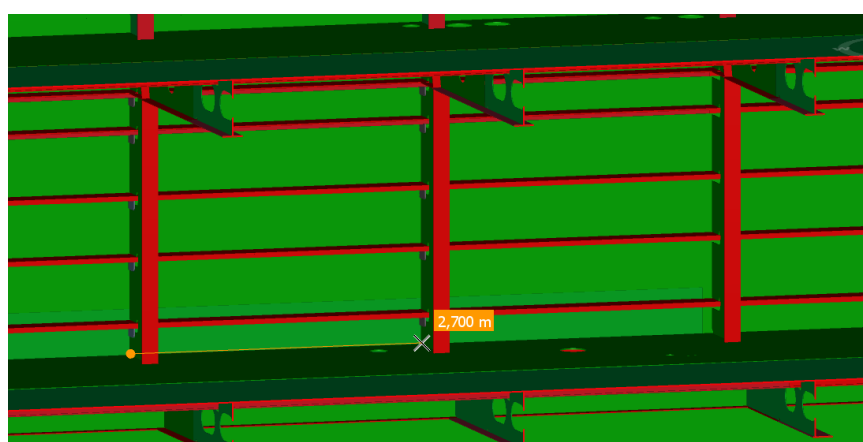


Figure 34: Representative stiffened panel for the vessel

5.3 Selected configurations for the analysis

Considering the previous structural arrangements present in the vessel, six structural configurations are selected to perform the further analysis. Three unstiffened plates and three stiffened panels. In addition, an enhanced model for each stiffened panel is selected considering the dimensions of the surrounding heavy members.

The structures selection aims to represent in a consistent way different arrangements to have a broader view of their behaviour in terms of buckling. The varying parameters are the thicknesses for plating and stiffener as well as the stiffener height.

The unstiffened plates are defined by the stiffeners and transverse spacing, considering thus the minimum unstiffened plate in the structure.

The selected configurations are summarized in the tables below:

Unstiffened plate configurations:

Length: 2.7 m (frame spacing)
Width: 600 mm (stiffener spacing)

	Plate
	Thickness [mm]
Unstiffened Plate 1	6
Unstiffened Plate 2	12
Unstiffened Plate 3	15.5

Table 1: Selected unstiffened plates for the analysis

Stiffened panel configurations:

Length: 2.7 m (frame spacing)
Width: 3 m (girder spacing)
Stiffener spacing: 600 mm

**The stiffener selected for the analysis is a flat-bar stiffener*

	PLATE	STIFFENER		FRAME			
	Thickness [mm]	Height [mm]	Thickness [mm]	Web Height [mm]	Web Thickness [mm]	Flange Width [mm]	Flange Thickness [mm]
Stiff. Panel 1	6	100	6	235	7	100	12
Stiff. Panel 2	12	140	8	485	10	150	15
Stiff. Panel 3	15.5	240	10	640	10	150	15

Table 2: Selected stiffened panels for the analysis

6. TYPICAL CLASS METHODS OF UNSTIFFENED AND STIFFENED STRUCTURES

The load-carrying capacity reduction when a structural member undergoes buckling causes a redistribution and increase of internal forces in unbuckled members, which may lead to the progressive occurrence of buckling failure and result in the collapse of the whole structure. This is why in old classification societies rules, buckling was not allowed in any structural member.

However, aiming a more rational design, capacity in post buckling strength and ultimate strength were introduced as design standard in Common Structural Rules (CSR) by IACS in early 2000s. Initially, two CSR were issued, one for Bulk carriers and another for Double Hull Oil Tankers. Later, these two were joined into Harmonized Structural Rules (H-CSR) which came into effect in 2015.

This chapter is based in typical class methods according to DNV-GL rules [6]. Accordingly, the following three methods are provided for the assessment of buckling and ultimate strength of load carrying members:

- Closed Form Method (CFM)
- PULS Code
- Non-Linear Finite Element

These methods assume a quasi-static formulation; hence the dynamic load effects are not being considered since the load varies slowly with time. This leads to a conservative assumption which applies to the environmental conditions the structure is going to operate in.

6.1 Closed form method (CFM)

This method is based on semi-empirical formulations and criteria is given as Closed Cell Formulas (CCF). It allows a buckling capacity assessment of different structural elements such as plate panels, stiffeners, stiffened panels, pillars or corrugated bulkheads.

The buckling capacity of the element is determined by applying the actual stress combination and then modifying the stresses proportionally until the interaction formulae are equal to 1. With respect to stiffened panels, the DNV-GL[6] considers three limit states which are presented below with their corresponding interaction formulas:

- **Overall Stiffened panel limit state:**

$$\frac{P_z}{c_f} = 1 \quad (37)$$

Where:

P_z : Nominal lateral load acting on the stiffener due to stresses σ_x, σ_y and τ in the attached plating in way of the stiffener midspan [N/mm²]

c_f : Elastic support provided by the stiffener [N/mm²]

- **Plate limit state:**

$$\left(\frac{\gamma_{c1}\sigma_x S}{\sigma'_{cx}}\right)^{e_0} - B \left(\frac{\gamma_{c1}\sigma_x S}{\sigma'_{cx}}\right)^{\frac{e_0}{2}} \left(\frac{\gamma_{c1}\sigma_y S}{\sigma'_{cy}}\right)^{\frac{e_0}{2}} + \left(\frac{\gamma_{c1}\sigma_y S}{\sigma'_{cy}}\right)^{e_0} + \left(\frac{\gamma_{c1}|\tau| S}{\tau'_c}\right)^{e_0} = 1 \quad (38)$$

$$\left(\frac{\gamma_{c2}\sigma_x S}{\sigma'_{cx}}\right)^{\frac{2}{\beta p^{0.25}}} + \left(\frac{\gamma_{c2}|\tau| S}{\tau'_c}\right)^{\frac{2}{\beta p^{0.25}}} = 1 \quad \text{for } \sigma_x \geq 0 \quad (39)$$

$$\left(\frac{\gamma_{c3}\sigma_y S}{\sigma'_{cy}}\right)^{\frac{2}{\beta p^{0.25}}} + \left(\frac{\gamma_{c3}|\tau| S}{\tau'_c}\right)^{\frac{2}{\beta p^{0.25}}} = 1 \quad \text{for } \sigma_y \geq 0 \quad (40)$$

$$\frac{\gamma_{c4}|\tau| S}{\tau'_c} = 1 \quad (41)$$

Where:

σ_x, σ_y : Applied normal stress to the plate panel

σ'_{cx} : Ultimate buckling stress in the direction parallel to the longer edge of the panel

σ'_{cy} : Ultimate buckling stress in the direction perpendicular to the shorter edge of the panel

τ : Applied shear stress

τ_c' : Buckling strength in shear

$\gamma_{c1}, \gamma_{c2}, \gamma_{c3}, \gamma_{c4}$: Stress multiplier factors at failure for each of the above limit states

B : Coefficient

e_0 : Coefficient

β_p : Plate slenderness

- **Stiffener limit state:**

$$\frac{\gamma_c \sigma_a + \sigma_b + \sigma_w}{R_{eH}} S = 1 \quad (42)$$

Where:

σ_a : effective axial stress, at mid span of the stiffener with the attached plating

σ_b : bending stress in the stiffener

σ_w : stress due to torsional deformation

R_{eH} : yield stress of the material

S : safety factor

Although numerical methods can produce very accurate results, they tend to use significant computational and time resources limiting their application. The combination of speed and reliability makes this method suitable for use especially in preliminary design phases for structural members [9].

6.2 PULS method

This chapter presents the theoretical basis and background behind PULS formulation and approach. A more developed and extended information is available in [1], [2] and [6].

PULS is a computerized code developed by DNV-GL and IACS for the purpose of doing a fast buckling and ultimate strength assessment of unstiffened and stiffened thin plate elements with an accuracy close to more advanced NFEM. It is based on a direct semi-analytical approach using non-linear plate theory capable of predicting the elastic buckling limit (eigenvalues) and the post-buckling behaviour up to the ultimate strength limit. A direct approach means that the equations describing the physical problem are established and a numerical strategy is used for solving them.

The strength assessment can be performed for combined loading as indicated in Fig. 35, considering:

- i. In-plane axial load in the direction of the stiffener, compression or tension (σ_1)
- ii. In-plane transverse load in the direction perpendicular to the stiffener, compression or tensions (σ_2)
- iii. In-plane shear (σ_3)
- iv. Lateral pressure

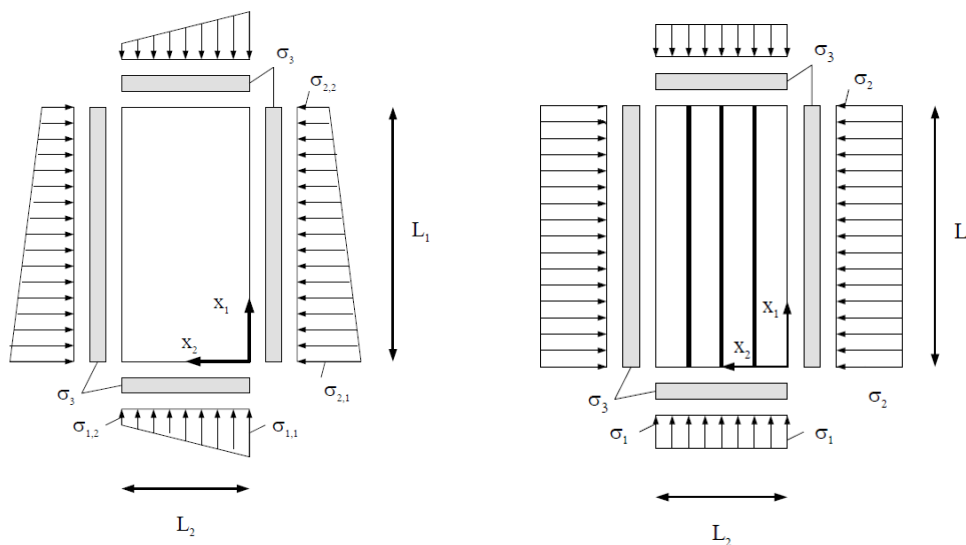


Figure 35: Schematic combined loading for unstiffened plate (left) and stiffened panel (right) [1]

Several types of elements are available covering regular stiffening, non-regular stiffening and corrugation arrangements as presented in Fig. 36. They are implemented in DNV-GL's NAUTICUS Hull program and the basic plate elements (U3, S3) are also available in Excel format, which offers an easy input of a large number of panels, and therefore makes parametric studies easier to perform. The current library presents four different structural elements:

- 1 Unstiffened rectangular plate, U3
- 2 Uni-axially or Orthogonally stiffened rectangular plate, S3
- 3 Non-regular stiffened plate, T1
- 4 Symmetric trapezoidal open corrugation, K3

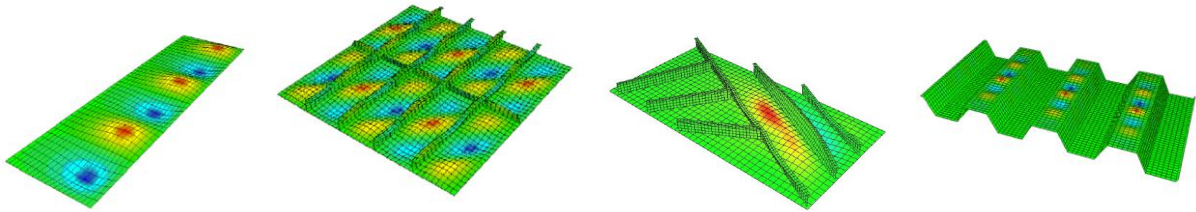


Figure 36: PULS available elements [6]

For all elements PULS provides the Buckling Strength (BS) and Ultimate Capacity (UC) for the specified load combination. Geometrical imperfections and residual stress effects are implicitly considered in the code with typical values for welded and fabricated steel plates as used in ships and offshore constructions.

For the purpose of code/rules checking, the results are presented in a single parameter: the usage factor. This factor provides a measure of the difference between the specified load and the corresponding UC or BS, giving an intuitive idea about how far the element is operating from its critical load.

6.2.1 Theory fundamentals

PULS method is classified as semi-analytical in the sense that is based on a recognized non-linear large deflection plate theory (Marguerre) in combination with a Rayleigh-Ritz discretization of deflections. This discretization method implies global trigonometric functions over the plate and stiffener surfaces through a Fourier series expansion. Thus, by using sufficiently terms in the series, relatively complex deflection shapes can be described.

The set of algebraic non-linear equilibrium equations are derived based on energy principles and solved using an incremental numerical perturbation scheme with arc length control. The von Mises yield strength in hot spot locations is controlled against the material yield condition for each load step and used as an indicator for when the ultimate strength is reached.

Taking the non-linear plate theory due to Marguerre, the kinematic and compatibility equations for plates including geometrical imperfections i.e the membrane strain-displacement relations are as follows:

$$\varepsilon_{11} = u_{1,1} + \frac{1}{2} w^2_{,1} + w_{,1} w_{0,1} \quad (43)$$

$$\varepsilon_{22} = u_{2,2} + \frac{1}{2} w^2_{,2} + w_{,2} w_{0,2} \quad (44)$$

$$\varepsilon_{33} = \frac{1}{2} (u_{1,2} + u_{2,1}) + \frac{1}{2} (w_{,1} w_{,2} + w_{,1} w_{0,2} + w_{,2} w_{0,1}) \quad (45)$$

The corresponding compatibility equation reads:

$$\nabla^4 F = E [w^2_{,12} - w_{,11} w_{,22} + 2 w_{0,12} w_{,12} - w_{0,11} w_{,22} - w_{0,22} w_{,11}] \quad (46)$$

where:

ε : Membrane strain tensor

$u_{\alpha,\beta}$: In – plane displacement gradients

$w_{,\alpha}$, $w_{,\alpha\beta}$, $w_{0,\alpha}$, $w_{0,\alpha\beta}$: Additional and initial out – of plane plate deflection gradients

F : Airy's stress function

The equilibrium equations are derived using energy principles. Taking the Virtual work principle on total form as:

$$\int_V \sigma_{\alpha\beta} \delta \varepsilon_{\alpha\beta} = \delta E \quad (47)$$

Where the left side represents the internal virtual work over the volume V , and the right side represents the external virtual work done by the external forces. For derivation of the equilibrium equations on incremental form (1th order of perturbation rate) the virtual work equation is derived as follows, where the dot over the symbol represent the incremental properties:

$$\int_V \dot{\sigma}_{\alpha\beta} \delta \varepsilon_{\alpha\beta} + \int_V \sigma_{\alpha\beta} \delta \dot{\varepsilon}_{\alpha\beta} = \delta \dot{E} \quad (48)$$

The lateral buckling deflection w due to the applied loads and initial stress-free geometrical imperfections w_0 are discretized by the Rayleigh-Ritz semi-analytical approach by a double Fourier series:

$$w = q_i f_i(x_1, x_2) = \sum_m \sum_n A_{mn} \sin\left(\frac{m\pi}{a} x_1\right) \sin\left(\frac{n\pi}{b} x_2\right) \quad (49)$$

$$w_0 = q_{i0} f_i(x_1, x_2) = \sum_m \sum_n A_{mn}^0 \sin\left(\frac{m\pi}{a} x_1\right) \sin\left(\frac{n\pi}{b} x_2\right) \quad (50)$$

The set of unknown Fourier parameters A_{mn} , A_{mn}^0 are given in single subscript notation where i and j runs from 1 to the total number of degrees of freedom N . Therefore, the deflection coefficient parameters A_{mn} with respect to the arc length variable η are the unknown parameters.

The final set of first order linear algebraic equations is compactly written as follows:

$$K_{ij} \dot{q}_j + G_{i\Lambda} \dot{\Lambda} = 0 \quad (51)$$

$$\dot{q}_i \dot{q}_i + \dot{\Lambda}^2 = 1 \quad (52)$$

where:

\mathbf{K}_{ij} : State dependent geometrical stiffness matrix

$\mathbf{G}_{i\Lambda}$: Incremental load vector – plane displacement gradients

\dot{q}_i : Deflection coefficient

$\dot{\Lambda}$: Load rate

The first order perturbation expansion, Eq. 51, provides a linearized set of N equations with $N+1$ unknown: N deflection parameters plus one load parameter. The additional equation, Eq. 52, is based on the definition of the arc length parameter which gives a single quadratic equation in the unknown coefficients.

In order to solve the equilibrium equations, the deflections and the load parameter in the state $s+1$ are expressed as a Taylor series expanded around the state s :

$$q_{1,s+1} = A_{11,s+1} = A_{11,s} + \dot{A}_{11,s} \Delta\eta + \dots \quad (53)$$

$$q_{2,s+1} = A_{12,s+1} = A_{12,s} + \dot{A}_{12,s} \Delta\eta + \dots \quad (54)$$

$$\vdots$$

$$\Lambda_{s+1} = \Lambda_s + \dot{\Lambda}_s \Delta\eta + \dots \quad (55)$$

where:

s : General state

$s + 1$: Next neighbouring state

$\Delta\eta$: Incremental prescribed arc length parameter between two states

The parameters \dot{A}_{ij} and $\dot{\Lambda}$ in the state s are directly used for finding deflections and loads for the next state $s + 1$. Moreover, in the perturbation expansion only the first order coefficients are used since the assumed incremental perturbation $\Delta\eta$ is very small. Generally, $\Delta\eta \approx 0.01$ gives sufficiently accurate solutions for practical applications implying a range from 50 to 100 steps to reach the ultimate capacity.

The algorithm described by the previous equations is schematically presented in Figure. 37:

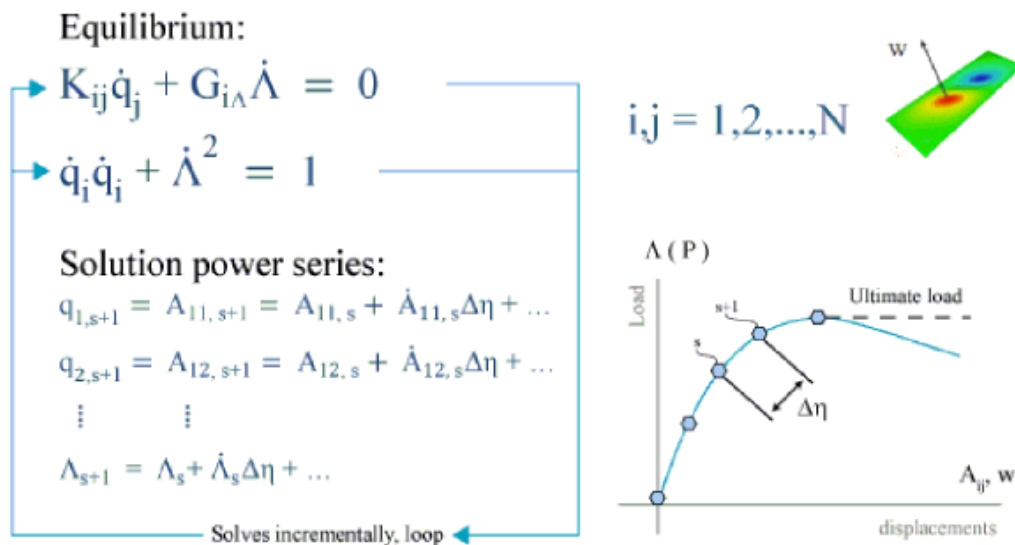


Figure 37: Incremental solution algorithm stepping a non-linear equilibrium path [6]

In order to determine the ultimate capacity of the structural member, the redistributed stress pattern is checked against von Mises yield criterion in six critical locations inside the element and along the edges as shown in Fig. 38. The redistributed stress pattern consists of the external applied stresses added to the second order stress distribution due to elastic buckling and due to the presence of geometrical imperfections. The evaluation of yielding is based on mid-plane membrane stress of each individual component. Thus, bending stresses across plate thickness are not included in the limit state yield criteria.

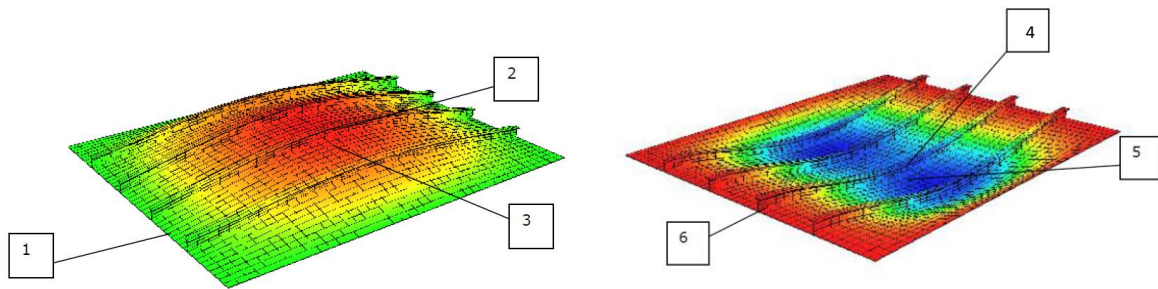


Figure 38: Stress control points for ultimate capacity assessment [1]

- **1, Plate edges:** Stress control along the supported edges.
- **2, Stiffener flange in tension:** Stress control at the stiffener midspan when the global panel deflects upwards.
- **3, Plate midspan in compression:** Stress control at plate midspan when the global panel deflects upwards.
- **4, Stiffener flange in compression:** Stress control at the stiffener midspan when the global panel deflects downwards.
- **5, Plate midspan in tension:** Stress control at plate midspan when the global panel deflects downwards.
- **4, Stiffener bending stress at support:** Stress control at the support of the stiffeners.

When yielding is reached, the incremental loading is stopped and the corresponding load is defined as ultimate capacity. By using this approach, the ultimate capacity for thin-walled structures is expected to be on the conservative side, hence some more capacity may be expected at the expense of some plastic redistribution of stresses.

In addition, the ideal elastic buckling stress (eigenvalue) and the corresponding eigenmode are calculated as described in section 2.2.1 by a linear elastic analysis considering the element with a perfect flat geometry. For the case of the unstiffened plate, there is a single elastic buckling stress while for the stiffened panel is split into Local Buckling (LEB) and Global Buckling (GEB).

In summary, results of the previous formulation are in terms of stresses and deflections, hence it is not very practical for rules checking purposes. To do so, the ultimate capacity factor Λ_u , which is itself a measure of the safety margin against collapse, is used to present the results as a single parameter: the utilization or usage factor η .

The factor is derived by:

$$\eta = \frac{1}{\Lambda_u} = \frac{\sqrt{\sigma_{10}^2 + \sigma_{20}^2 + \sigma_{30}^2}}{\sqrt{\sigma_{1U}^2 + \sigma_{2U}^2 + \sigma_{3U}^2}} \quad (56)$$

The concept of this factor is to give an intuitive idea of how far the structural element is operating from its ultimate load. This is illustrated in Fig. 39 with an UC failure surface for the 3D load space $(\sigma_1, \sigma_2, \sigma_3)$ which defines the strength of the element for different load combinations.

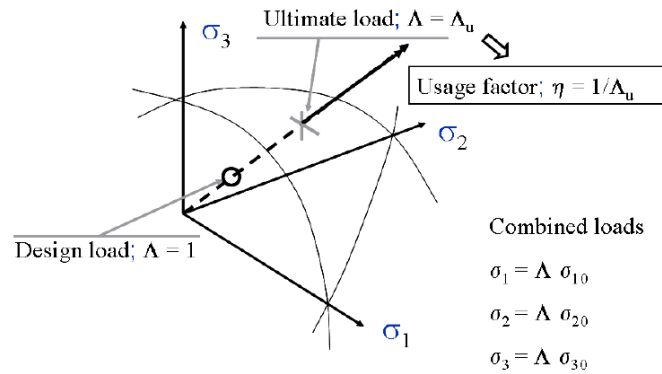


Figure 39: Ultimate capacity surface in load space [6]

In order to be approved by PULS, the element shall remain within the volume defined by the surface under the design loads, that is to operate with a usage factor lower than 1.

6.2.2 Buckling modes for stiffened panels

For the analysis of stiffened panels PULS splits the calculation procedure into two modes: Global and Local.

For the *local level*, the eigenvalue is assessed for the isolated component plates considering a perfect flat geometry. Then, the buckling mode is used to set initial deflections and the post-buckling strength is derived.

In addition, orthotropic macro coefficients representing in-plane and out-of-plane stiffness are derived. These coefficients are used in the global model to account for the effect of buckling in local components. The approach is based on a six-dimensional orthotropic macro material law given by Eq. 57 in an incremental relation between in-plane loads N_i , Moments M_i and the corresponding strains ε_i and curvatures κ_i in the plating:

$$\begin{bmatrix} \Delta N_1 \\ \Delta N_2 \\ \Delta N_3 \\ \Delta M_1 \\ \Delta M_2 \\ \Delta M_3 \end{bmatrix} = \begin{bmatrix} C_{11} & C_{12} & C_{13} & Q_{11} & Q_{12} & Q_{13} \\ C_{21} & C_{22} & C_{23} & Q_{21} & Q_{22} & Q_{23} \\ C_{31} & C_{32} & C_{33} & Q_{31} & Q_{32} & Q_{33} \\ Q_{11} & Q_{21} & Q_{31} & D_{11} & D_{12} & D_{13} \\ Q_{12} & Q_{22} & Q_{32} & D_{21} & D_{22} & D_{23} \\ Q_{13} & Q_{23} & Q_{33} & D_{31} & D_{32} & D_{33} \end{bmatrix} \begin{bmatrix} \Delta \varepsilon_1 \\ \Delta \varepsilon_2 \\ \Delta \varepsilon_3 \\ \Delta \kappa_1 \\ \Delta \kappa_2 \\ \Delta \kappa_3 \end{bmatrix} \quad (57)$$

where:

C_{ij} : In – plane stiffness

D_{ij} : Torsional stiffness

Q_{ij} : Interaction of in – plane and torsional stiffness

The previous stiffness components are decomposed into linear and non-linear terms. The non-linear term accounts for the drop of in-plane stiffness when an element undergoes local buckling.

For the *global level*, the stiffened panel is assessed using the classical orthotropic plate theory with modified orthotropic macro material coefficients accounting for the local buckling effects. By this way, the interaction between local and global modes is accounted for.

The calculation procedure is similar to the local level. First, the eigenvalue is assessed disregarding initial deflections. Then, the buckling mode is used to set initial deflections and the post-buckling strength is derived.

6.2.3 Boundary conditions

The most common type of boundary conditions assumed regarding buckling and ultimate capacity strength assessment are described in more detail in section 2.3. In this section is defined how PULS considers the boundary conditions for unstiffened plates and stiffened panels:

- **Out-of-plane support:** the out-of-plane support along the outer edges is assumed to be rigid in the lateral direction while free to rotate for the unstiffened plate. This corresponds to the classical simply supported boundary conditions.

For the stiffened panel, all four edges are considered as simply supported for the global buckling mode. For the local model, the longitudinal edges are elastically restrained as along the primary stiffeners while the transverse edges are simply supported.

- **In-plane support:** The in-plane support along the outer edges is constrained to remain straight but movable in-plane. With respect to stiffened panels, the rotational restraint of the plate within the panel is determined by the influence of the stiffener. With this assumption, PULS assume the elements to be integrated in laterally rigid structures.

By taking the previous assumptions with respect to the boundaries of the element, PULS assume the element to be integrated in laterally rigid structures such as frames or bulkheads in ship structure. However, it should be noted that this effect is just accounted with respect the in-plane support. The out-of-plane support is simply supported which means there is no rotational constraint from the surrounding elements

6.2.4 Initial imperfections

PULS set by default model tolerances according to normal fabrication standards of welded integrated structures used in shipbuilding and offshore industry. For the unstiffened plate there is only one model tolerance amplitude δ_{p0} corresponding to the maximum initial plate amplitude and set by default as $s/200$ where s is the stiffener spacing.

For the stiffened panel there are three imperfection amplitudes δ_{p0} , δ_{s0} and δ_{t0} as presented in Figure 40. Amplitude δ_{t0} corresponds to the displacement of the stiffener and δ_{s0} to the vertical deflection of the stiffener coming from the global eigenmode. Both amplitudes are set by default as Plate length/1000.

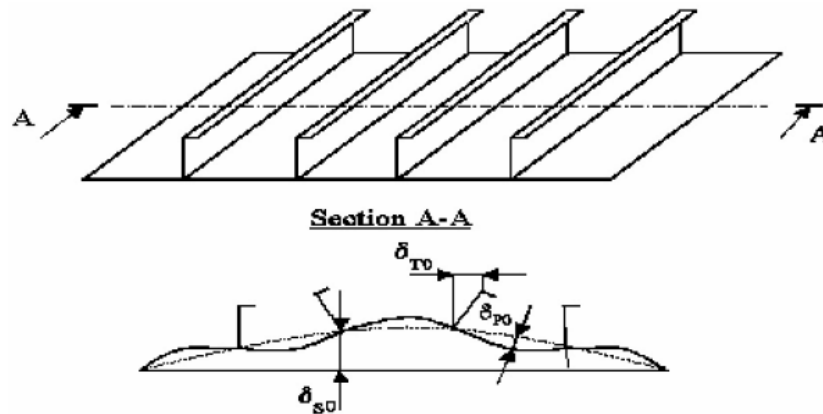


Figure 40: Definition of geometrical imperfections [1]

The imperfection shape cannot be controlled by the user, it is automatically taken by combining local and global eigenmodes and applying the previously defined amplitudes.

6.2.5 Design Principles

In this section are defined the design principles the elements are based in order to set the cut-off values in terms of strength. By considering an ULS design approach, the following principles apply:

- i. **Elastic local buckling of components is accepted**
- ii. **Permanent buckles are not accepted**
- iii. **Global (Overall) buckling of the panel is not accepted**

By ensuring the maximum membrane stress in the element to stay below the yield stress, excessive permanent deformations and buckles are prevented. This responds to the capacity of plates to sustain further loading in the elastic regime, even if in-plane stiffness decreases significantly after the inception of buckling. However, when the element undergoes buckling in the inelastic regime, significant residual strength is not expected.

In addition, given that the overall buckling stiffened panel is considered as a significant instability, it is not accepted to take place. By this constraint, it is ensured that the panel has sufficient out-of-plane bending stiffness to avoid this deformation mode.

In summary, the ULS approach allows the element to undergo deflection in the elastic buckling regime while preventing excessive permanent damages. This principle constrains the elements to have minimum stiffness properties for an efficient load transfer. It also helps to improve the performance of the structure by saving weight. In terms of loads, ULS for ship and offshore structures corresponds to designing the structure for the largest loading that may be experienced in a typical period of 25 years.

In contrast, in some cases it may not be acceptable that the structural element undergoes elastic buckling and thereby large deflections. This corresponds to a Serviceability approach (SLS) which implements the elastic buckling stress as an upper limit of allowable loading. In terms of element thickness and proportions, this means that they are to be increased as compared to the previous ULS approach. This represents a useful approach for heavy members such as frames, girders or bulkheads since it ensures a robust design with additional margins to take additional redistributed loads coming from the previous approach of accepting elastic buckling in surrounding structures.

6.3 Non-linear Finite Element Method

This method represents the “state of the art” becoming the most powerful and accurate approach for assessing buckling and ultimate capacity strength. Its power arises from the possibility of including the following non-linear basic effects:

- i. Non-linear geometrical behaviour
- ii. Non-linear and inelastic material behaviour
- iii. Contact
- iv. Fracture

According to DNV-GL [6], for buckling and ultimate strength assessment of ship structures, non-linear material and geometrical behaviour are always to be included while contact and fracture are normally not relevant for this analysis.

Another of the very powerful capabilities of this approach is the possibility to handle very complex geometries that cannot be solved in an analytical manner.

In addition, providing an adequate extension of the model such several frame spacings or even cargo holds, it is possible to account for complicated effects and interactions that are generally not considered when considering small isolated sections of the structure.

However, the main drawback is the requirement of large computational effort due to the large number of unknowns and numerical integration procedures such as obtaining the non-linear stiffness matrices for the element as it deforms. That is why it is not a practical approach for design purposes and tends to be reserved to research focus activities.

6.3.1 Non-linear geometrical behaviour

This effect arises from the large deflections and changes in the geometry of the structure due to external loading. This leads to a non-linear relation between load and deflection when deflection becomes large enough in comparison with the structure dimensions.

For a compressive load acting on a plate, the effect is pronounced already for deflections of the order of half the plate thickness. This effect is most pronounced for slender structures where large deflections will be present before the material non-linearity starts [6].

6.3.2 Non-linear material behaviour

This effect is associated with the inelastic behaviour of the material. For low strain values the behaviour of most metals is considered as linear, but when yielding in the material takes place the relationship between stress and strain becomes non-linear.

With respect to metallic materials, it is usually characterized by:

-*Stress-strain curve*: It can be approximated as a multi-linear curve. For steels with a marked yield plateau a bi-linear approach is usually considered with a low plastic tangent module ($E_t = 1000 \text{ MPa}$) as illustrated in Fig. 41 or as a perfect elastic-plastic curve ($E_t = 0$). For buckling analysis the strains are small and distinction between engineering strain and true strain are negligible. [6]

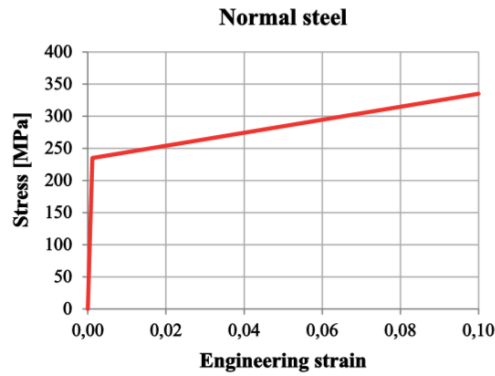


Figure 41: Bi-linear idealization of non-linear material behaviour [6]

-*Yield criteria for metallic materials*: The von Mises yield criterion is accepted and widely used for all metallic materials. It allows to represent an arbitrary multi-axial stress state as a single stress value which is used to predict yielding in the material. The von Mises stress is derived as follows:

$$\sigma_{VM} = \sqrt{\sigma_x^2 + \sigma_y^2 - \sigma_x \sigma_y + 3\tau^2} \quad (58)$$

-*A hardening model* (isotropic or kinematic): It describes how the yield condition varies when stresses reach and undergo yielding. The most used models are isotropic and kinematic hardening models.

6.4 Comparison between presented methods

PULS and CFM are partly supplementary. Both approaches cover uni-axially stiffened panels and unstiffened plates, while CFM also covers pillars, beams, web plates with cut-outs and curved shells. PULS covers orthogonally stiffened panels, irregular stiffened panels and corrugated panels.

The main difference between PULS and CFM is that PULS applies non-linear plate theory and thus additional information is available with respect to the structural behaviour of the element. That provides a better insight and understanding on the failure mechanism in terms of weakest failure modes or stress redistribution supported by a 3D graphical representation. In contrast, CFM presents the results as a single parameter with no insight or additional information with respect to the behaviour of the element. In addition, PULS provides an integrated check of all the failure modes and load shedding for the stiffened panel while for CFM different elements such as the plate, the stiffener and the overall stiffened panel capacity have to be assessed separately.

The NFEM approach provides a direct assessment of the structural behaviour considering both material and geometrical non-linearities. Other complex behaviours which cannot be analysed by analytical methods such as complicated geometries or interactions due to the extension of the model can be included. Due to the increased accuracy of the results, class societies such as DNV-GL considers the acceptance criteria and partial safety factors in strength on a case by case [6]. That means that reduced safety factors may be applied in comparison with rule-based designs leading to an optimization of the design.

In summary, from least to most accurate it is found CFM, PULS, and NFEM. Their use and applicability are mainly restricted to the design stage they are to be applied. For initial design stages, CFM may be useful to perform an initial assessment of the buckling and ultimate strength of the structure. Then, for more advanced design stages PULS and NFEM can provide a better insight on the actual failure mode and mechanism of the structure. NFEM will provide the most accurate results but at a significant higher computational cost. In addition, the results must be carefully checked and verified since different sources of errors may appear from inappropriate modelling or wrong input data.

7. NUMERICAL ANALYSIS

This section presents the analysis of the selected configurations defined in section 5.3 as well as an enhanced model for the stiffened panels. This enhancement consists in six stiffened panels which surrounds the studied panel in order to account for the effects of heavy members on boundary conditions as defined in Table 4. The studied configurations are summarized below:

	Plate
	Thickness [mm]
Unstiffened Plate 1	6
Unstiffened Plate 2	12
Unstiffened Plate 3	15.5

Table 3: Summary of unstiffened plate configurations

	PLATE	STIFFENER		HEAVY MEMBER			
	Thickness [mm]	Height [mm]	Thickness [mm]	Web Height [mm]	Web Thickness [mm]	Flange Width [mm]	Flange Thickness [mm]
Stiff. Panel 1	6	100	6	235	7	100	12
Stiff. Panel 2	12	140	8	485	10	150	15
Stiff. Panel 3	15.5	240	10	640	10	150	15

Table 4: Summary of stiffened panel configurations

The aim of the analysis is to perform a buckling and ultimate strength assessment of the selected configurations comparing the results obtained by NFEM and results delivered by PULS.

The first part consists in the derivation of boundary conditions to represent the actual behaviour of the structure and a convergence study to select an accurate mesh size to perform the analysis.

Afterwards, a linear eigenvalue buckling analysis is carried out to compare the elastic buckling stress obtained from numerical methods (FEM), semi-analytical methods (PULS) and analytical formulation when available depending on the structure considered.

Then, the ultimate capacity of the structures is computed based on a non-linear analysis including material and geometrical non-linearities. The initial deflections in the structure are introduced based in the eigenmodes obtained from the linear eigenvalue analysis.

7.1 Material properties and behaviour

The material properties considered throughout the analysis are presented below:

- Structural steel (mild-high tensile steel) A36
- Yield strength, $\sigma_y = 355 \text{ MPa}$
- Young's Modulus, $E = 200000 \text{ MPa}$
- Poisson's ratio, $\nu = 0.3$

With respect to the non-linear analysis, the material behaviour is characterized as illustrated in Fig. 42 according to DNV-GL rules [6] as Bilinear Isotropic hardening as following:

- Plastic tangent modulus: $E_T = 1000 \text{ MPa}$

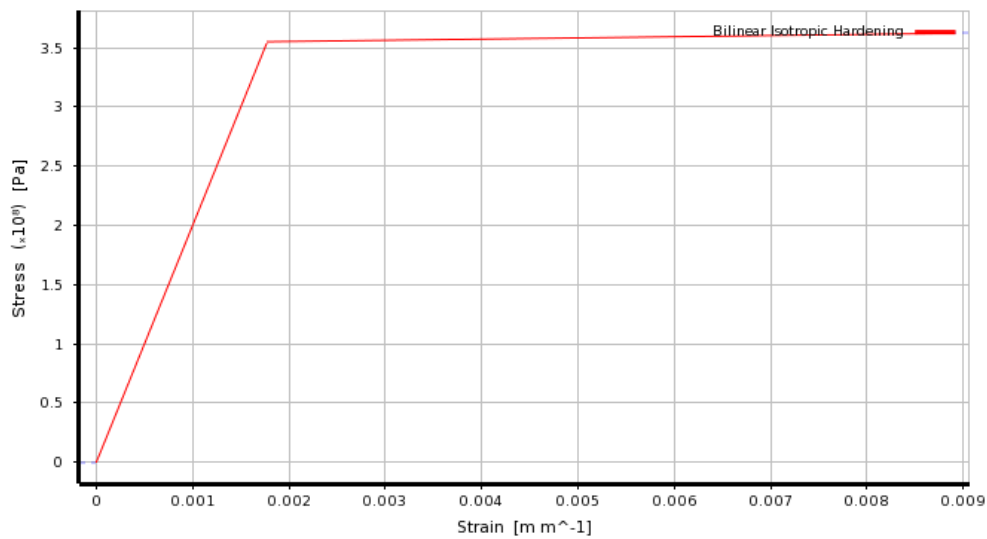


Figure 42: Non-linear material behaviour used in the analysis

7.2 Boundary conditions

The boundary conditions to constrain the structures are taken as follows:

- **Out-of-plane support:** Simply supported for all four edges. Rigid in lateral directions while free to rotate. Mainly affect the elastic buckling stress (eigenvalue).
- **In-plane support:** Outer edges constrained to remain straight but movable in-plane. Have influence in the post-buckling behaviour and so in the ultimate capacity of the structure.

This corresponds to the most common assumption regarding buckling and ultimate capacity strength assessment. In fact, this is the approach PULS implement in the computation code. Thus, same boundary conditions are reproduced in the numerical analysis to have a consistent comparison.

To implement these boundary conditions a coupled behaviour is introduced at the edges of the model in the proper degrees of freedom as illustrated in Figures 43, 44 and 45. By this way the edges are constrained to remain straight.

The stiffeners are constrained so they remain in-plane at the edges representing the joint with the frames or girders. For the enhanced model, just the outer edges are constrained, the inner elements are free to deform in order to capture the influence of the heavy members in the stiffened panel.

For unstiffened plate:

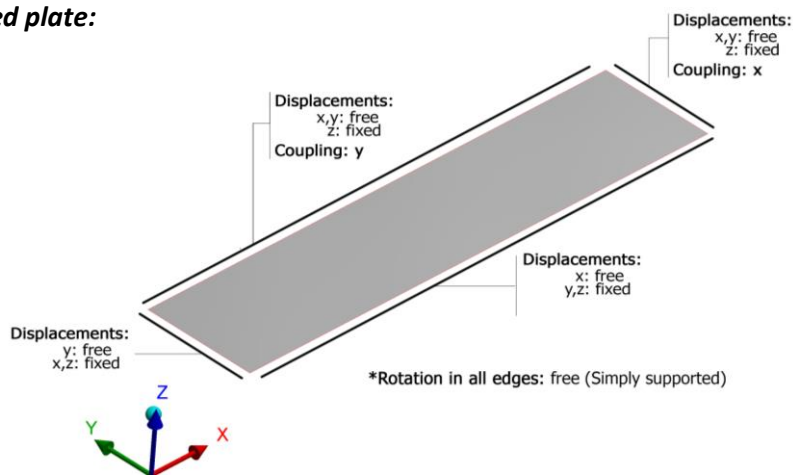


Figure 43: Boundary conditions and coupling applied in unstiffened plate model

For stiffened panel:

*The annotations pointing to one single stiffener apply to all the stiffeners on that edge of the panel

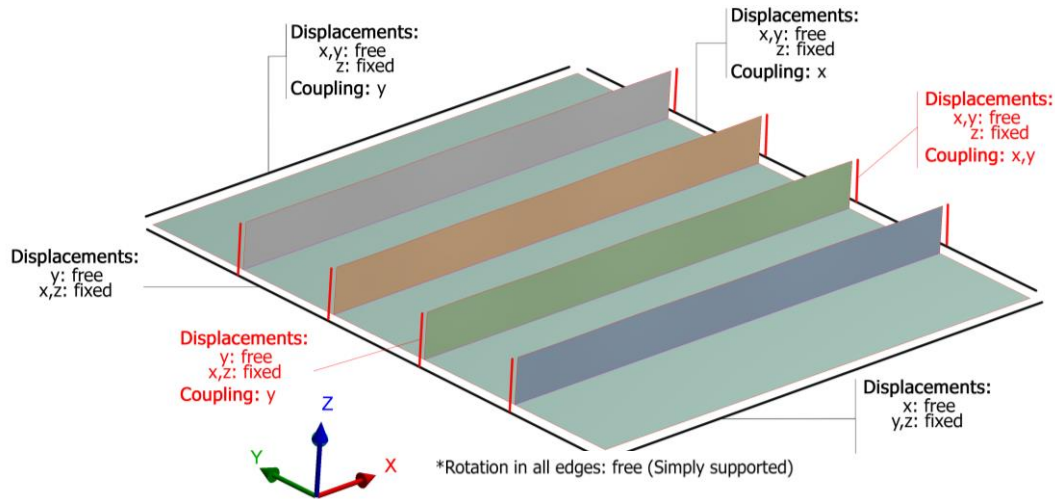


Figure 44: Boundary conditions and coupling applied in stiffened panel model

For enhanced model:

*The annotations pointing to one single stiffener or heavy member apply to all the stiffening members on that edge of the model.

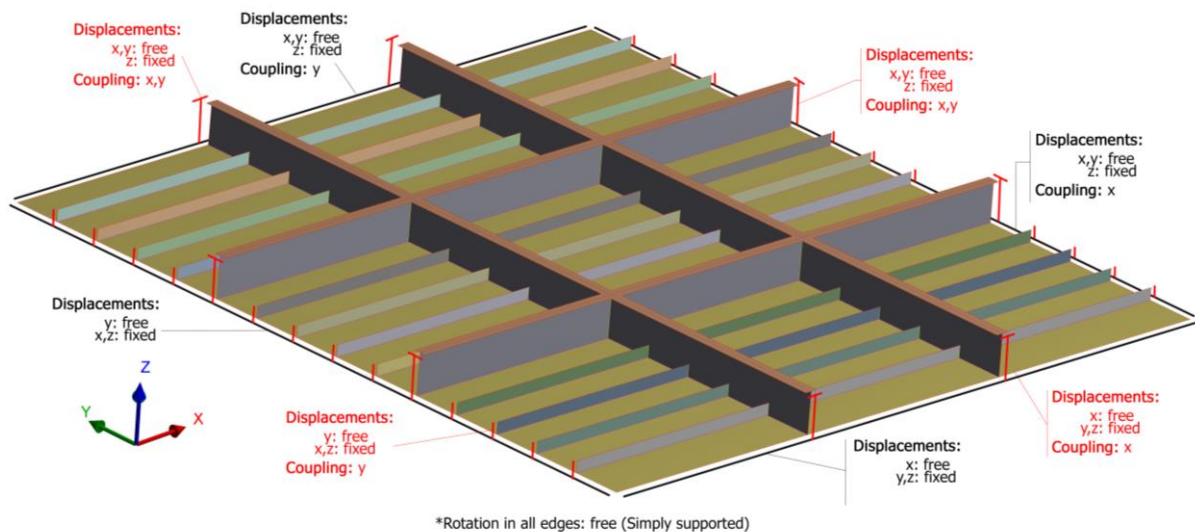


Figure 45: Boundary conditions and coupling applied in enhanced model

7.3 Convergence study

This section presents a convergence study for both elements, unstiffened plates and stiffened panels. The aim is to ensure that results obtained from numerical calculations are consistent with analytical formulations and a mesh refinement produce a negligible change in the solution considering thus that the result has converged.

The study is performed for the structures more sensitive in buckling which are the unstiffened plate and stiffened panel with 6mm plate thickness.

In addition, since the buckling eigenmode is to be used to introduce initial imperfections, the variation of the buckling eigenmode according to the mesh size is also studied to ensure an accurate representation with respect theoretical background.

In further sections, the term failing or applied load refers to the load for which PULS considers the panel to have failed either due to buckling or UC.

Finally, a mesh size of 50mm is selected representing a good compromise between computation effort and accuracy in the results. In this section just the results for this mesh size are presented to avoid an overloading of this section. The complete convergence study including results from other mesh sizes is available in Annex 11.1.

7.3.1 Elastic buckling stress and buckling factor

For unstiffened plates, the analytical elastic buckling stress σ_E is derived by Eq. 11. Then, combining Eq. 11 and 15, the buckling factor k for unstiffened plates is obtained as:

$$k = \sigma_E \frac{D \pi^2}{b^2 t} \quad (59)$$

Taking into account the elements are simply supported, analytical formulation delivers the following results for unstiffened plates:

	PLATE 1 - 6mm			PLATE 4 - 12 mm			PLATE 6 - 15.5 mm		
	Longitudinal	Transverse	Combined	Longitudinal	Transverse	Combined	Longitudinal	Transverse	Combined
Elastic Buckling stress [MPa]	73,11	19,91	18,97	292,44	79,62	75,88	487,91	132,84	126,59
Buckling factor	4,04	1,10	-	4,04	1,10	-	4,04	1,10	-

Table 5: Analytical solutions for elastic buckling stress and buckling factor for unstiffened plates

With respect to the numerical analysis, the elastic buckling stress is derived based in the Load Multiplier obtained from the FEM computation as:

$$\sigma_E = \lambda \sigma_{applied} \quad (60)$$

where:

λ : Load multiplier

$\sigma_{applied}$: Load for which PULS considers the element to have failed

The results obtained for the *unstiffened plate* of 6mm thickness and final mesh size of 50 mm are presented in Table 6. It is observed that for all loading cases, the load multiplier is very close to one, indicating thus the beginning of elastic buckling.

The elastic buckling stress is obtained with a good accuracy with respect to the analytical solutions with a maximum variation of 0.7%. Moreover, the solution presents a good convergence state with a maximum variation of 1% with respect to the previous solution with a mesh size of 75 mm.

	Mesh size of 50 [mm]		
	Longitudinal	Transversal	Biaxial
Applied load [MPa]	73	19.9	18.9
N° of elements	648	648	648
Half-waves of Buckl. Mode	5	1	1
1st mode Load multiplier	1.0106	1.0104	1.0141
Elastic Buckling stress	73.77	20.11	19.17
<i>Variation with resp. Prev. Solution</i>	0.98%	0.27%	0.26%
<i>Variation with resp. Analytical sol.</i>	0.66%	0.20%	0.20%
Buckling coefficient	4.0813	1.1123	1.0603
<i>Variation with resp. Prev. Solution</i>	0.05%	0.02%	0.01%
<i>Variation with resp. Analytical sol.</i>	0.04%	0.03%	-

Table 6: Results summary for unstiffened plate of 6 mm plate thickness with 50 mm mesh size

The convergence of elastic buckling stress for the different loading cases is presented in Fig. 46 for longitudinal loading and Fig. 47 for transversal and biaxial loading.

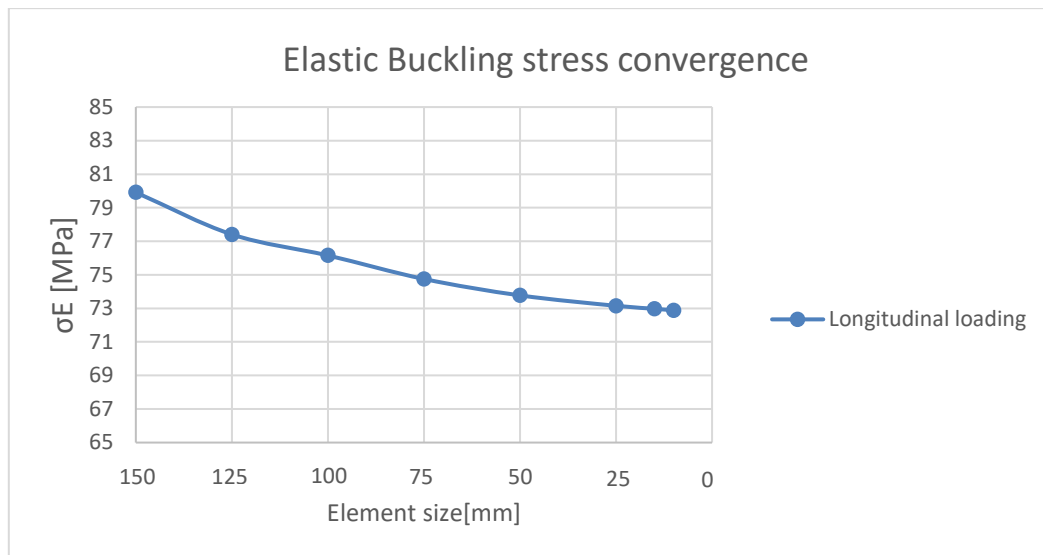


Figure 46: Elastic Buckling stress convergence unstiffened plate of 6 mm thickness under longitudinal loading

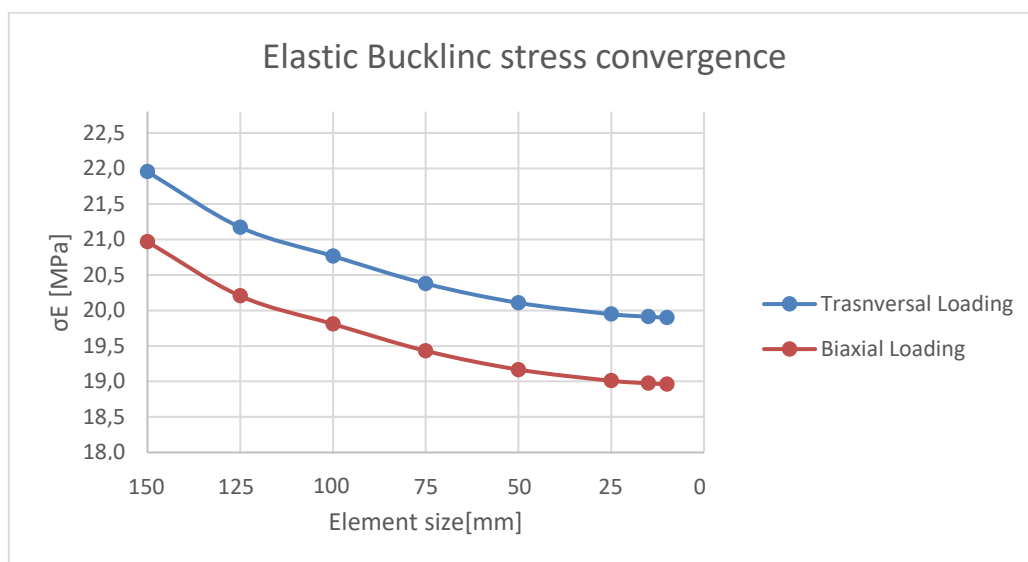


Figure 47: Elastic Buckling stress convergence for unstiffened plate of 6 mm thickness under transversal and biaxial loading

In general, both loading situations present a fast convergence trend. For the longitudinal case there is a maximum variation of 7 MPa between the coarsest and the finest mesh while for the transversal and biaxial loading case is around 2 MPa.

The results obtained for the *stiffened panel* of 6mm plate thickness and final mesh size of 50 mm are presented in Table 7. For these configurations just the numerical computation is considered due to the lack of analytical formulations. It is observed that for all loading cases, the elastic buckling stress presents a good convergence state with a maximum variation of 1,15% with respect to the previous solution performed with a mesh size of 75 mm.

	Mesh size of 50 [mm]		
	Longitudinal	Transversal	Biaxial
STIFFENED PANEL 1 (6mm)			
Applied Load [MPa]	79	20.25	19.25
N° of elements	3888	3888	3888
Half-waves of Buckl. Mode	5	1	1
1st mode Load multiplier	0.9900	1.0079	1.0097
Elastic Buckling stress [MPa]	78.21	20.41	19.44
Variation with resp. Prev. Solution	1.15%	0.28%	0.30%

Table 7: Results summary for stiffened panel of 6 mm plate thickness with 50 mm mesh size

The convergence of elastic buckling stress for the different loading cases is presented in Fig. 48 for longitudinal loading and Fig. 49 for transversal and biaxial loading.

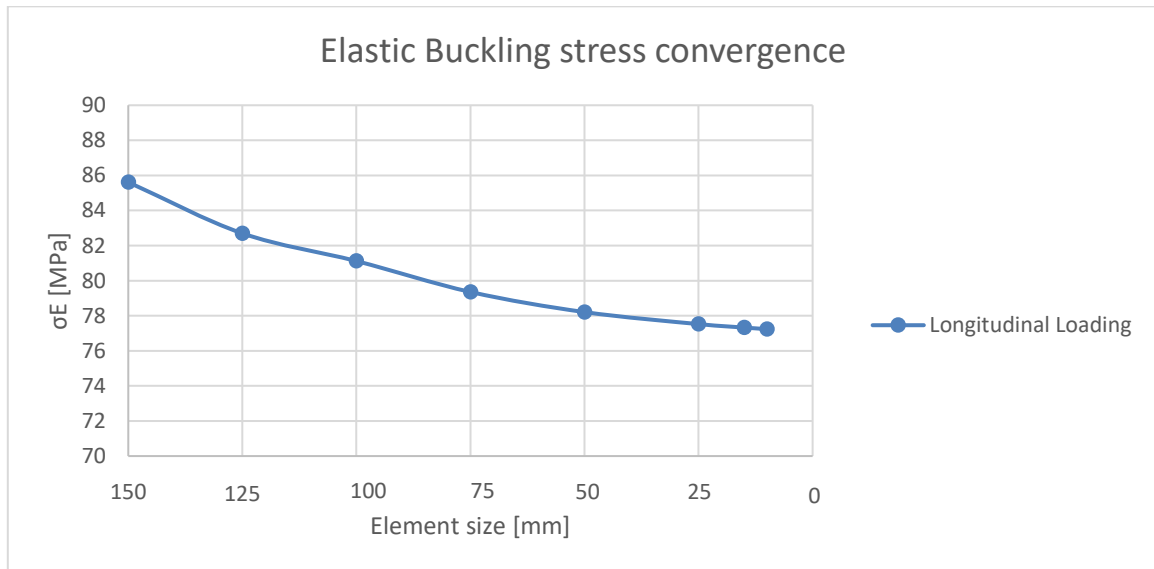


Figure 48: Elastic Buckling stress convergence for stiffened panel of 6 mm plate thickness under longitudinal loading

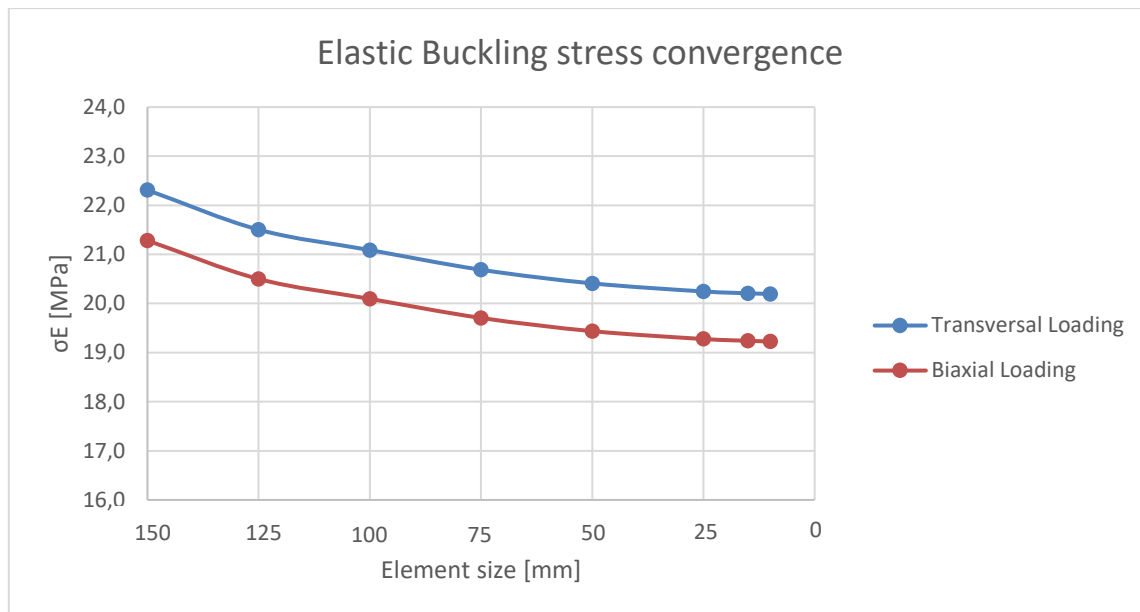


Figure 49: Elastic Buckling stress convergence for stiffened panel of 6mm plate thickness under transversal and biaxial loading

In the same way that unstiffened plates, stiffened panels also present a fast convergence trend. For the longitudinal case there is a maximum variation of 8 MPa between coarsest and the finest mesh while for the transversal and biaxial loading case is around 2 MPa.

In summary, the elastic buckling stress presents a fast convergence for unstiffened plates and stiffened panels. For both configurations, it can be considered that with a mesh size of 50 mm, the result converges to a reasonable level of accuracy. For the unstiffened plate there is a variation of 1% with respect to the previous mesh size of 75 mm, and a variation of 0.6% with respect to the analytical solution. Likewise, for the stiffened panel there is a variation of 1.15% with respect to the previous solution.

It could be argued that a bigger mesh could still lead to a good accuracy level saving some computational effort. However, another parameter should be considered in order to select the mesh which is the representation of the eigenmode since it is the way to introduce the initial imperfections for the non-linear analysis. This aspect is considered in the following section justifying the selection of a 50 mm mesh size.

7.3.2 Eigenmodes

This section presents the variation of the eigenmode with respect to the mesh size. It represents an important factor in the analysis since it is the way the initial imperfections are introduced in the structures to perform the non-linear analysis.

According to analytical formulations and theoretical background provided in section 2.5, the buckling modes expected for unstiffened plates as considered for this analysis are presented in Fig. 50:

Unstiffened plate dimensions:

Length:	2700 mm
Width:	600 mm
Aspect ratio	$a/b = 4.5$

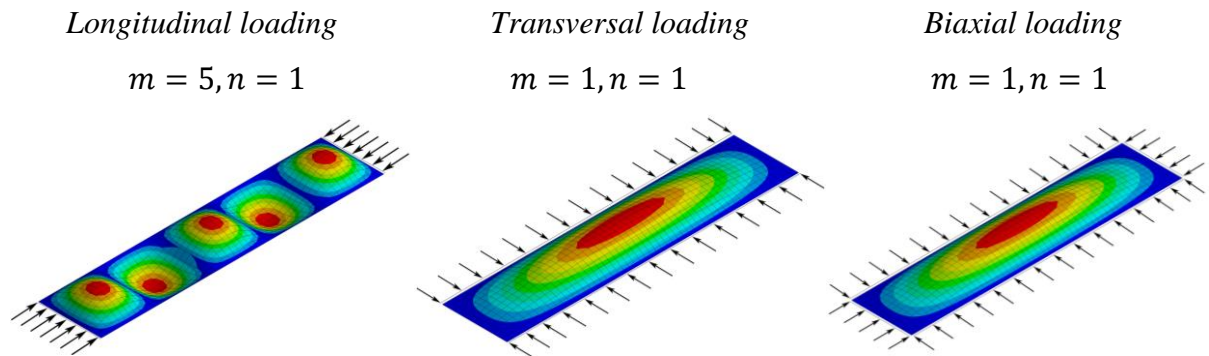


Figure 50: Buckling modes according to analytical formulation for the considered unstiffened plate

It is observed how for the longitudinal loading case, five half-waves are formed along the longitudinal direction while only one is formed in the transversal direction. In contrast for the transversal and biaxial (with same load applied at both edges) loading case, the buckling mode present one half-wave in the longitudinal direction as well as transversal direction.

For the stiffened panel, the previous pattern defined by the unstiffened plate will be reproduced within the structure, in the sense that plating between stiffeners and stiffeners web will deform like previous unstiffened plate.

With the respect to the eigenmode analysis, just the longitudinal load case is shown since for transversal and biaxial loading even the coarsest mesh considered is able to reproduce the number of half-waves according to analytical background.

For the *unstiffened plate* under longitudinal loading, coarse meshes produce a non-consistent eigenmode with respect to previous analytical considerations, showing four half-waves along the plate instead of five. It is not up to a mesh size of 75 mm when the correct eigenmode is produced as illustrated in Fig. 51.

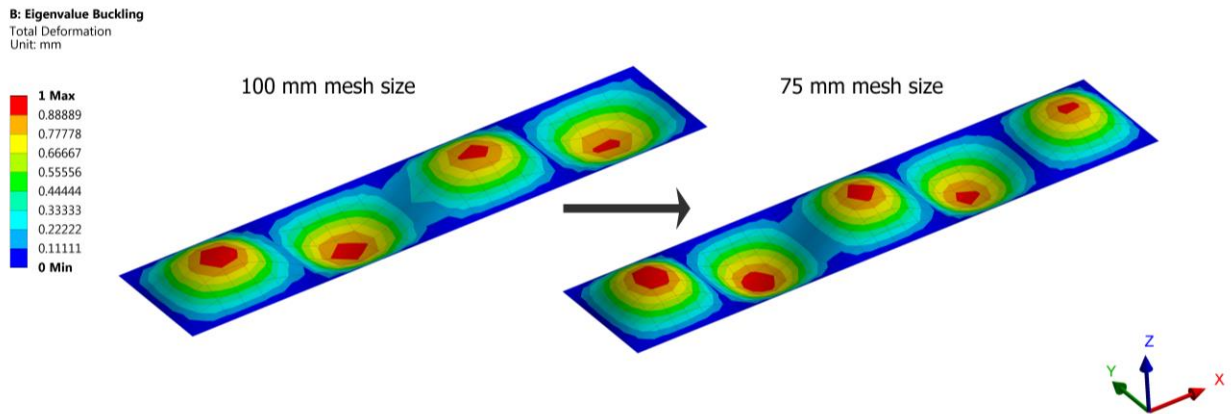


Figure 51: Threshold mesh size for a consistent representation of eigenmode under longitudinal loading for unstiffened plate of 6 mm thickness

In the same way, for *stiffened panels* under longitudinal loading, it is not up to a mesh size of 100 mm when the correct eigenmode is produced as illustrated in Fig. 52.

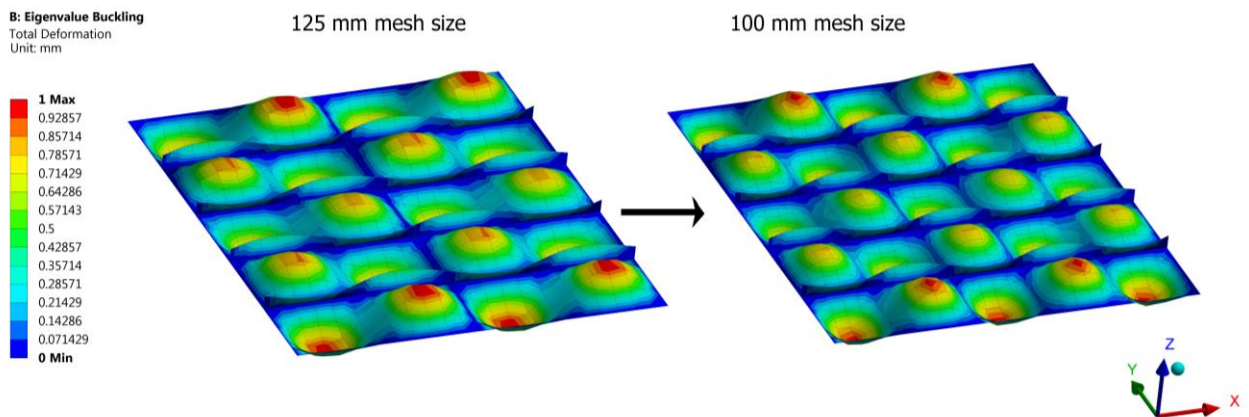


Figure 52: Threshold mesh size for a consistent representation of eigenmode under longitudinal loading for stiffened plate of 6mm plate thickness

Given the previous results, the minimum mesh size to represent a consistent buckling eigenmode for both structures is 75 mm. However, it can be observed from the previous figures that with this mesh size the shape is not smoothly represented.

Since the way the buckling eigenmode is obtained is determinant in how the imperfections are going to be introduced for the non-linear analysis, it is decided to select a mesh size of 50 mm. This size provides accurate results as present in the previous section and a smooth and consistent eigenmode representation as illustrated in Fig. 53.

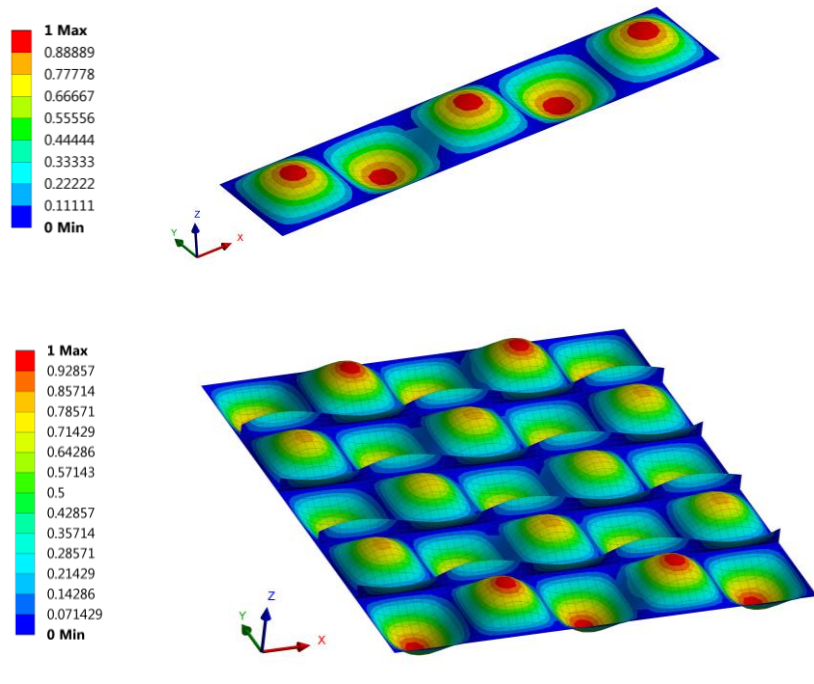


Figure 53: Longitudinal eigenmodes for unstiffened plate of 6 mm thickness (up) and stiffened panel of 6 mm plate thickness (down)

This need of such an accurate mesh size to represent consistently the buckling eigenmode is produced by the selected aspect ratio of 4,5. As illustrated in Fig.16, this value is located very close to the analytical value where the buckling mode changes from $m=4$ to $m=5$ half-waves, which corresponds to $\sqrt{20} \approx 4,47$. This leads to the need of a finer mesh to represent the correct buckling eigenmode than it would be needed with an aspect ratio of 4 or 5.

7.4 Mesh

As provided by the convergence study, the selected mesh size is 50 mm. According to DNV-GL guidelines for assessment of buckling and ultimate capacity by NFEM [6], in order to capture all relevant local buckling deformations and localized plastic behaviour the mesh in the models has the following attributes:

- More than 5 elements across plating between stiffeners
- Minimum of 3 elements across stiffener web height
- Element aspect ratio 2 or lower in critical areas susceptible to buckling
- The structural elements and areas susceptible to buckling and collapse are modelled as shell elements.

The type of element used for the analysis is a 4-node shell element.

Unstiffened Plates

	Unstiffened plates (all configurations)
Total elements	648
Elements in Long. direction	54
Elements in Transv. Direction	12

Table 8: Unstiffened plates mesh description

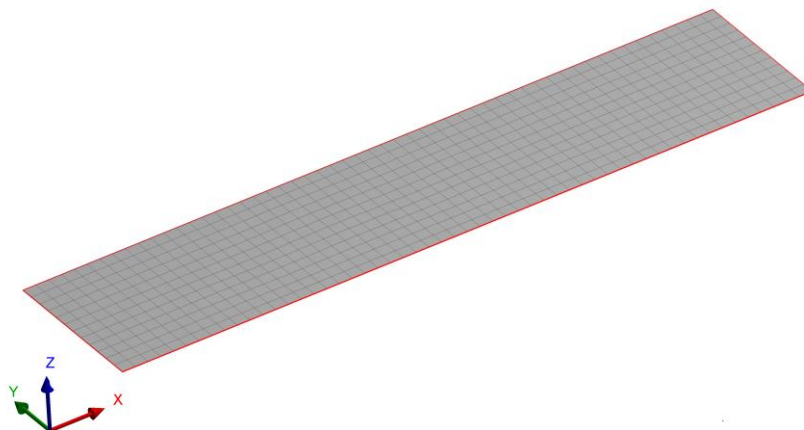


Figure 54: Unstiffened plate mesh

Stiffened Panels

	Stiff. Panel 1	Stiff. Panel 2	Stiff. Panel 3
Total elements	3888	3888	4320
Elements in Long. direction	54	54	54
Elements in Transv. Direction	60	60	60
Elements along stiffener height	3	3	5

Table 9: Stiffened panels mesh description

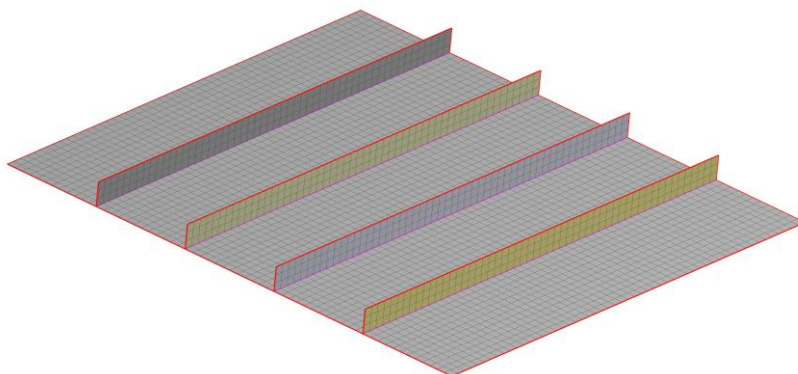


Figure 55: Stiffened panel mesh

Enhanced model

	Stiff. Panel 1	Stiff. Panel 2	Stiff. Panel 3
Total elements	41148	44568	50508
Elements in single* stiff. Panel	3888	3888	4320
Girder (individual* section)			
Elements along web length	54	54	54
Elements along web height	7	10	13
Elements along flange length	54	54	54
Elements along flange width	2	4	4
Frame(individual section)			
Elements along web length	60	60	60
Elements along web height	7	10	13
Elements along flange length	60	60	60
Elements along flange width	2	4	4

Table 10: Enhanced models mesh description

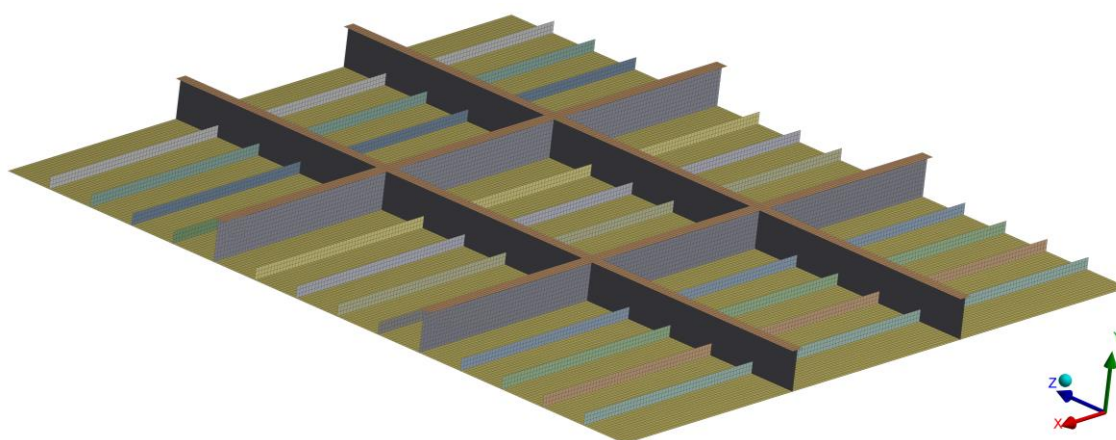


Figure 56: Enhanced model mesh

7.5 Linear Eigenvalue Buckling Analysis

This section deals with the calculation of the elastic buckling stress or eigenvalues for the different structures and comparison of results delivered from PULS, FEM and analytical formulations. The procedure and theoretical background are described in further detail in section 2.2.1.

The elastic buckling stress has not a direct relation for actual structures since they will start to buckle from the beginning of the loading instead of a sudden buckling at a critical load. However, this section aims to study the degree of accuracy of PULS with respect to FEM and analytical formulations. In addition, the obtained results (eigenmodes) of this section are used to introduce the initial imperfections for the further non-linear analysis.

Initially, the structures are modelled into PULS to obtain the failing load and the mechanism they fail by, either buckling or ultimate capacity. Then, the obtained failing load is introduced in the FEM model to obtain the load multiplier, hence the elastic buckling stress.

For the cases where the load multiplier is not close to one is because the structure is failing due to ultimate capacity. However, it can be seen that the elastic buckling stress is well predicted in comparison with analytical formulation.

The results obtained for *unstiffened plates* are presented in Table 11:

		PLATE 1 - 6mm			PLATE 2 - 12 mm			PLATE 3 - 15.5 mm		
		Long.	Transv.	Comb.	Long.	Transv.	Comb.	Long.	Transv.	Comb.
PULS	Failing Load [Mpa]	73	19,9	18,9	258	79,5	75,5	309	132,5	126
	Elast. Buckling stress	73	19,9	18,9	292	79,5	75,5	488	132,5	126
	Ultimate capacity	159	51	48	259	110	105	309	155	152
	Failure Mode	Buckling	Buckling	Buckling	UC	Buckling	Buckling	UC	Buckling	Buckling
FEM	Load multipl. Mode 1	1,011	1,010	1,014	1,139	1,010	1,014	1,582	1,010	1,013
	Elast. Buckling stress	73,77	20,11	19,17	293,94	80,33	76,57	488,71	133,88	127,61
	Margin with resp. PULS	1,05%	1,03%	1,39%	0,66%	1,03%	1,40%	0,15%	1,03%	1,26%
ANALYTICAL	Elast. Buckling stress	73,11	19,91	18,97	292,44	79,62	75,88	487,91	132,84	126,59
	Margin with resp. PULS	0,15%	0,03%	0,36%	0,15%	0,15%	0,49%	-0,02%	0,26%	0,47%
	Margin with resp. FEM	0,90%	1,00%	1,03%	0,51%	0,88%	0,91%	0,16%	0,77%	0,80%

Table 11: Comparison between results obtained for unstiffened plates

For all loading cases, the elastic buckling stress obtained by FEM computations presents a good accuracy with respect to PULS and analytical formulations. The maximum variation from analytical solution derived by FEM is about 1% while for PULS is 0.5%.

Regarding buckling eigenmodes, the results are presented in Fig. 57, with a graphical comparison between modes derived by FEM and PULS. Given that the eigenmodes for different thicknesses present very similar shapes, just the configuration with 12 mm thickness is presented.

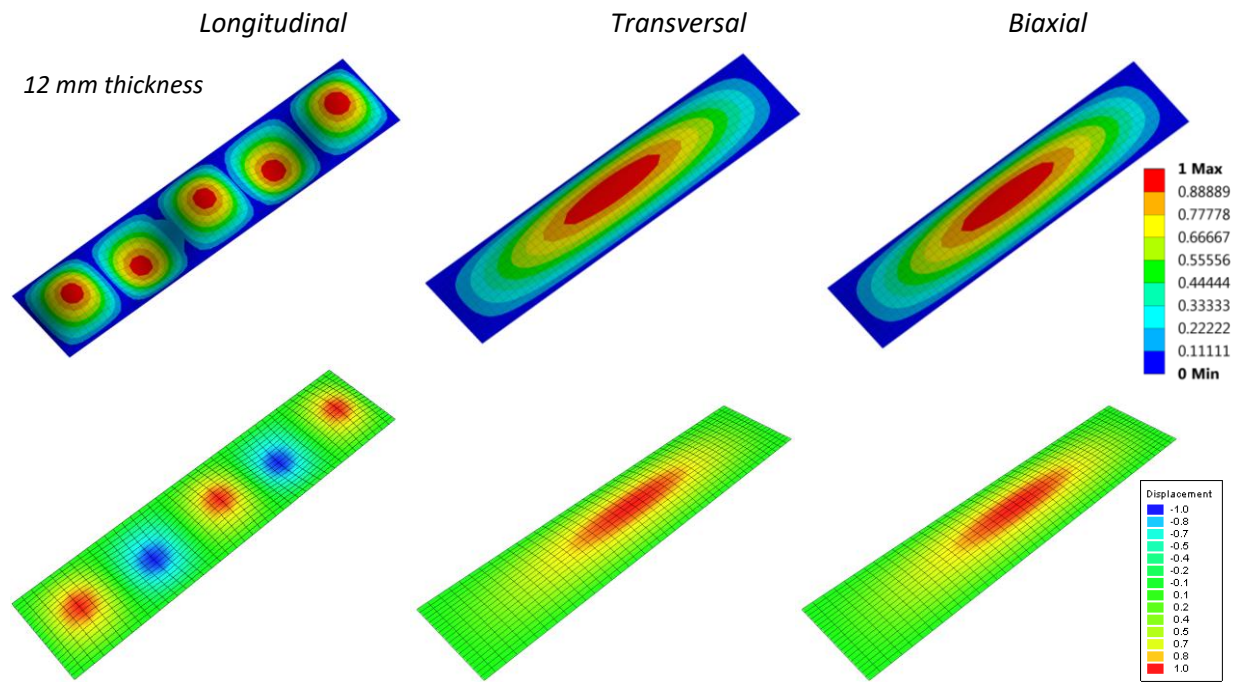


Figure 57: Comparison of eigenmodes between FEM and PULS for unstiffened plate of 12 mm thickness

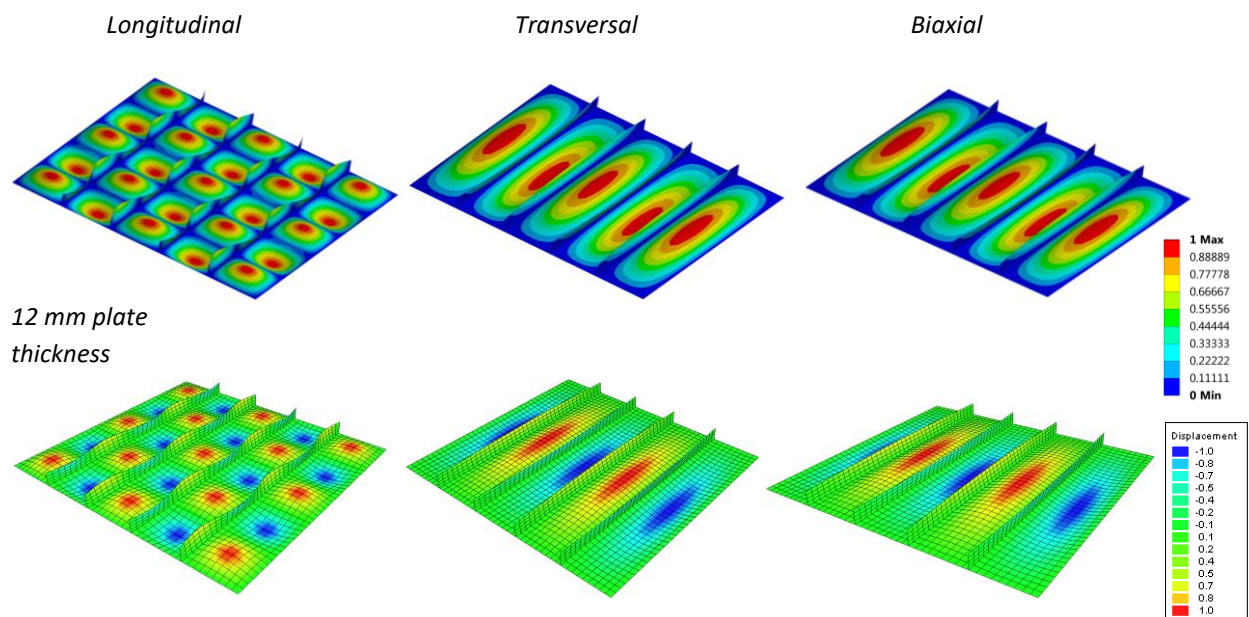
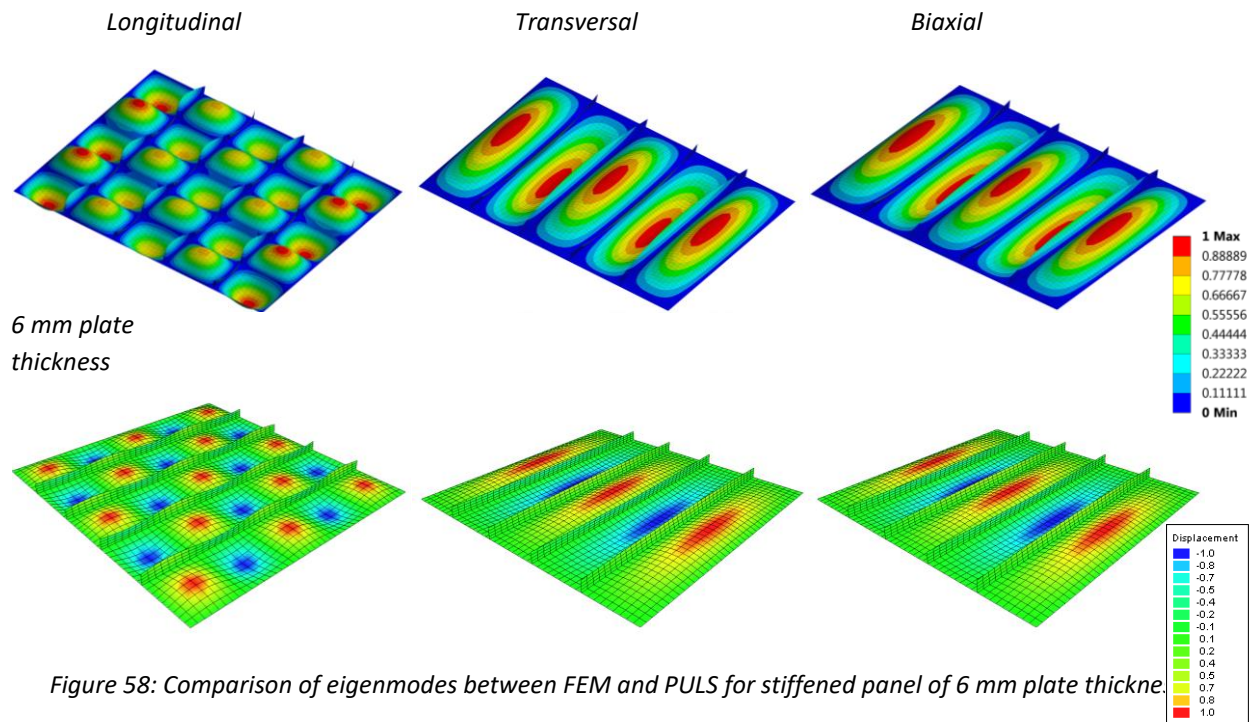
With respect to the stiffened panels, just the FEM computations are considered for the comparison. The results obtained for *stiffened panels* are presented in Table 12:

		STIFFENED PANEL 1 - 6mm			STIFFENED PANEL 2 - 12 mm			STIFFENED PANEL 3- 15.5 mm		
		Long.	Transv.	Comb.	Long.	Transv.	Comb.	Long.	Transv.	Comb.
PULS	Failing Load [Mpa]	79	20,25	19,25	162	67,5	57	257	134,5	124
	Global elast. Buckling	127	25	23	258	73	63	952	188	171
	Local elast. Buckling	79	20,25	19,25	292	80	76	372	134,5	127
	Ultimate capacity	99	25	23	162	67,5	57	257	141	124
	Failure Mode	LEB	LEB	LEB	UC	UC	UC	UC	LEB	UC
FEM	Load multipl. Mode 1	0,990	1,008	1,010	1,816	1,198	1,349	1,408	1,006	1,030
	Elast. Buckling stress	78,21	20,41	19,44	294,24	80,83	76,89	361,73	135,36	127,77
	Margin with resp. PULS	-1,0%	0,8%	1,0%	0,8%	1,0%	1,2%	-2,8%	0,6%	0,6%

Table 12: Comparison between results obtained for stiffened panels

In the same way, for all loading cases the elastic buckling stress obtained by FEM computations presents a good accuracy with respect to PULS with a maximum variation of 3%.

Regarding buckling eigenmodes, the results for stiffened panels are presented in Fig. 58, 59 and 60 with a graphical comparison between modes derived by FEM and PULS.



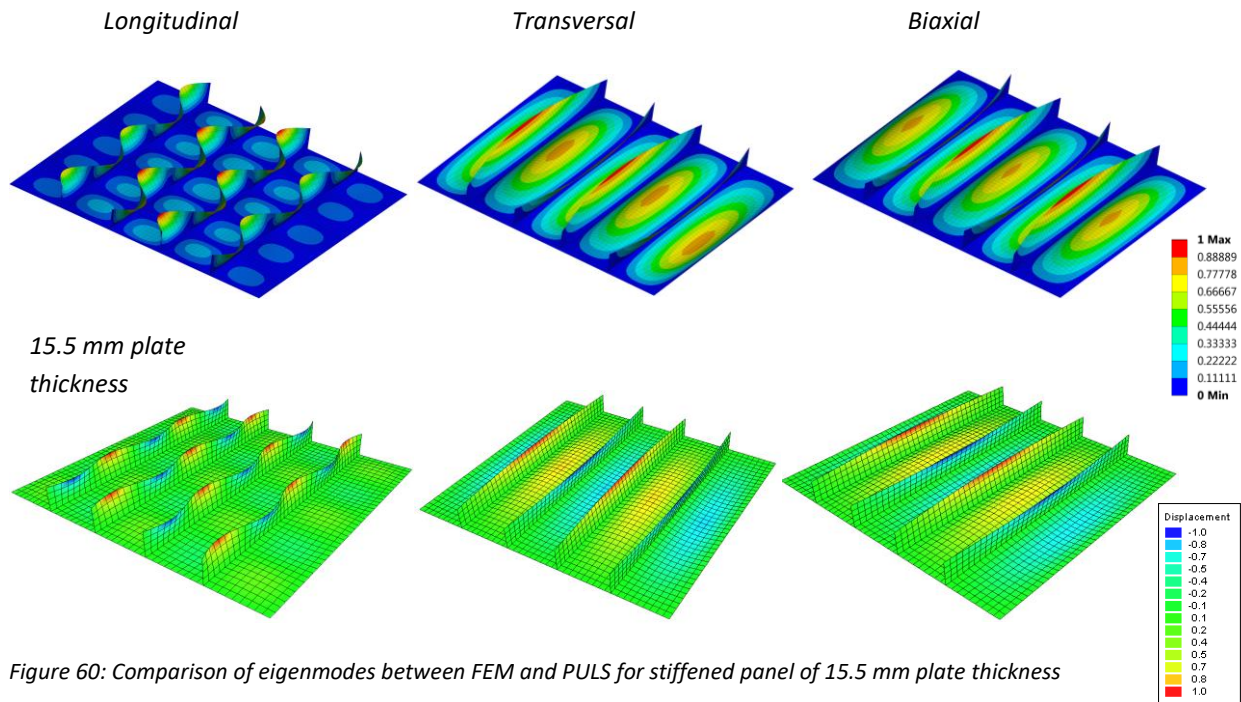


Figure 60: Comparison of eigenmodes between FEM and PULS for stiffened panel of 15.5 mm plate thickness

In summary, PULS and FEM delivers elastic buckling stress with a good accuracy in comparison with analytical formulations for the case of unstiffened plates. For stiffened panels a good agreement is found between both approaches. In addition, the eigenmodes delivered by PULS are consistent with those delivered by FEM.

In general, it is observed how the pattern produced for single unstiffened plates is reproduced within the panel with the same behaviour but with the junction between the stiffener and the plate acting as a nodal line in the buckling pattern.

With respect to the deformation of the stiffener, it is observed that the higher the stiffener is the higher amplitudes are obtained in the buckling pattern as illustrated in Fig. 61. In the same way, the amplitude of the buckling pattern for plating between stiffeners decreases as the stiffener height and thickness are increased.

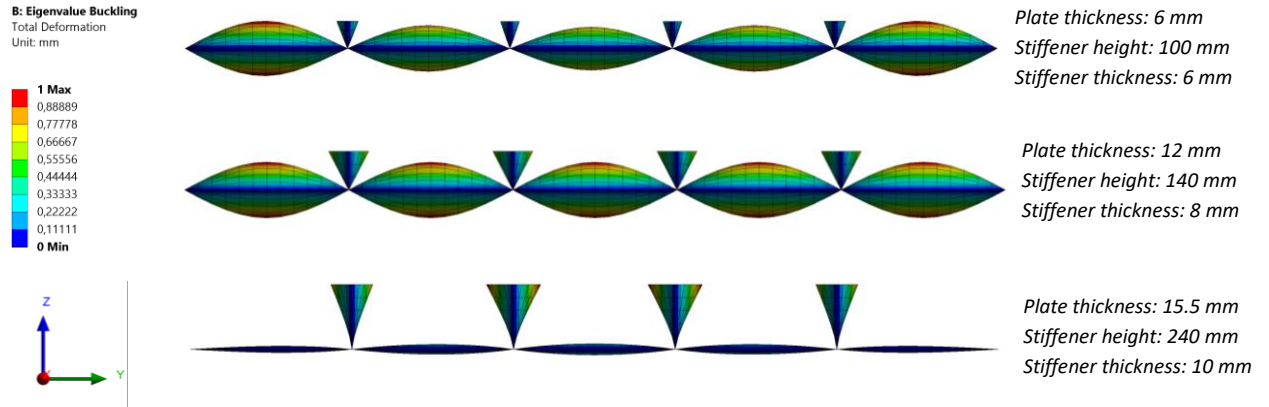


Figure 61: Eigenmode variation under longitudinal loading for different stiffened panels

Furthermore, the buckling pattern of plating for stiffened panels show an asymmetrical pattern as illustrated in Fig. 62 where one plate side tends to buckle upwards and the adjacent plate element tends to deflect downwards.

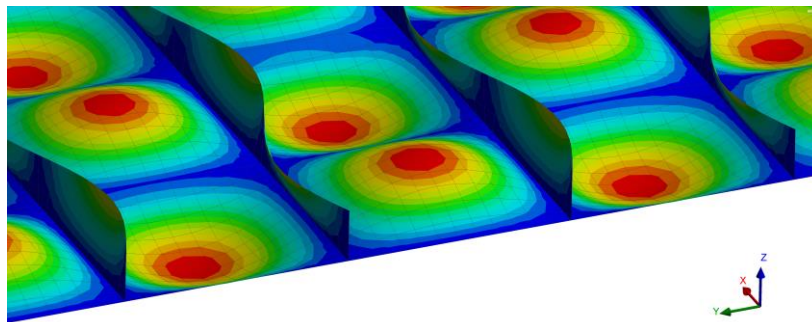


Figure 62: Asymmetrical Buckling pattern of plating between stiffeners obtained by FEM

This is a common buckling behaviour when pure dominant in-plane compressive loads, as considered in this study, are applied. However, if lateral pressure is considered and large enough the buckling pattern of the structure can tend to be symmetrical and each plate side will buckle in the direction of the lateral pressure loading producing the so called thin-horse mode.

With respect to transversal and biaxial loading case, both provide an elastic buckling stresses very close to each other. In the same way, the buckling eigenmodes are represented with the same pattern. This is very much influenced by the election of the loading ratio, which in this case is one, hence the same stress is applied in both edges. Therefore, for the next non-linear analysis just the longitudinal and transversal loading cases are considered.

7.6 Non-Linear Analysis

In this section a non-linear FEM analysis is performed for the different structures considered including non-linear effects from material plasticity, large deformation and initial imperfections. The aim is to compute the ultimate capacity of the different structures and compare the results with those derived by PULS.

As provided in previous section, given that biaxial loading case presents a very similar behaviour with respect to the transversal loading, this case is omitted in this analysis.

The non-linear material behavior is considered as stated in section 7.1 which consist in a yielding stress σ_y of 355 MPa and a plastic tangent modulus E_T of 1000 MPa.

For the non-linear solution procedure, the Full Newton-Raphson method is applied. This, approach computes the tangent stiffness matrix for each iteration step as illustrated in Fig. 63. It is a very effective and powerful method although it presents a relatively high computational effort.

$$[K_{n,i}^T]\{\Delta u_i\} = \{F_n^a\} - \{F_{n,i}^{nr}\} \quad (61)$$

where:

$[K_{n,i}^T]$: Tangent matrix for the time step n , iteration i

$\{\Delta u_i\}$: Displacement increment from i to $i + 1$

$\{F_n^a\}$: Total applied force vector at time step n

$\{F_{n,i}^{nr}\}$: Restoring force vector for time step n , iteration i

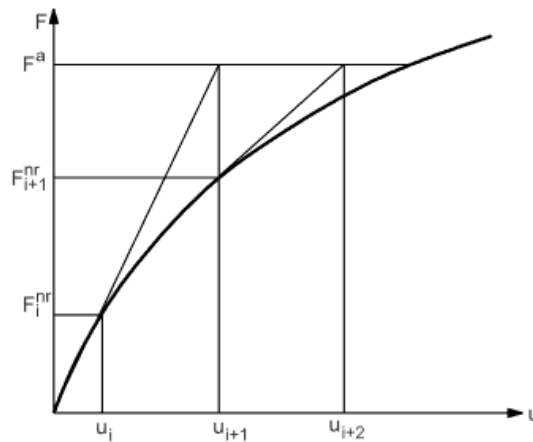


Figure 63: Newton-Raphson scheme for non-linear solution approach [10]

In addition, as a way to contrast the obtained results, for stocky structures undergoing plasticity before the inception of buckling the Johnson-Ostenfeld approach is used. It is a widespread method to account for this behaviour and has been applied in most classification societies [5] to account for the effect of plasticity in Buckling. It is given as follows:

$$\sigma_{cr} = \begin{cases} \sigma_E & \text{for } \sigma_E \leq 0.5 \sigma_y \\ \sigma_y \left[\frac{1 - \sigma_y}{4 \sigma_E} \right] & \text{for } \sigma_E > 0.5 \sigma_y \end{cases} \quad (62)$$

where:

σ_{cr} : Critical buckling stress

σ_E : Elastic buckling stress

σ_y : Yielding stress

7.6.1 Initial imperfections

The initial deflections are introduced in the structures based on the buckling eigenmode obtained from the Linear eigenvalue buckling analysis. The amplitude of the eigenmode is scaled according to fabrication standards of welded integrated structures in shipbuilding and offshore industry. As described in section 6.2.4, for unstiffened plates there is just one amplitude which corresponds to $s/200$ where s is the stiffener spacing. For the selected configurations that means that the scaling amplitude for the buckling eigenmode is taken as 3.

The procedure is performed by linking the linear eigenvalue analysis to the non-linear analysis as illustrated in Fig. 64. In this way the solution from the eigenvalue analysis as well as material properties are transferred and used as an input for the non-linear analysis.

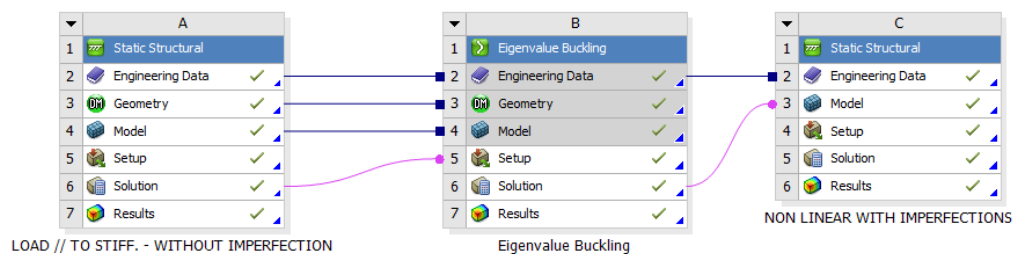


Figure 64: Implementation of initial imperfections for unstiffened plates

For stiffened panels, PULS implement the initial imperfection by combining the local and global eigenmodes as illustrated in Fig. 40. However, the buckling modes provided by FEM consider the effect of the stiffeners and produce different eigenmodes which differ from the global mode. In addition, due to difficulties in finding a procedure to combine two eigenmodes to produce the final model, an alternative approach is used.

In order to reproduce the initial imperfections as PULS does, the local eigenmode is taken and scaled by 3. Then, to produce the effect of the global mode, a force is applied onto the stiffeners to introduce the vertical elevation in the stiffeners with respect to the baseline as illustrated in Fig. 65 for the longitudinal loading. For transversal loading the same approach is used.

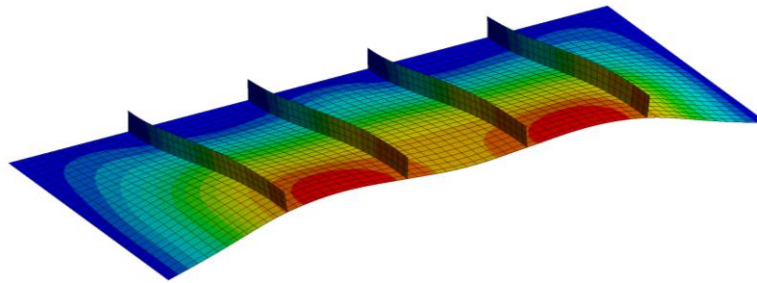


Figure 65: Initial imperfections for stiffened panel under longitudinal loading. Mid-stiffened panel section

For the enhanced model, it is not found a reasonable and practical way to introduce the imperfections through ANSYS Workbench and a script is developed by Dipl.-Ing. Stefan Griesch to be executed in ANSYS Mechanical APDL.

The script follows the previous approach, firstly a linear eigenvalue analysis is performed according to the type of loading considered for a single stiffened panel. The obtained buckling eigenmode is scaled according to PULS amplitude. Then, the stiffened panel with the imperfections is copied in the neighbouring regions. Finally, the heavy members are modelled and the nodes are merged accordingly producing the enhanced model. The heavy members are perfectly modelled without initial imperfections.

7.6.2 Unstiffened plates

In this section the results for unstiffened plates are presented and discussed. In order to not overload the size of the section and given that the graphical results are similar for the considered thicknesses, just the configuration of 6mm plate thickness is presented.

Results for all configurations are summarized in 13:

	PLATE 1 - 6mm		PLATE 2 - 12 mm		PLATE 3 - 15.5 mm	
	Longitudinal	Transverse	Longitudinal	Transverse	Longitudinal	Transverse
Failure type	Buckling	Buckling	UC	Buckling	UC	Buckling
Failure load in PULS	73	19,9	259	79,5	309	132,5
Elast. Buckl. Stress Analytical	73,11	19,91	292,44	79,62	487,91	132,84
Elast. Buckl. Stress PULS	73	19,9	292	79,5	488	132,5
Elast. Buckl. Stress Non-lin NFEM	61	13	-	50	-	75
First yielding PULS	159	51	259	110	309	155
First yielding NFEM-Top/bottom	147	46	216	94	242	120
First yielding NFEM-Middle	162	52	249	105	293	139
Variation between FEM and PULS	2%	2%	-4%	-5%	-5%	-10%
U.C PULS	159	51	259	110	309	155
U.C NFEM	178	56	253	105	297	139
U.C Johnson-Ostenfeld	-	-	247	-	290	-
Variation between FEM and PULS	12%	10%	-2%	-5%	-4%	-10%
Variation between FEM and J-O	-	-	2%	-	2%	-
Reserve after mid-plane yielding FEM	16	4	4	0	4	0
Buckling Usage factor PULS	1,00	1,00	0,89	1,00	0,63	1,00
Buckling Usage factor NFEM	1,20	1,53	-	1,59	-	1,77
UC Usage factor PULS	0,46	0,39	1,00	0,72	1,00	0,85
UC Usage factor NFEM	0,41	0,36	1,02	0,76	1,04	0,95

Table 13: NFEM results for unstiffened plates

As sustained by theoretical considerations, NFEM provides lower elastic buckling stress values since it considers initial imperfections and non-linear effects. Thus, the buckling usage factor obtained by FEM is always bigger than one.

The first yielding point on mid-plane between PULS and FEM present a good match in general with a maximum variation of 10%. It should be remarked that PULS considers as UC the first yielding on the mid-plane of the component. That is why the comparison with respect UC provide higher margins than for the first yielding on the mid-plane of the component.

A trend can be observed in the variation of results where for thin plates PULS provide lower values than NFEM while for thicker plates PULS provide higher values. This may arise from the assumption of neglecting the effect of bending stress in the limit state yield criteria which tends to become significant as the thickness increase.

In addition, the reserve of strength after mid-plane has reached yielding present more reserve for thin plates than for thick plates. For the thin configuration of 6 mm there is a reserve of 19 MPa until it reaches its ultimate capacity. However, for the thicker configurations of 12 and 15.5 mm, the reserve experiences a significant decrease with an available margin of 4 MPa and for some cases the margin is neglectable.

The ultimate capacity curves for *longitudinal loading* is presented in Fig. 66:

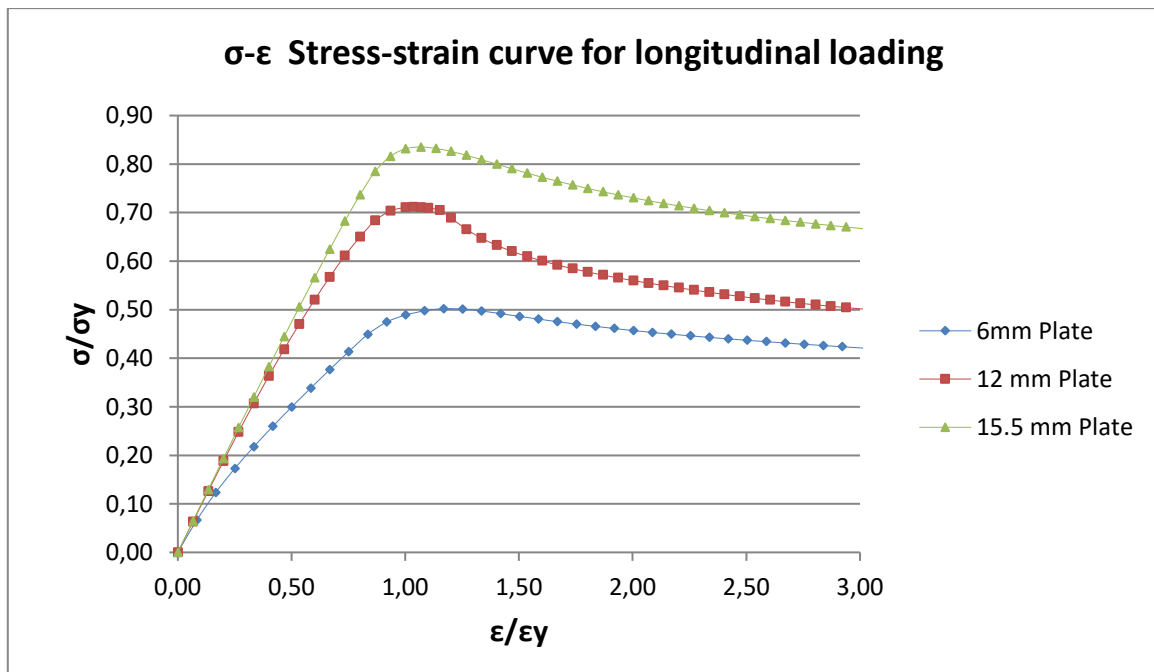


Figure 66: Ultimate capacity curves for unstiffened plates under longitudinal loading

As illustrated by the Figure, for the thin plating of 6 mm the failure mechanism is driven by buckling. The curve shows an early stiffness drop off much before than the ultimate capacity is reached. This indicates that load-shedding will be redistributed onto supporting members such as stiffeners or heavy members. Then, when first yielding takes place, the stiffness starts again to decrease until it becomes zero and ultimate capacity is reached.

In contrast, for the thicker configurations the failure mechanism is driven by ultimate capacity. In this case there is no stiffness drop until ultimate capacity is attached. Thus, the load-shedding will not take place unless the structure is compressed beyond the peak load.

Graphical results obtained by NFEM for the unstiffened plate of 6mm thickness under longitudinal loading are presented in Fig. 67. The von Mises stress at different stages during the failure is compared with result derived by PULS.

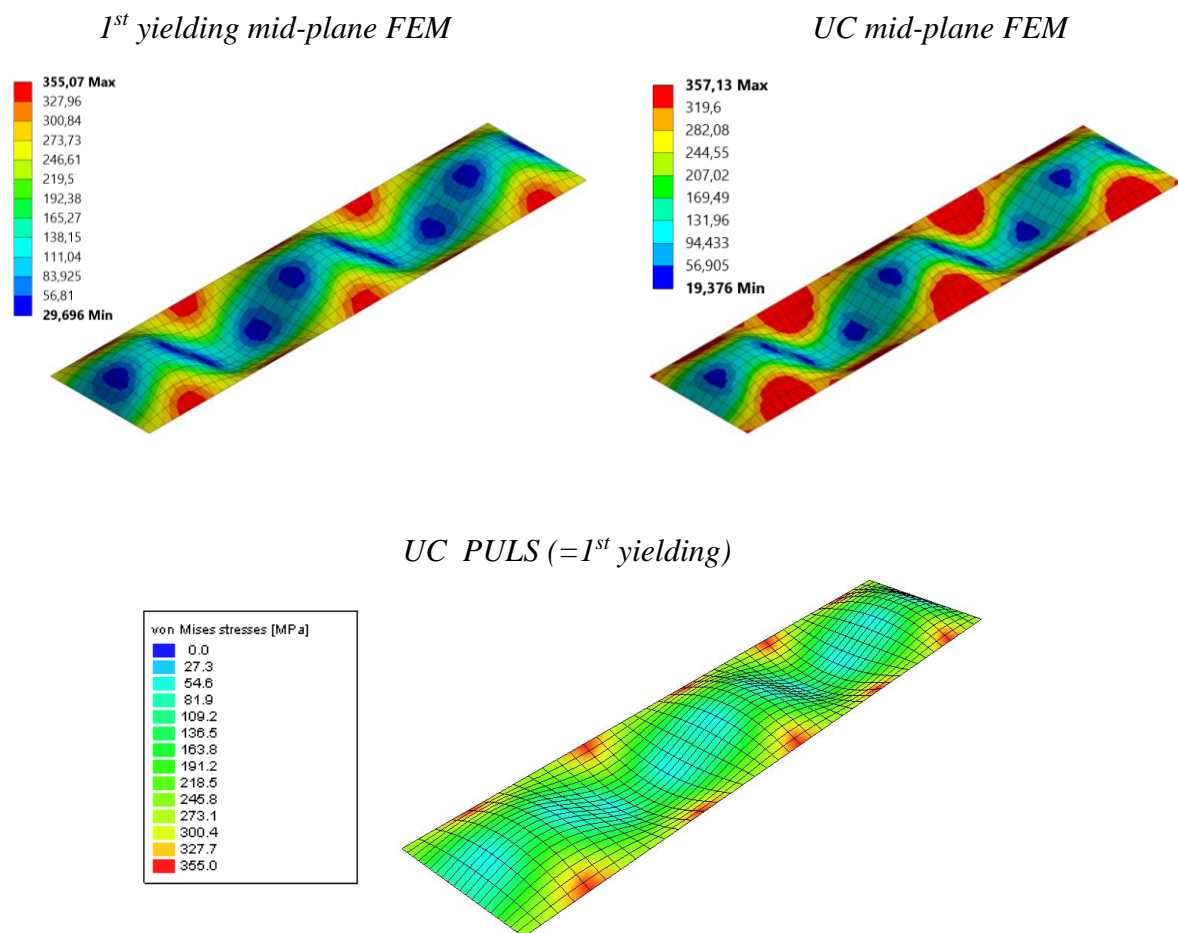


Figure 67: von Mises comparison between NFEM and PULS for unstiffened plate of 6 mm thickness under longitudinal loading

In general, there is a good agreement with the stress distribution provided by PULS and NFEM, where the maximum stress is developed around the edges that remain straight while the minimum occurs at the middle of the plate.

The ultimate capacity curves for *transverse loading* is presented in Fig.68:

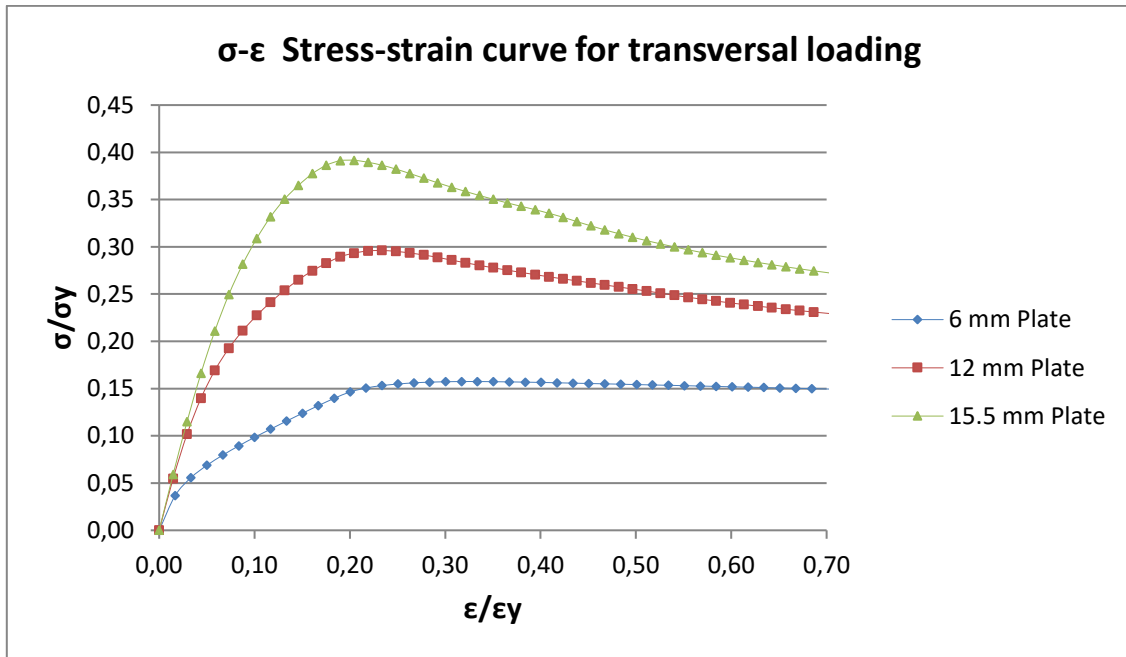


Figure 68: Ultimate capacity curves for unstiffened plates under transverse loading

For transverse loading, the failure mechanism for all configuration is driven by Buckling. All the curves present a stiffness drop of before than ultimate capacity is reached. For the curve of 6 mm plate thickness, it can be observed the sensitivity of this phenomenon regarding slenderness, with a much more pronounced drop in stiffness than the other two configurations.

In contrast with longitudinal loading, the post-collapse behaviour is softer and descend gradually without abrupt changes.

Graphical results obtained by NFEM and PULS for the unstiffened plate of 6mm thickness under transverse loading are presented in Fig. 69.

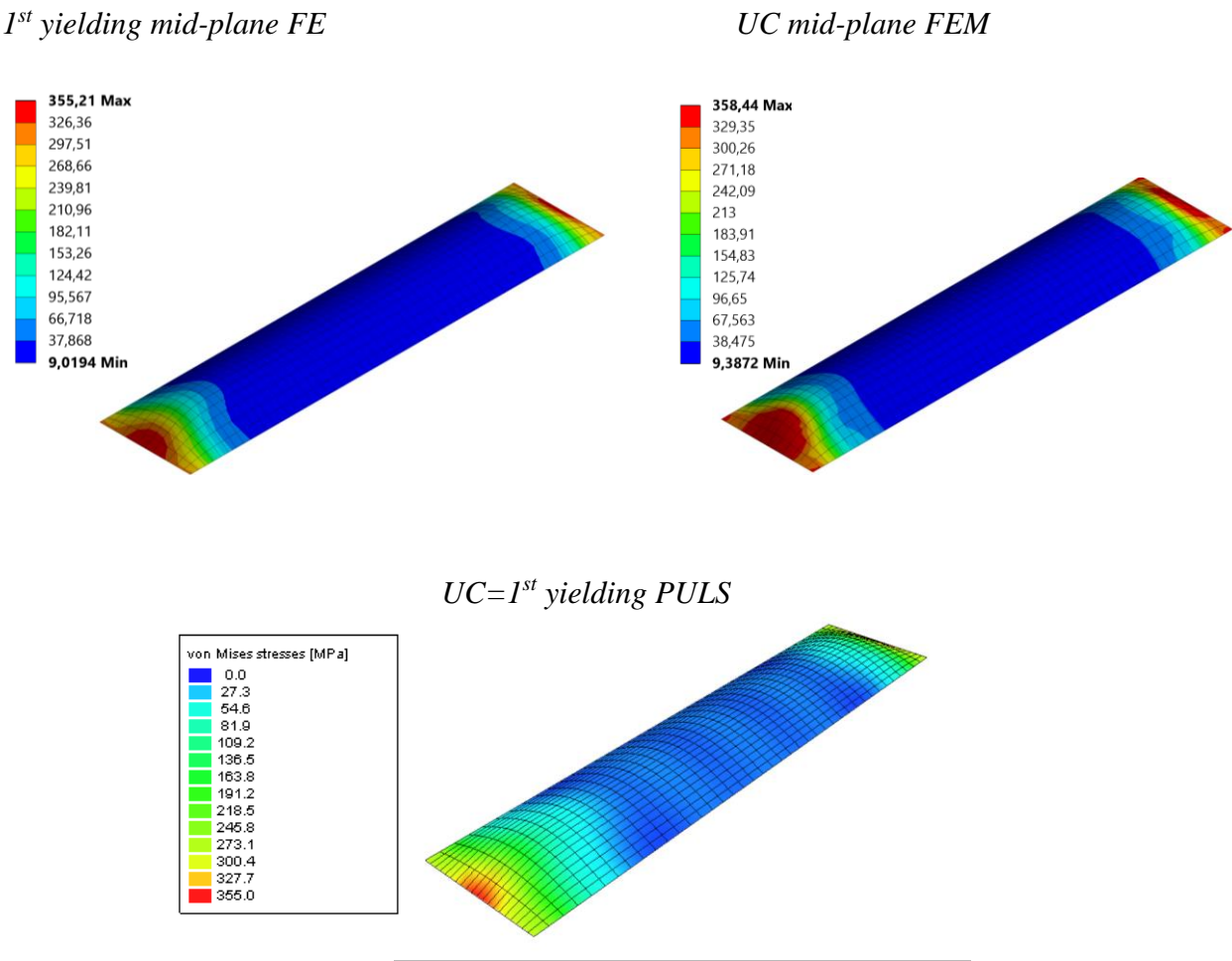


Figure 69: von Mises comparison between NFEM and PULS for unstiffened plate of 6 mm thickness under transverse loading

In the same line than for longitudinal loading, there is a good agreement with the stress distribution provided by PULS and NFEM, where the maximum stress is developed around the edges that remain straight while the minimum occurs at the middle of the plate.

7.6.3 Stiffened panels

In this section the results for stiffened panels are presented and discussed. In order to not overload the size of the section and given that the graphical results are similar for the considered thicknesses, just the configuration of 6mm plate thickness is presented.

Results for all configurations are summarized in Table 14:

	STIFF PANEL 1 - 6mm		STIFF PANEL 2 - 12 mm		STIFF PANEL 3 - 15.5 mm	
	Longitudinal	Transverse	Longitudinal	Transverse	Longitudinal	Transverse
Failure type	LEB	LEB	UC	UC	UC	LEB
Failure load in PULS	79	20,25	162	67,5	257	134,5
Global Elast. Buckl. Stress PULS	127	25	258	73	952	188
Local Elast. Buckl. Stress PULS	79	20,25	292	80	372	134,5
Elast. Buckl. Stress Non-lin NFEM	57	20	-	49	-	65
First yielding PULS	99	38	162	67,5	258	141
First yielding NFEM-Top/bottom	138	45	197	88	228	124
First yielding NFEM-Mid-plane	162	54	234	104	294	144
Variation between FEM and PULS	63,6%	42%	44%	54%	14%	2%
U.C PULS (=First yielding mid-plane)	99	38	162	67,5	258	141
U.C NFEM	166	57	236	105	303	145
U.C Johnson-Ostenfeld	-	-	247	-	270	-
Variation between FEM and PULS	68%	50%	46%	56%	17%	3%
Variation between FEM and J-O	-	-	-4%	-	12%	-
Reserve after mid-plane yielding FEM	4	3	2	1	9	1
Buckling Usage factor PULS	1,00	1,00	0,55	0,84	0,69	1,00
Buckling Usage factor NFEM	1,39	1,01	-	1,63	-	2,07
UC Usage factor PULS	0,80	0,53	1,00	1,00	1,00	0,95
UC Usage factor NFEM	0,48	0,36	0,69	0,64	0,85	0,93

Table 14: NFEM results for stiffened panels

First yielding point and UC between PULS and NFEM present a wider variation than for unstiffened plates with a maximum variation of around 60% for the thinnest configuration. However, the same trend than for unstiffened plates is observed. As thickness increase, PULS provide higher results since it neglects the effect of bending stresses and the variation between both methods is reduced.

Moreover, for the cases failing by UC, results provided by NFEM are in good agreement with Johnson-Ostenfeld approach with a maximum variation of 12%.

The variations in usage factors are according to the variations between PULS and NFEM results. In general, according to NFEM there is an improvement in terms of UC for all the configurations with respect to PULS. However, this just applies to the configurations failing due to UC since the ones failing by buckling have a lower cut-off value provided by the eigenvalue.

Ultimate capacity curves for *longitudinal loading* are presented in Fig. 70 :

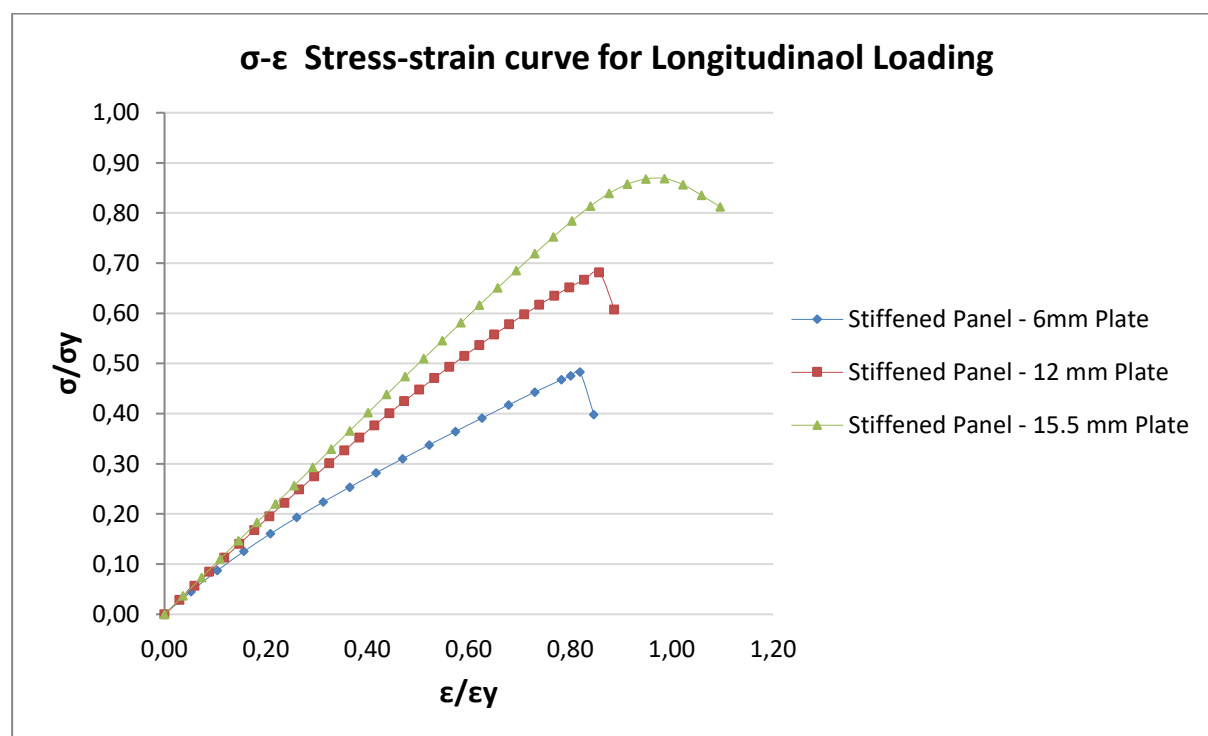


Figure 70: Ultimate capacity curves for stiffened panels under longitudinal loading

The stiffened panel with plating of 6 mm presents an early stiffness drop off much before ultimate capacity is reached, being the failure mechanism driven by Buckling. The stiffness drop due to buckling leads to stress redistribution towards the support members such as frames, girders or bulkheads.

In contrast, for the other two configurations with plating of 12 and 15.5 mm the failure mechanisms is driven by yielding and thus ultimate capacity. Thus, there is no drop off in the curve until the ultimate capacity is attached.

Graphical results obtained by NFEM and PULS for the stiffened panel with plating of 6 mm are presented in Fig. 71:

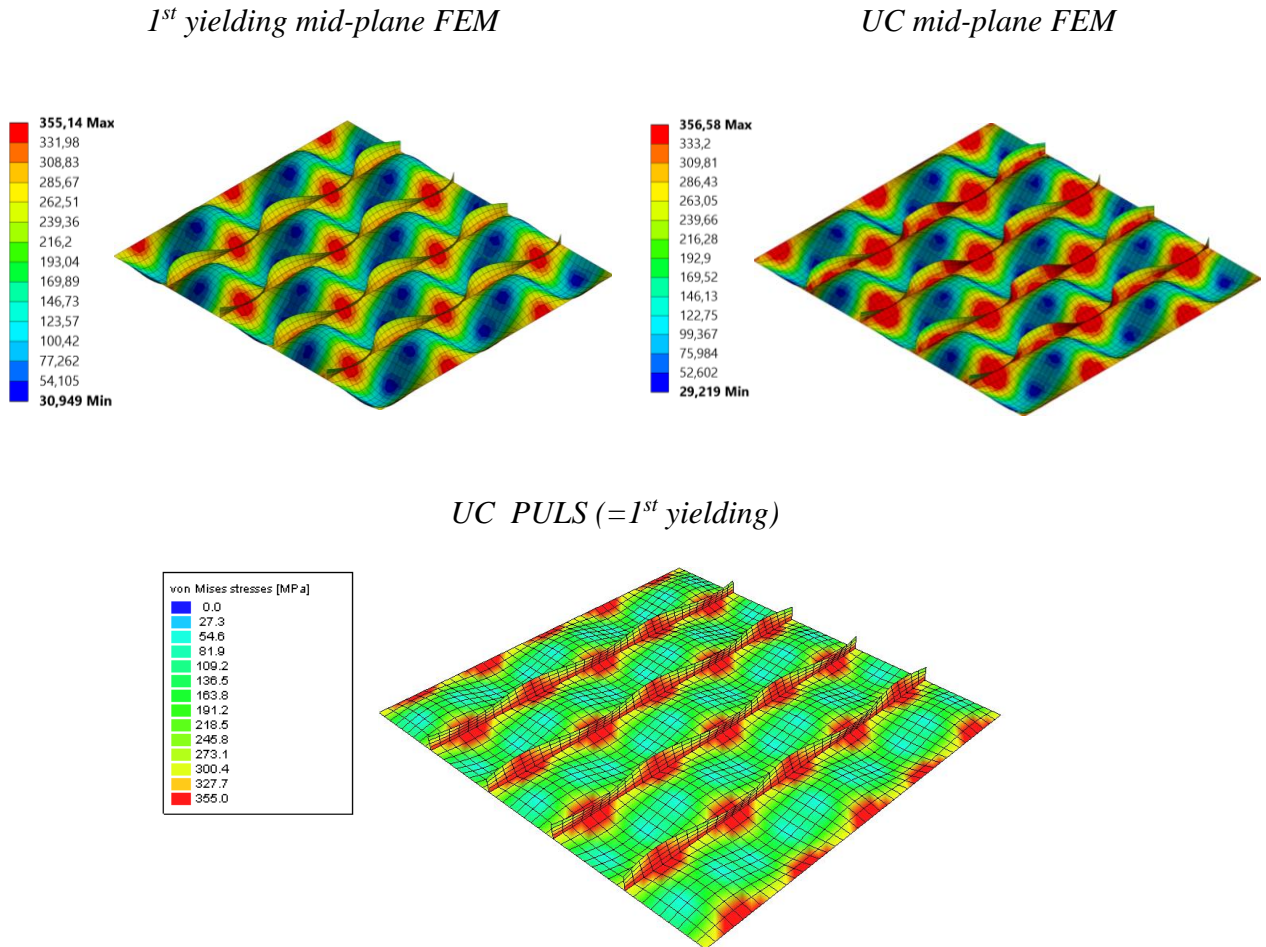


Figure 71: von Mises comparison between NFEM and PULS for stiffened panel with plating of 6 mm under longitudinal loading

In general, there is a good agreement with the stress distribution provided by PULS and NFEM, where the maximum stress is developed around the outer edges forced to remain straight and the plate-stiffener connection while the minimum occurs at the middle of the plate between stiffeners.

Ultimate capacity curves for *transverse loading* are presented in Fig. 72:

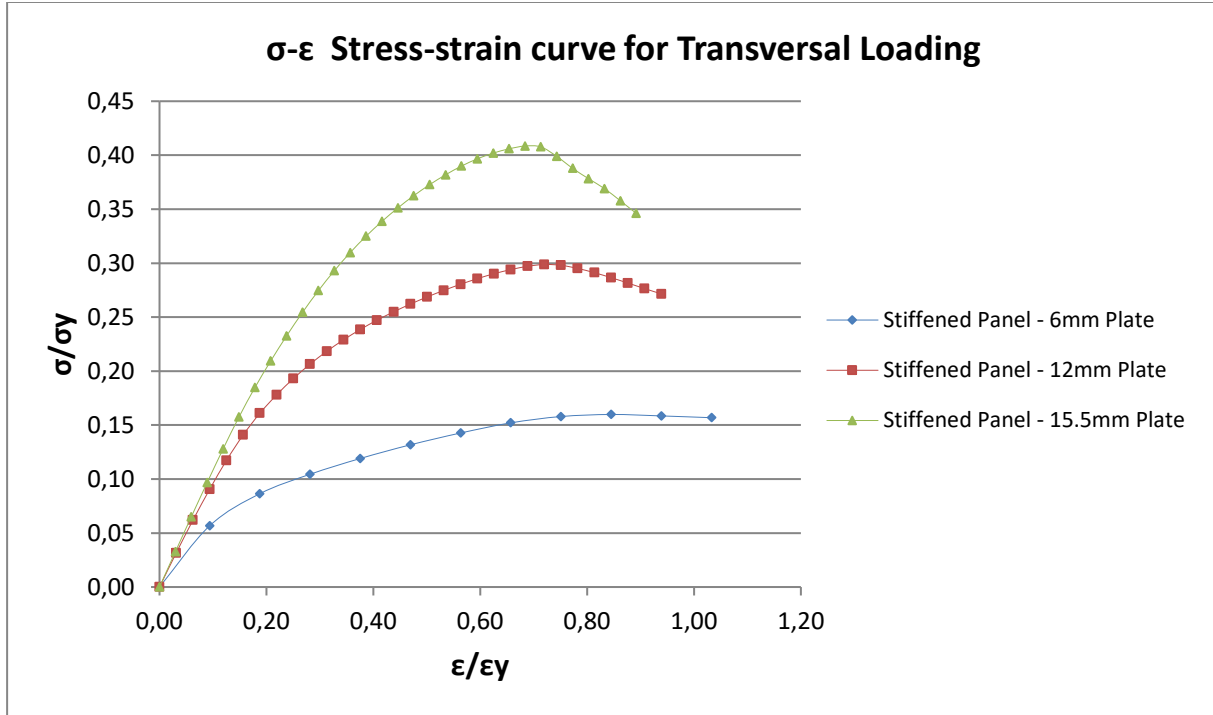


Figure 72: Ultimate capacity curves for stiffened panels under transverse loading

For transverse loading, stiffened panels with 6 and 15.5 mm plate thickness fail due to buckling while the stiffened panel with 12 mm fail due to ultimate capacity. However, in this case all the structures, even the configuration of 12 mm thickness, present a stiffness drop off well before ultimate capacity is attained. This means that for such structures, the load-shedding and so redistribution is a characteristic feature.

It is observed also the sensitivity of low thicknesses to the change of slope in the stress-strain curve, where the configuration of 6 mm presents a much more pronounce and earlier drop in stiffness than the other configurations.

Graphical results obtained by NFEM and PULS for the stiffened panel with plating of 6 mm is presented in Fig.73.

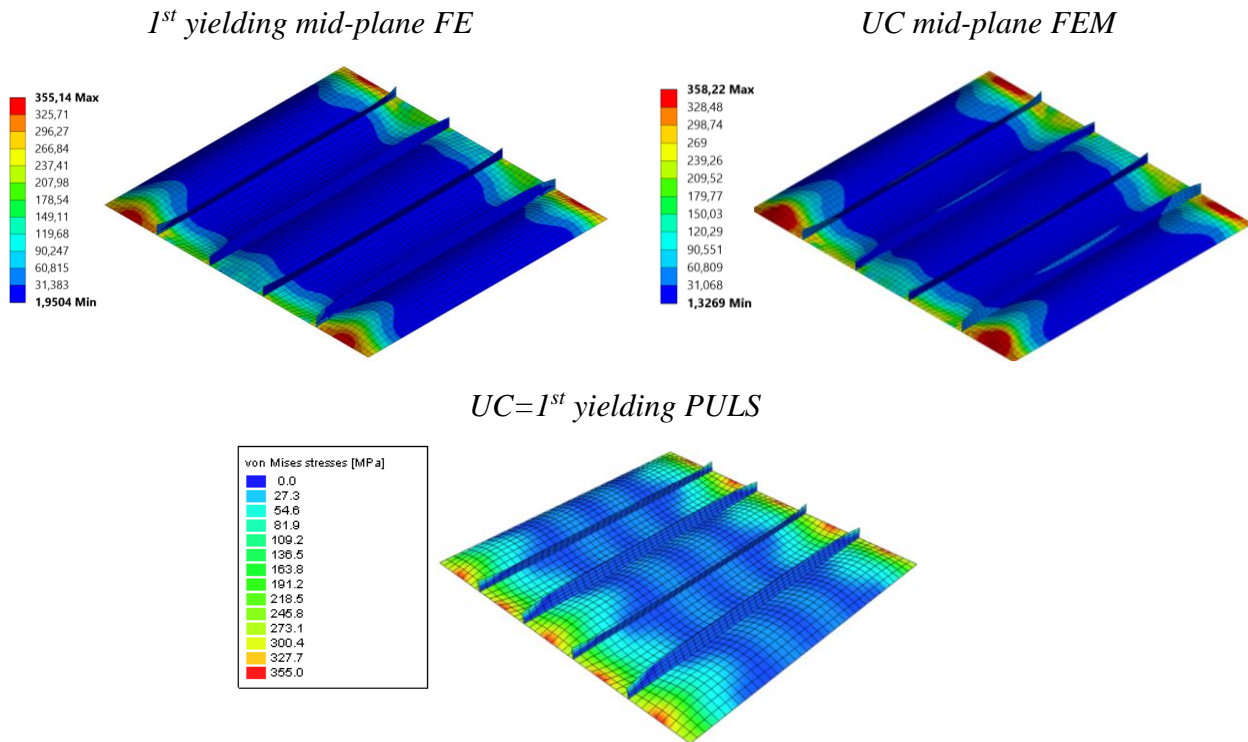


Figure 73: von Mises comparison between NFEM and PULS for stiffened panel of 6 mm plating under transverse loading

In the same line than for longitudinal loading, there is a good agreement with the stress distribution provided by PULS and NFEM, where the maximum stress is developed around the extreme part of edges that remain straight while the minimum occurs at the middle of the plate.

For NFEM stress distributions, yielding is concentrated in the outer regions of the plate while for PULS is evenly distributed along the edges to remain straight. This may arise from the fact that for stiffened panels PULS consider the longitudinal edges elastically restrained as along the stiffeners while the transverse edges are simply supported. In contrast, for the NFEM analysis the outer edges are idealized as simply supported.

7.6.4 Enhanced models

In this section the results for the enhanced models are presented and discussed. First, the results of the enhanced model considered as a whole are presented. Then, results focused on the behaviour of the inner stiffened panel surrounded by the heavy members in comparison with the single stiffened panel are considered. Finally, the usage factors provided by PULS are recalculated according to results derived by NFEM applying an ULS approach.

Due to time and technical difficulties in developing the script, the enhanced models for the plating of 12 and 15.5 mm under longitudinal loading cannot be developed.

In order to not overload the size of the section and given that the graphical results are similar for the considered thicknesses, just the configuration of 6mm plate thickness is presented.

Results for all configurations based on the overall structure are summarized in 15:

	STIFF PANEL 1 - 6mm		STIFF PANEL 2 - 12 mm		STIFF PANEL 3 - 15.5 mm	
	Longitudinal	Transverse	Longitudinal	Transverse	Longitudinal	Transverse
Failure type	LEB	LEB	UC	UC	UC	LEB
Failure load in PULS	79	20,25	162	67,5	257	134,5
Global Elast. Buckl. Stress PULS	127	25	258	73	952	188
Local Elast. Buckl. Stress PULS	79	20,25	292	80	372	134,5
Elast. Buckl. Stress Non-lin NFEM	50	19	-	51	-	64
First yielding PULS	99	38	-	68	-	141
First yielding NFEM-Top/bottom	154	46	-	95	-	130
First yielding NFEM-Middle	175	57	-	115	-	152
Variation between NFEM and PULS	77%	50%	-	69%	-	8%
U.C PULS (=First yielding)	99	51	259	68	309	141
U.C FEM	180	85	-	125	-	159
Variation between NFEM and PULS	82%	67%	-	84%	-	13%
Reserve after mid-plane yielding NFEM	5	28	-	10	-	7
Buckling Usage factor PULS	1,00	1,00	-	0,84	-	1
Buckling Usage factor NFEM	1,58	1,07	-	1,32	-	2,10
UC Usage factor PULS	0,80	0,40	-	0,99	-	0,95
UC Usage factor NFEM	0,44	0,24	-	0,54	-	0,85

Table 15: NFEM results for enhanced models

Ultimate capacity curves for the enhanced model and single stiffened panel under *longitudinal* loading are presented in Fig. 74:

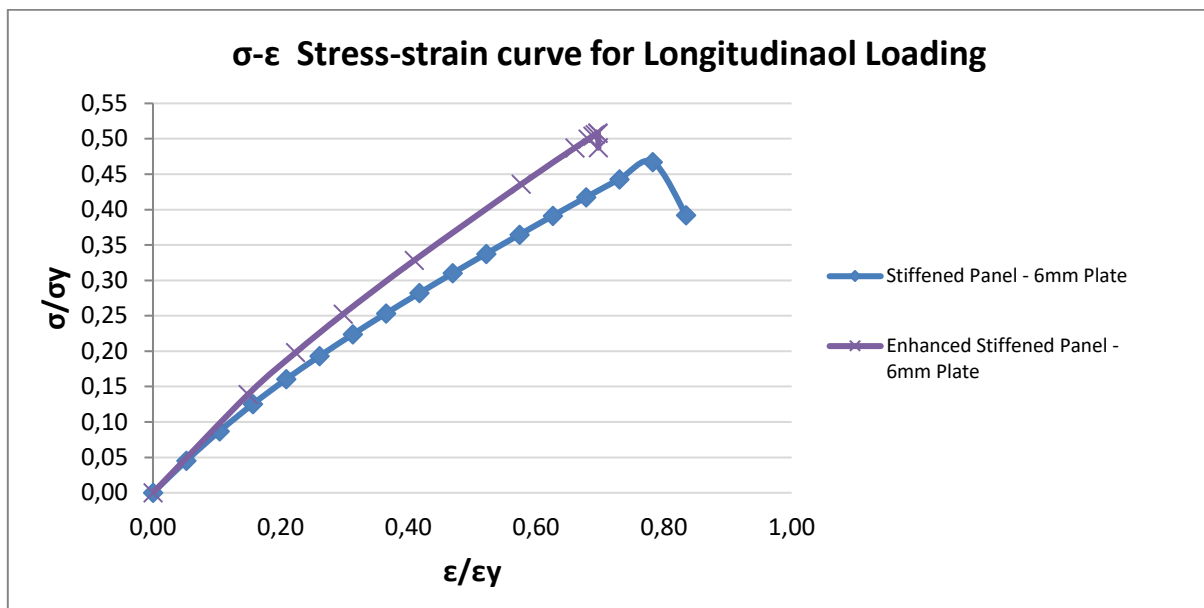


Figure 74: UC curves comparison for single stiffened panel and enhanced model under longitudinal loading

Ultimate capacity curves for the enhanced model and single stiffened panel under *transverse* loading are presented in Fig. 75:

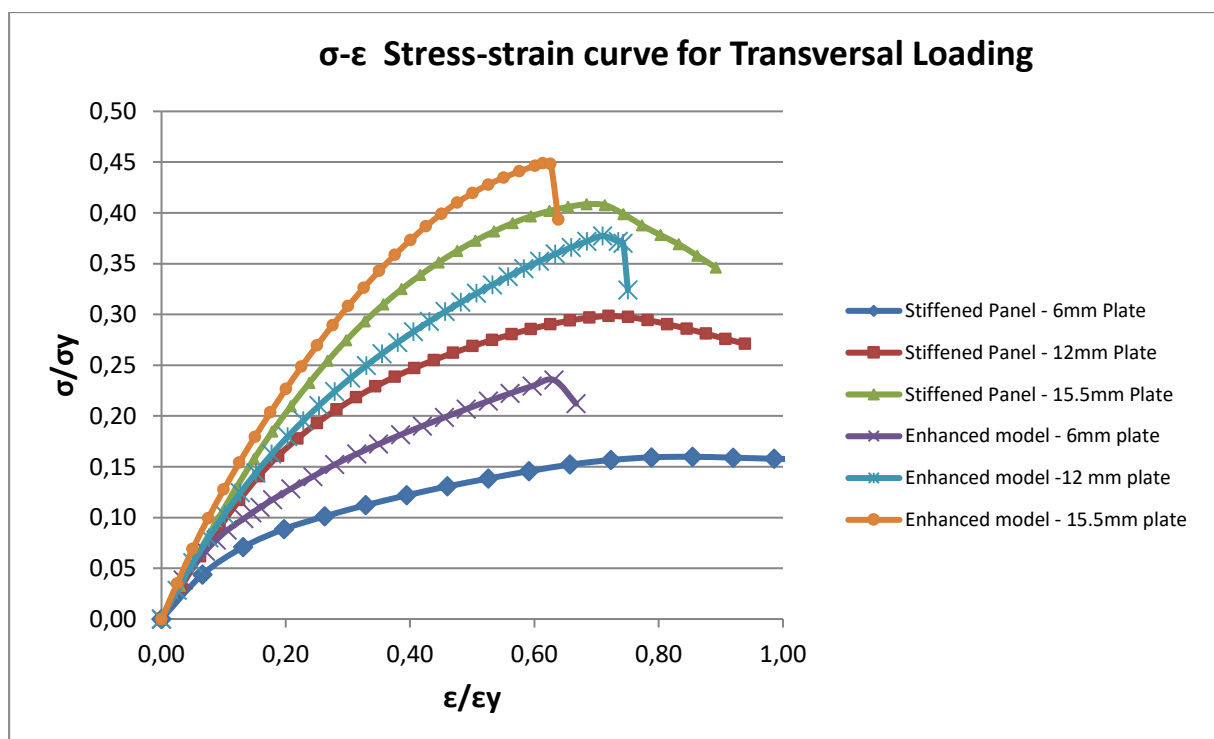


Figure 75: UC curves comparison for single stiffened panel and enhanced model under transverse loading

For both loading conditions, it is observed a later occurrence of the stiffness drop off in the average stress-average strain curve. This is due to the increase in rotational restraint introduced by the heavy members.

For longitudinal loading, just the thin configuration of 6 mm is analysed. The enhanced model presents an increase in UC of 8% with respect to the single stiffened panel. That means from 166 to 180 MPa.

For transversal loading, even the thicker configurations present a drop off in the stiffness before UC is reached. Thus, load shedding is a characteristic feature for this kind of loading which can lead to an increase of capacity due to load redistribution. The curves present the same trend observed for previous configurations where the variation between results decrease as the thickness of the element increases as presented in Table. 16.

	6 mm	12 mm	15,5 mm
Single stiffened panel			
U.C [σ/σ_y]	0,16	0,3	0,41
U.C [MPa]	57	105	145
Enhanced stiffened panel			
U.C [σ/σ_y]	0,24	0,38	0,45
U.C [MPa]	85	133	159
Increase in strength [Mpa]	49%	27%	10%

Table 16: Increase in strength for transverse loading

It is of special interest to have a closer view in how the inner centred panel surrounded by heavy members behaves in comparison with the isolated stiffened panel analysed in the previous section.

For all enhanced configurations, failure and collapse is driven by the surrounding panels in the outer regions where the edges are assumed to be simply supported. The heavy members are also assumed to be simply supported on the extremes and free to deform within the model. Therefore, first yielding in top/bottom and mid-plane are taken as a significant measure for strength comparison between both structures.

Results for all configurations with focus on the strength behaviour of the inner stiffened panel surrounded by heavy members are summarized in Table 17:

	STIFF PANEL 1 - 6mm		STIFF PANEL 2 - 12 mm		STIFF PANEL 3 - 15.5 mm	
	Longitudinal	Transverse	Longitudinal	Transverse	Longitudinal	Transverse
Single stiffened panel						
First yielding NFEM (Top/Bottom)	138	47	197	88	228	124
First yielding NFEM (Middle)	162	51	234	104	294	144
UC NFEM	166	57	236	105	303	145
Panel restrained by heavy members						
First yielding NFEM (Top/Bottom)	155	83	-	115	-	148
First yielding NFEM (Middle)	180	85*	-	125*	-	159*
Increase First yielding at Top/bottom	12%	77%	-	31%	-	19%
Increase First yielding at Mid-plane	11%	67%	-	20%	-	10%

**For these configurations, the inner central panel does not reach yielding in the mid-plane. For comparison purposes, this value is taken as the UC of the overall structure.*

Table 17: NFEM results for the inner stiffened panel within the enhanced models

Regarding first yielding in the mid-plane between PULS and NFEM, the same trend than for isolated stiffened panels is observed with slightly higher margins. The difference between both approaches decrease as the thickness increase. The increased margins provided by enhanced models arise from the influence of the heavy members, which introduce a rotational constraint in the edges of the panel increasing its Buckling strength as illustrated in Fig. 76.

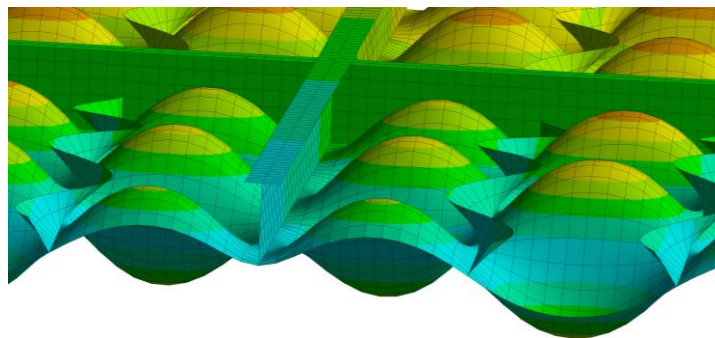


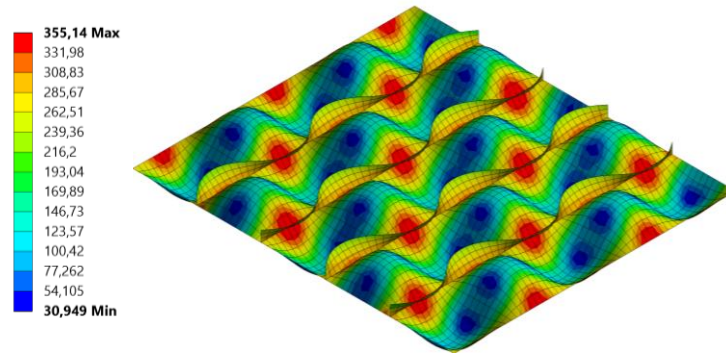
Figure 76: Rotational constraint introduced by heavy members in stiffened panel

This behaviour of the edges which tends more to a clamped condition may be influenced from the way that the initial imperfections are introduced. The fact of introducing the imperfections symmetrically with respect to the heavy member as shown in Fig. 76, may lead to the edges to behave more like clamped.

In addition, this increase in structural capacity is also due to the load redistribution into surrounding structures. When one stiffened panel starts to buckle, the load can be redistributed in comparison with a single stiffened panel. Also, it should be considered that the heavy members are taking part of the load in some extent.

Graphical results obtained by NFEM for the enhanced model in comparison with the isolated model of stiffened panel are presented in Fig. 77. It can be noticed the difference in stress distribution for the isolated stiffened panel with plating of 6 mm and the enhanced model with same thickness. Both structures show the stress distribution for which the single stiffened panel undergoes yielding in the mid-plane.

First yielding on mid-plane for isolated panel: 162 MPa



Stress distribution presented by the enhanced model when loaded with 162 MPa

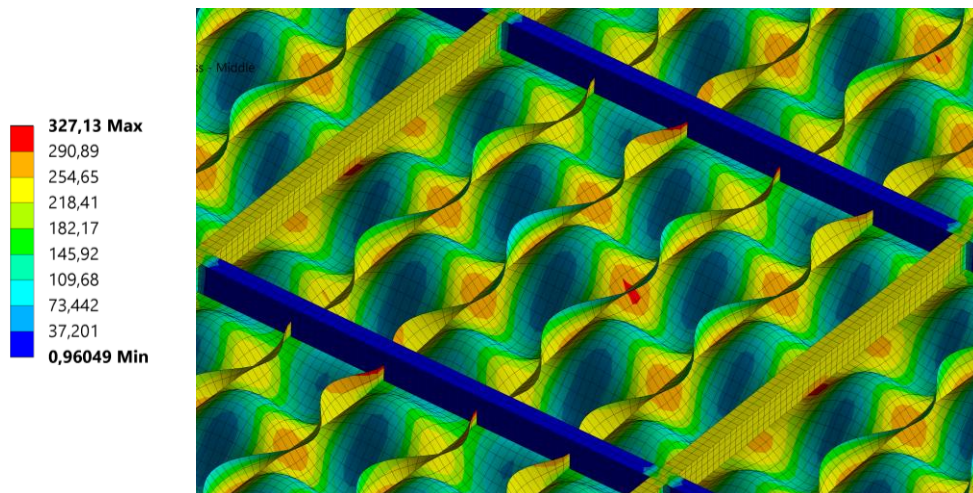
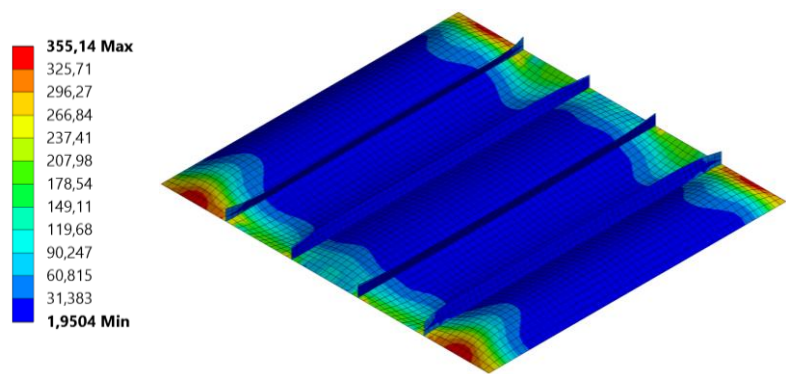


Figure 77: NFEM stress distribution comparison between single stiffened panel and enhanced model

Graphical results obtained by NFEM for the enhanced model in comparison with the isolated model of stiffened panel are presented in Fig. 78. The Figure shows the difference in stress distribution for the isolated stiffened panel with plating of 6 mm and the enhanced model with same thickness. Both structures show the stress distribution for which the single stiffened panel undergoes yielding in the mid-plane.

First yielding on mid-plane for isolated panel: 52 MPa



Stress distribution presented by the enhanced model when loaded with 52 MPa

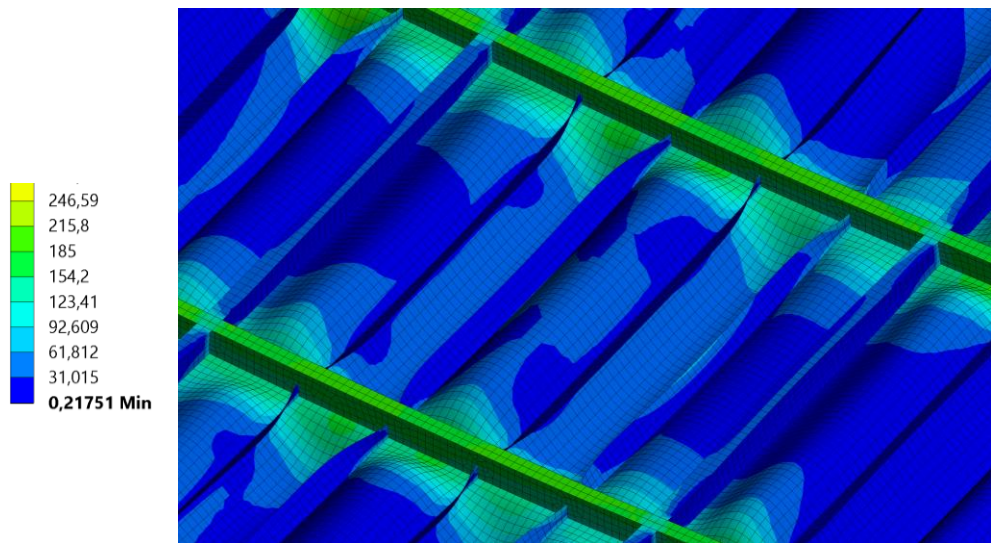


Figure 78: NFEM stress distribution comparison between single stiffened panel and enhanced model

PULS implements by default an SLS approach since the elastic buckling strength is used as an upper loading limit of allowable loading. This leads to an increase in the element thickness and proportions in comparison with an ULS approach. An SLS approach is consistent for heavy members such as frames, girders or bulkheads ensuring a robust design and allowing additional margins to support redistributed loads.

According to the design principles of ULS approach, described in section 6.2.5, the usage factors and failure loads are recalculated based in the results obtained by NFEM for the enhanced model. Since permanent buckles are not accepted, the strength parameter used is the first yielding in the top/bottom. Thus, the failure load for ULS is taken as the minimum between the global elastic buckling stress and the first yielding in the top/bottom.

The results are presented in Table 18:

	STIFF PANEL 1 - 6mm		STIFF PANEL 2 - 12 mm	STIFF PANEL 3 - 15.5 mm
	Longitudinal	Transverse	Transverse	Transverse
Global Elast. Buckl. Stress PULS	127	25	73	188
Local Elast. Buckl. Stress PULS	79	20,25	80	134,5
Elast. Buckl. Stress Non-lin NFEM	50	19	51	64
First yielding PULS	99	38	67,5	141
First yielding FEM-Top/bottom	155	83	116	148
Failure type PULS (SLS)	<i>LEB</i>	<i>LEB</i>	<i>UC</i>	<i>LEB</i>
Failure load in PULS (SLS)	79	20,25	67,5	134,5
Buckling usage factor (SLS)	1,00	1,00	0,92	1,00
UC usage factor (SLS)	0,80	0,53	1,00	0,95
Failure type PULS (ULS)	<i>GEB</i>	<i>GEB</i>	<i>GEB</i>	<i>UC</i>
Failure load in PULS (ULS)	127	25	73	148
Buckling usage factor (ULS)*	0,62	0,81	0,84	0,72
UC usage factor (ULS)*	0,51	0,24	0,58	0,91
Strength increase with respect to SLS	61%	23%	8%	10%

**These usage factors take the failing load of SLS to reflect the actual usage factor that the structure would have if ULS is applied.*

Table 18: Results for the stiffened panels based in an ULS approach

The results obtained are in the same line than previous sections where the strength increase tends to reduce as the thickness of the component increase. This is due to the fact that PULS neglects the effect of bending stress which becomes significant as the thickness increase.

For the stiffened panel 1 and 2, both configurations fail by Buckling. Under SLS they are not allowed to buckle elastically while for ULS the cut-off value is set as the global buckling stress since this mode introduces a significant instability in the structure.

The usage factors for ULS are calculated taking as an applied load the failure load of SLS and the maximum load allowed under ULS approach. For instance, for the stiffened panel with plating of 6 mm under longitudinal load, the failure load given by SLS is 79 MPa while under an ULS the structure can be loaded up to 127 MPa. This provides an actual usage factor of 0.62, which means that just a 62% of the ultimate capacity is being used.

In summary, an increase in strength is observed when applying an ULS instead of an SLS approach. Given that global buckling tends to occur at higher loads than local buckling, the failure load is based in the minimum between the global buckling stress and the first yielding on top/bottom of the structure. When the structure undergoes buckling in the elastic regime it can normally sustain further loading until first yielding is attached. Thus, an ULS approach provides an increase in the performance of the structure in terms of weight

7.7 Verification

In this section are presented some results from recognized and trusted sources such as class rules from DNV [6] and Yao and Fukujibo [4] in order to verify and validate the results obtained throughout the analysis.

7.7.1 Unstiffened Plates

The average stress-average strain curve for an unstiffened plate of 10 mm thickness under longitudinal loading and transversal loading is presented in Fig.79 and Fig. 80 respectively. The curves are derived as function of geometrical imperfections where X represents the amplitude factor and W_{max} the maximum deflection.

Longitudinal loading Length: 4000 mm σ_y : 315 MPa
Width: 1000 mm
Thickness: 10 mm

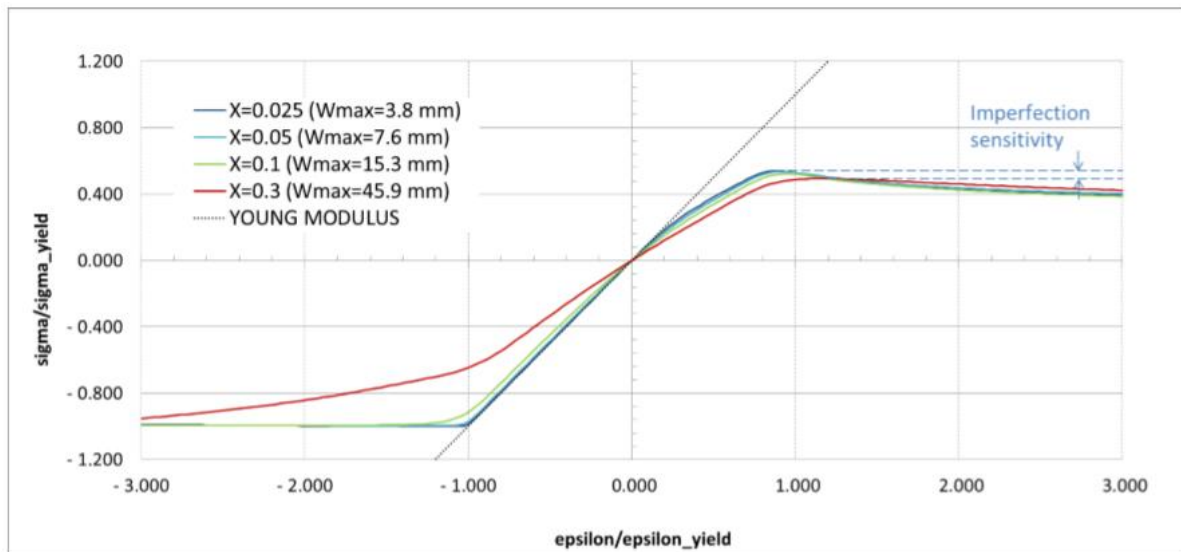


Figure 79: UC curve for thin unstiffened plate under longitudinal loading as function of imperfection size [6]

According to Fig. 79, for an imperfection amplitude of 3.8 mm the peak ratio between applied load and the yielding stress is 0.6. This presents a good agreement with the results obtained in the analysis which present a range from 0.5 for the thin configuration up to 0.84 for the configuration of 15.5 mm.

Transversal loading

Length: 4000 mm	σ_y : 315 MPa
Width: 1000 mm	λ : 3.86
Thickness: 10 mm	

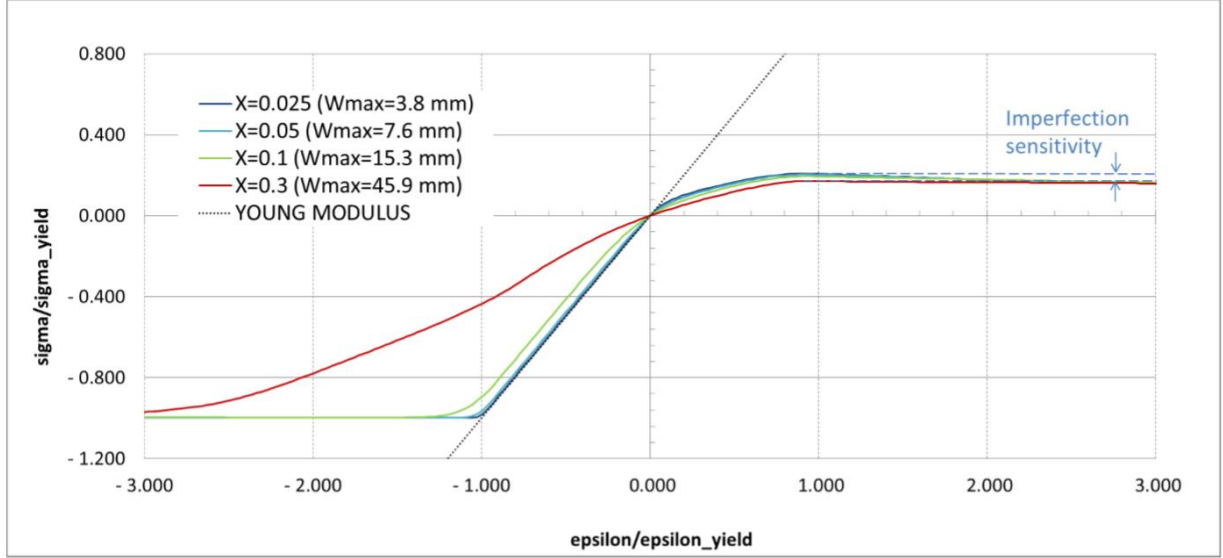


Figure 80: UC curve for thin unstiffened plate under transverse loading as function of imperfections size [6]

According to Fig. 80, for an imperfection amplitude of 3.8 mm the peak ratio between applied load and the yielding stress is around 0.2. This presents a good agreement with the results obtained in the analysis which present a range from 0.16 for the thin configuration up to 0.39 for the configuration of 15.5 mm.

7.7.2 Stiffened Panel

For this section it is taken as a reference a large study performed by Tanaka et al. (2014) [11] where a large numbers of stiffened panels from a bulk carrier and a tanker are analysed. The length of the stiffened panel is taken as 2550 mm while the stiffener spacing is taken as 850 mm. The term *size 3* refers to the dimensions of the stiffener, which are a height of 150 mm and a thickness of 17 mm. The term *n* refers to the number of longitudinal stiffeners.

The comparison of UC between PULS and NFEM as function of the slenderness is presented in Fig. 81 for two aspect ratios $a/b = 3$ and $a/b = 5$.

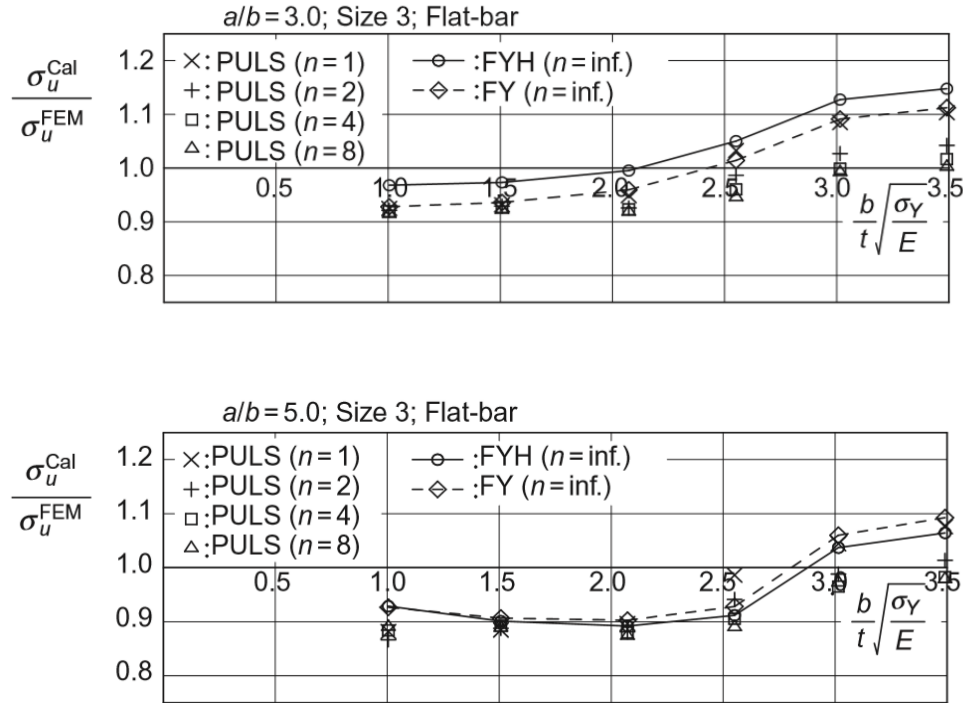


Figure 81: Comparison of UC between PULS and NFEM for stiffened panels as function of slenderness [11]

The stiffened panels considered for the analysis have an aspect ratio $a/b = 4,5$ which fit within the range provided by the mentioned study. Results obtained throughout the whole analysis present a similar pattern as presented in the Figure, where for thin structures PULS tend to provide lower results than NFEM while for thick structures it works in the opposite way. The range where the trend tends to change lies within a slenderness ratio between 2 and 3 approximately.

Given the previous contrast between results obtained by trusted and reputable sources, it is considered that the results obtained during the analysis are consistent.

8.CONCLUSION

Buckling is of crucial importance for the overall structural strength of stiffened panels. It is a complex phenomenon that includes the interdependence of a large number of factors, some of the most influent being: geometric and material properties, boundary conditions, initial imperfections and residual stresses. It is important to understand the buckling behaviour of stiffened panels to have a better insight into the failure mechanism in order to apply consistent design procedures. This arise from the existing reserves of capacity after the structure undergoes buckling which leads to an improved efficiency in the design.

Regarding elastic buckling stress and eigenmodes, PULS present a good agreement with analytical results as well as NFEM. For all the configurations, the elastic buckling stress derived by NFEM is lower than those provided by linear eigenvalue analysis. This is because NFEM consider initial imperfection and non-linear effects and so the structure buckles at an earlier stage, actually since the beginning of loading. Due to this fact, a sudden buckling point such as under linear analysis does not appear.

For all the configurations, a trend is observed in the variation of results for first yielding in the mid-plane between NFEM and PULS. As the thickness is increased, the variation between NFEM and PULS decrease as illustrated in Fig. 82 and Fig. 83 for longitudinal and transverse loading respectively.

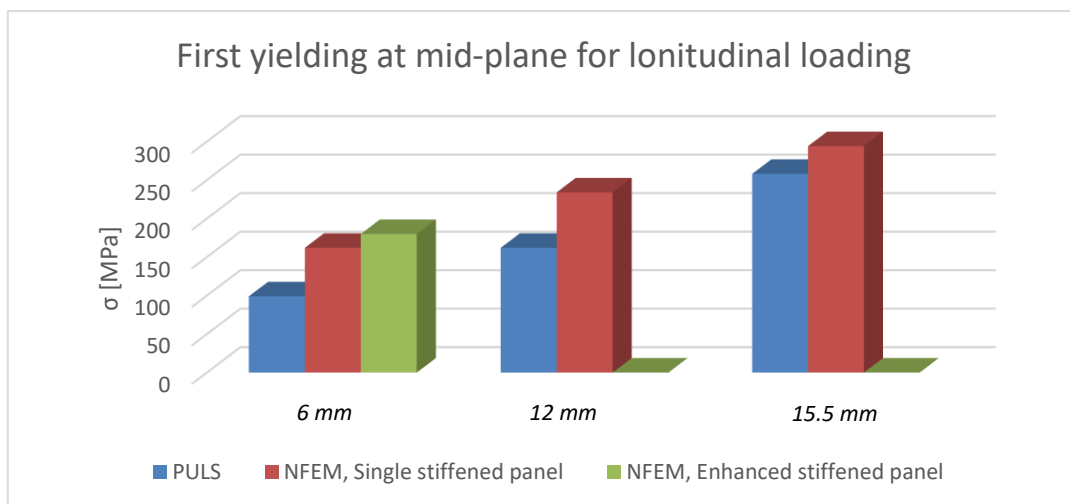


Figure 82: First yielding at midplane under longitudinal for the configurations considered

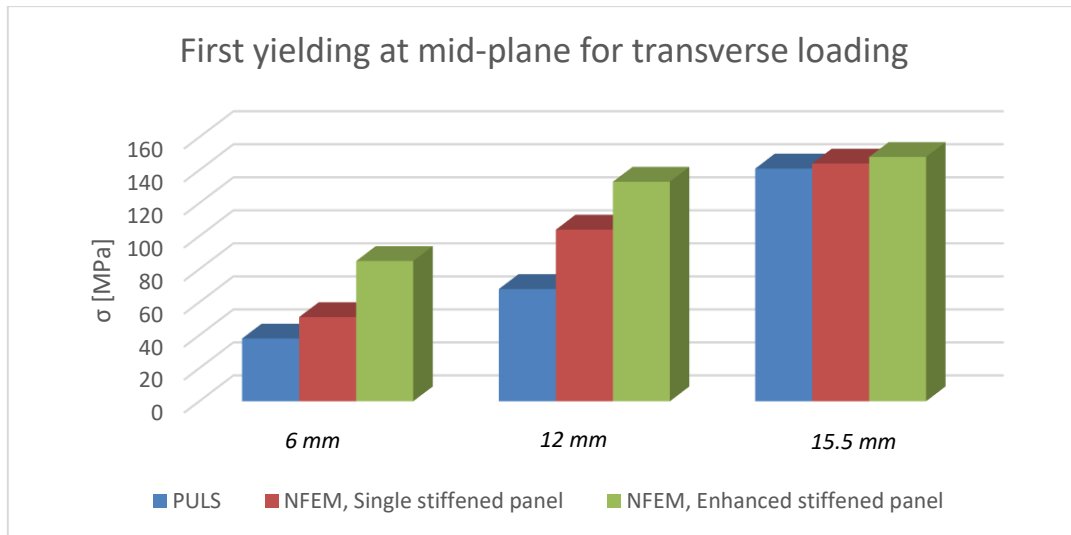


Figure 83: First yielding at midplane under transverse loading for the configurations considered

The Figures present the variation in the first yielding at mid-plane for the different models considered. The enhanced model results are based in the inner centred panel. It should be noted that for the enhanced model failure takes place in the outer regions and for the configurations of 12 and 15.5 mm the inner panel does not undergo yielding at mid-plane. However, for comparison purposes this value is taken as the UC of the enhanced model, but slightly higher strength is expected for the centred panel.

This trend arises from PULS assumption of neglecting the effect of bending stress in the limit state yield criteria, which tends to become significant as the thickness increase. This trend is in the same line than results found by Tanaka et al. (2014) [11], where for slenderness values higher than 2.5 PULS provide higher results than NFEM.

In addition, the assumption of taking the first yielding in the mid-plane represents a consistent way to account for the UC of the structure. Even if some reserves are found for thin plating, in general the UC is reached soon after the yielding in the mid-plane.

The enhanced model presents a significant increase with respect to the single stiffened panel due to the following facts:

One of the most influent facts in the increase of strength is the influence of the heavy members in the rotational restraint. PULS provide a model for integrated plates in larger plate constructions, but just in terms of in-plane boundary conditions where the edges are forced to remain straight. The out-of-plane boundary conditions is just partly considered, for the global model all four edges are simply supported. For the local model, the longitudinal edges are elastically restrained as along the primary stiffeners while the transverse edges are simply supported. Therefore, it should be noticed that in actual integrated ship structures, the supporting heavy members provide a higher rotational restraint than that provided by a smaller stiffener within the panel. This is observed in the enhanced model where the heavy members provide a rotational restraint which tends to behave more like clamped than simply supported. However, further research in this matter is needed since the way that the initial imperfections are introduced may affect the behaviour of the edge. The initial imperfections are introduced symmetrically with respect to the girder, where in both sides the plate is deformed upwards.

The increase in rotational restraint and so in buckling strength is also observed in the obtained UC curves for the enhanced model, where a later occurrence of the stiffness drop is observed for longitudinal and transverse loading. In addition, it is observed the sensitivity to buckling phenomenon for thin plating of 6 mm with a much earlier stiffness drop than other configurations of 12 and 15,5 mm.

The effect of load redistribution into surrounding structures provides an additional strength margin in comparison with an isolated stiffened panel. When a part of the structure starts to buckle, the load-carrying capacity is decreases and there is a redistribution of internal forces towards unbuckled members. This aspect is disregarded by PULS where a single panel is considered.

Finally, PULS implements by default an SLS approach where the elastic buckling strength is used as cut-off value. The comparison between SLS and ULS approaches using results derived by NFEM provide an increase of strength for all the considered configurations.

For thin and moderate thick plating, the increase in strength is constrained by the global elastic buckling stress, since it is normally below the first yielding. In contrast, for thick plating the global elastic buckling takes place at higher values and the structure undergoes yielding first. Therefore, the application of ULS approach for the stiffened panel leads to an increase in the performance of the structure in terms of weight.

9. FURTHER WORK

As a continuation of the present work and to provide a deeper knowledge in the topic the following work is proposed.

As a first step, the enhanced models for the moderate and thick configurations of 12 and 15.5mm could be modelled. This would complete the initial selected configurations and would allow to compare the results with the thin configuration of 6 mm.

The field where more work can be performed is in the initial imperfections. Given the unpredictable behaviour of the initial imperfections, a further investigation applying other type of patters would contribute largely to the knowledge in the matter. These could be mainly based in two approaches. The first one consists in a symmetrical distribution of deflections where the plating between stiffeners deflect upwards, also known as hungry-horse mode. This mode tends to appear in the stiffened panel when a large lateral pressure is applied. On the other hand, the second deflection pattern could be based in empirical measurements from deflections in real stiffened panels.

Regarding the enhanced model, it could be improved by introducing also imperfections in the heavy members since for the analysis they are perfectly modelled. In addition, to further study the influence of the initial imperfections in the rotational restraint of the edges along the heavy members, the same analysis could be performed by introducing the initial deflections asymmetrically with respect to the girders and frames.

10. REFERENCES

- [1] DNV-GL, 2015. Nauticus Hull-PULS User Manual.
- [2] Rigo, P. and Rizzuto E., 2003. Analysis and design of ship structure. In: T. Lamb, ed. *Ship Design and Construction*. Jersey city: SNAME, Chapter 18
- [3] Byklum, E., 2002. *Ultimate strength analysis of stiffened steel and aluminium panels using semi-analytical methods*. Doctoral thesis. (Dr.-Ing). Norwegian University of Science and Technology (NTNU)
- [4] Yao, t. and Fujikubo, M., 2016. *Buckling sand ultimate strength of ship and ship-like floating structures*. Cambridge: Butterworth-Heinemann
- [5] Paik, J.K. and Thayamballi, A.K, 2003. *Ultimate limit state design of steel-plated structures*. Chichester: John Wiley& Sons.
- [6] DNV-GL, 2018. Buckling. *Class guideline*
- [7] Bak, M., 2014. Non-linear Buckling analysis using Workbench v15. CAE Associates
- [8] MV Werften. 2019. *Giants made in MV, the global class* [online]. Available from: <https://www.mv-werften.com/en/ships/global.html> [Accessed 2 May 2019]
- [9] Herencia, J., Weaver, P. and Friswell, M., 2010. Closed-Form solutions for buckling of long anisotropic plates with various boundary conditions under axial compression. *Journal of Engineering Mechanics*. (ASCE) EM.1943-7789.0000158
- [10] SHARCNET. *Newton-Raphson procedure* [online]. Available from: https://www.sharcnet.ca/Software/Ansys/16.2.3/en-us/help/ans_thry/thy_tool10.html [Accessed 13 June 2019]
- [11] Tanaka, S., Yanagihara, D., Yasuoka, A., Harda, M., Okazawa, S., Fukujibo, M. et al., 2014. Evaluation of ultimate strength of stiffened panels under longitudinal thrust. *Mar Struct*, 36:21-50.

11. ANNEXES

11.1 Convergence study

This section presents the full results of the convergence study for the unstiffened plate and stiffened panel of 6 mm thickness under longitudinal, transversal and biaxial loading:

For unstiffened plates:

	Mesh size [mm]							
	150	125	100	75	50	25	15	10
LONGITUDINAL LOADING (Applied load: 73 Mpa)								
N° of elements	72	110	162	288	648	2592	7200	16200
Half-waves of Buckl. Mode	4	4	4	5	5	5	5	5
1st mode Load multiplier	1.0947	1.0604	1.0432	1.024	1.0106	1.0021	0.9997	0.99836
Elastic Buckling stress	79.91	77.41	76.15	74.75	73.77	73.15	72.98	72.88
<i>Variation with resp. Prev. Solution</i>	-	2.50%	1.26%	1.40%	0.98%	0.62%	0.18%	0.10%
<i>Variation with resp. Analytical sol.</i>	6.80%	4.30%	3.04%	1.64%	0.66%	0.04%	-0.13%	-0.23%
Buckling coefficient	4.4209	4.2824	4.2129	4.1354	4.0813	4.0469	4.0372	4.0318
<i>Variation with resp. Prev. Solution</i>	-	0.14%	0.07%	0.08%	0.05%	0.03%	0.01%	0.01%
<i>Variation with resp. Analytical sol.</i>	0.38%	0.24%	0.17%	0.09%	0.04%	0.00%	-0.01%	-0.01%
TRANSVERSAL LOADING (Applied load: 19.9 Mpa)								
N° of elements	72	110	162	288	648	2592	7200	16200
Half-waves of Buckl. Mode	1	1	1	1	1	1	1	1
1st mode Load multiplier	1.1032	1.0639	1.0435	1.024	1.0104	1.0024	1.0006	0.99987
Elastic Buckling stress	21.95	21.17	20.77	20.38	20.11	19.95	19.91	19.90
<i>Variation with resp. Prev. Solution</i>	-	0.78%	0.41%	0.39%	0.27%	0.16%	0.04%	0.01%
<i>Variation with resp. Analytical sol.</i>	2.05%	1.27%	0.86%	0.47%	0.20%	0.04%	0.01%	-0.01%
Buckling coefficient	1.2145	1.1712	1.1488	1.1273	1.1123	1.1035	1.1016	1.1008
<i>Variation with resp. Prev. Solution</i>	-	0.04%	0.02%	0.02%	0.01%	0.01%	0.00%	0.00%
<i>Variation with resp. Analytical sol.</i>	0.11%	0.07%	0.05%	0.03%	0.01%	0.00%	0.00%	0.00%
BIAXIAL LOADING (Applied load: 18.9 Mpa)								
N° of elements	72	110	162	288	648	2592	7200	16200
Half-waves of Buckl. Mode	1	1	1	1	1	1	1	1
1st mode Load multiplier	1.1094	1.069	1.0481	1.0281	1.0141	1.0058	1.0039	1.0032
Elastic Buckling stress	20.97	20.20	19.81	19.43	19.17	19.01	18.97	18.96
<i>Variation with resp. Prev. Solution</i>	-	0.76%	0.40%	0.38%	0.26%	0.16%	0.04%	0.01%
<i>Variation with resp. Analytical sol.</i>	2.00%	1.24%	0.84%	0.46%	0.20%	0.04%	0.00%	-0.01%
Buckling coefficient	1.1600	1.1177	1.0959	1.0750	1.0603	1.0516	1.0497	1.0489
<i>Variation with resp. Prev. Solution</i>	-	0.04%	0.02%	0.02%	0.01%	0.01%	0.00%	0.00%

Table 19: Convergence study results for unstiffened plate of 6 mm thickness

Under Longitudinal Loading

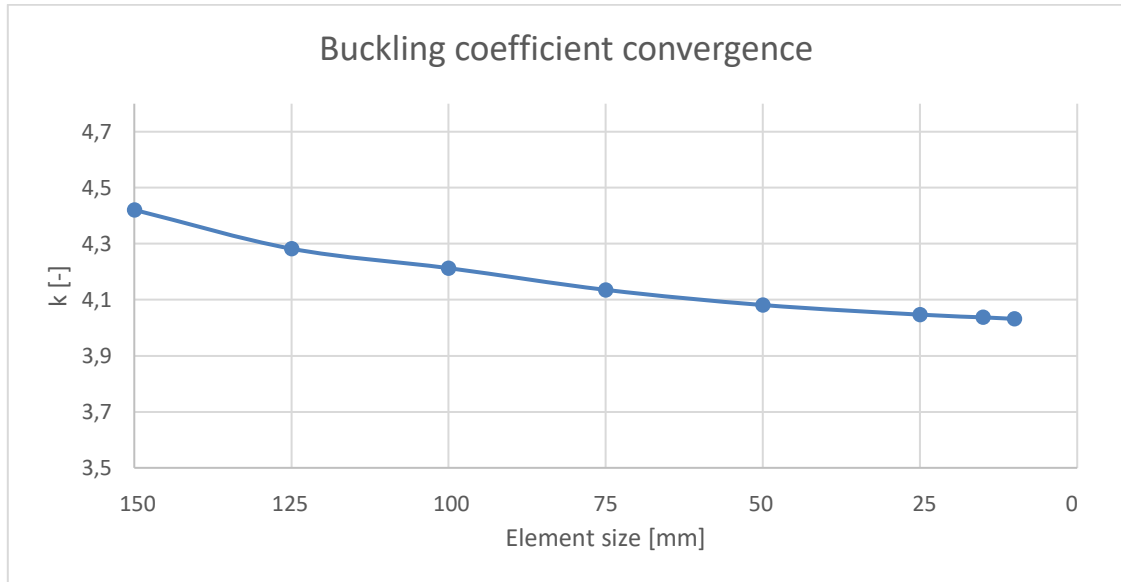


Figure 84: Buckling coefficient convergence for 6 mm unstiffened plate under longitudinal loading

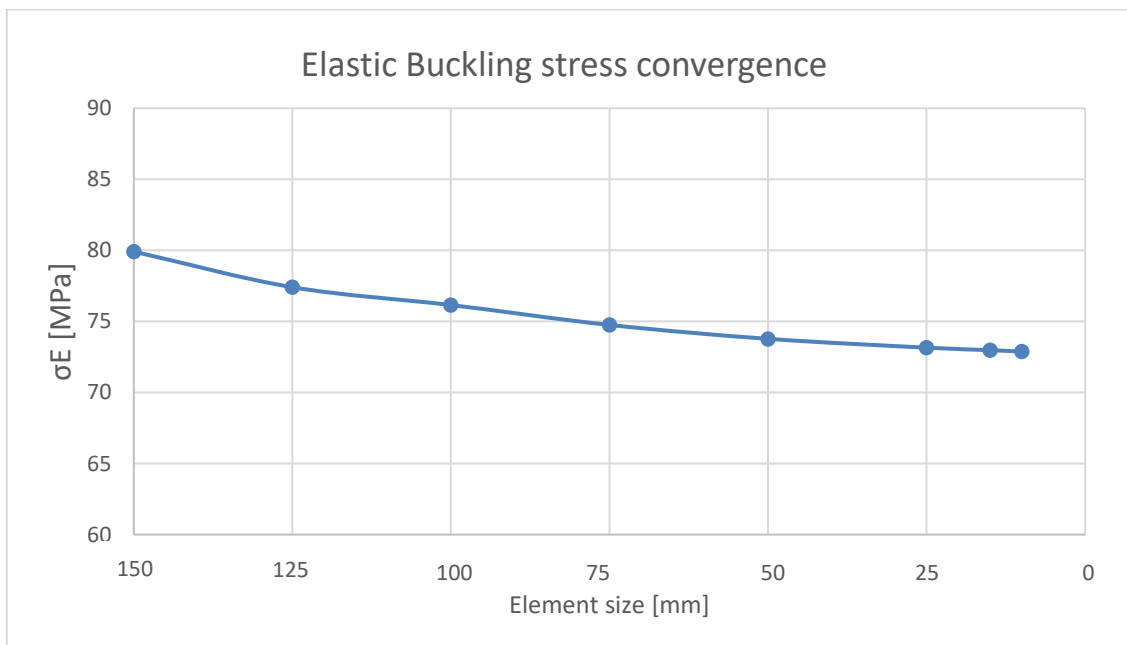


Figure 85: Elastic Buckling stress convergence of 6mm unstiffened plate under longitudinal loading

Under transversal and biaxial loading

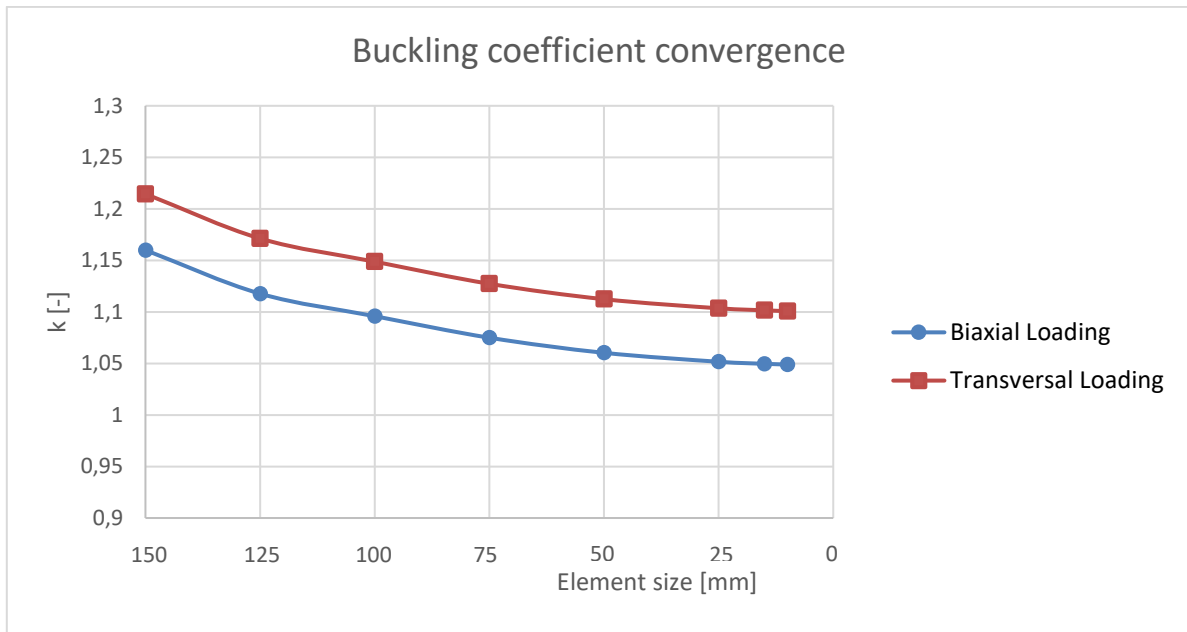


Figure 86: Buckling coefficient convergence of 6 mm unstiffened plate under transversal and biaxial loading

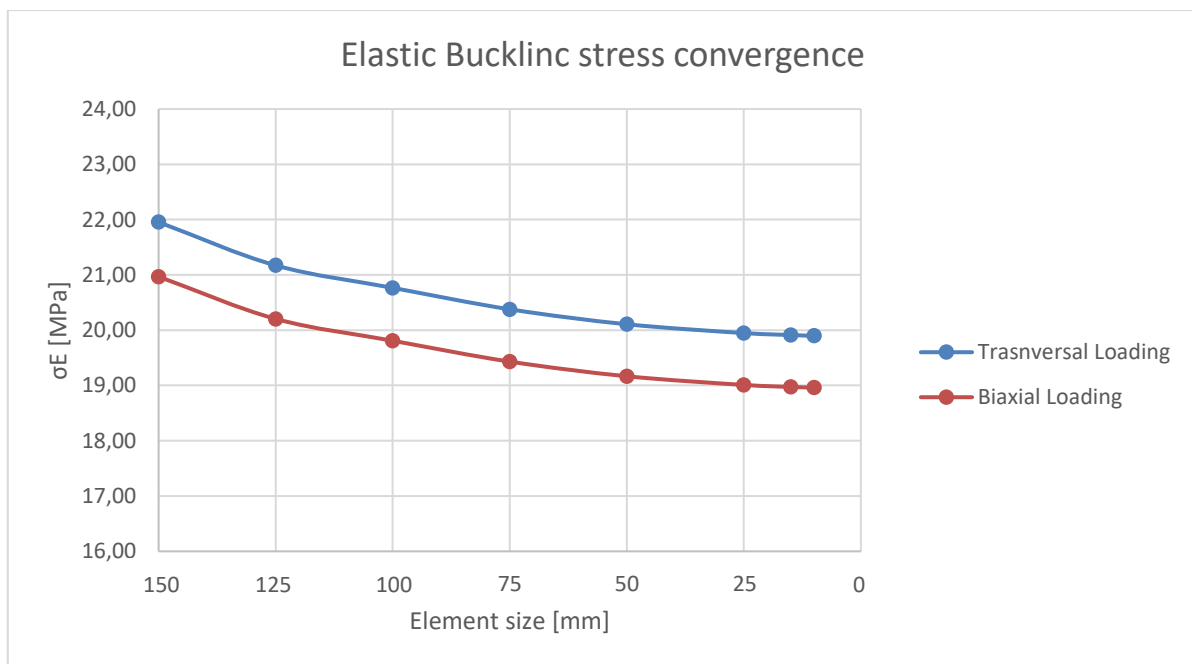


Figure 87: Elastic buckling stress convergence of 6 mm unstiffened plate under transversal and biaxial loading

For stiffened panels:

	Mesh size [mm]							
	150	125	100	75	50	25	15	10
LONGITUDINAL LOADING (Applied load: 79 Mpa)								
N° of elements	432	638	918	1728	3888	14688	41040	91800
Half-waves of Buckl. Mode	4	4	5	5	5	5	5	5
1st mode Load multiplier	1.0837	1.0468	1.0268	1.0045	0.98997	0.98131	0.97882	0.97767
Elastic Buckling stress [MPa]	85.61	82.70	81.12	79.36	78.21	77.52	77.33	77.24
Variation with resp. Prev. Solution	-	2.92%	1.58%	1.76%	1.15%	0.68%	0.20%	0.09%
TRANSVERSAL LOADING (Applied load: 20.25 Mpa)								
N° of elements	432	638	918	1728	3888	14688	41040	91800
Half-waves of Buckl. Mode	1	1	1	1	1	1	1	1
1st mode Load multiplier	1.1017	1.0619	1.0414	1.0216	1.0079	0.99978	0.99793	0.99728
Elastic Buckling stress [MPa]	22.31	21.50	21.09	20.69	20.41	20.25	20.21	20.19
Variation with resp. Prev. Solution	-	0.81%	0.42%	0.40%	0.28%	0.16%	0.04%	0.01%
BIAXIAL LOADING (Applied load: 19.25 Mpa)								
N° of elements	432	638	918	1728	3888	14688	41040	91800
Half-waves of Buckl. Mode	1	1	1	1	1	1	1	1
1st mode Load multiplier	1.1056	1.0649	1.0439	1.0237	1.0097	1.0014	0.99949	0.99881
Elastic Buckling stress [MPa]	21.28	20.50	20.10	19.71	19.44	19.28	19.24	19.23
Variation with resp. Prev. Solution	-	0.78%	0.40%	0.39%	0.27%	0.16%	0.04%	0.01%

Table 20: Convergence study for stiffened panel of 6mm thickness

For Longitudinal Loading

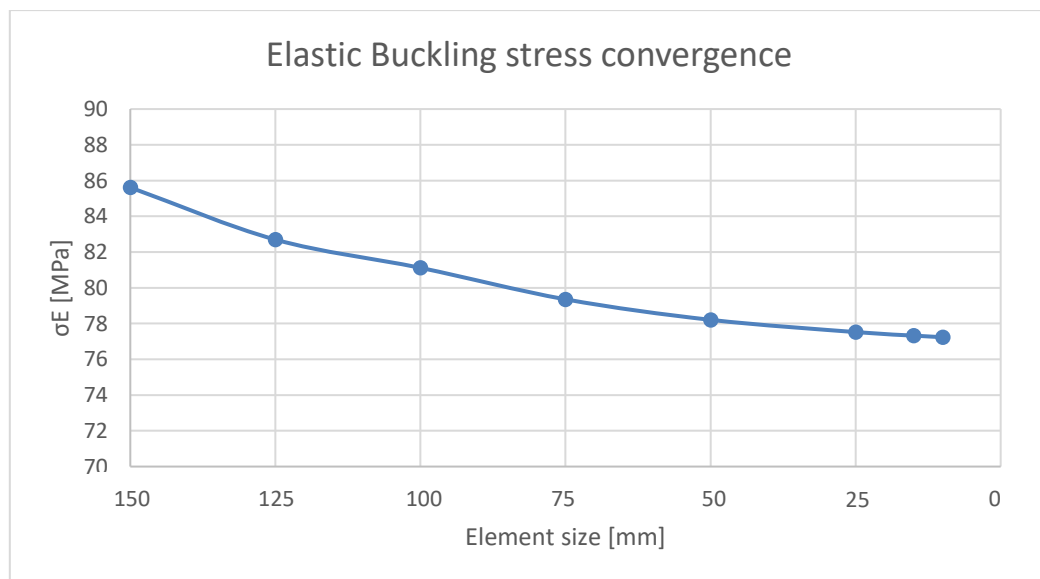


Figure 88: Elastic buckling stress convergence of 6 mm stiffened panel under longitudinal loading

For Transversal and Biaxial Loading

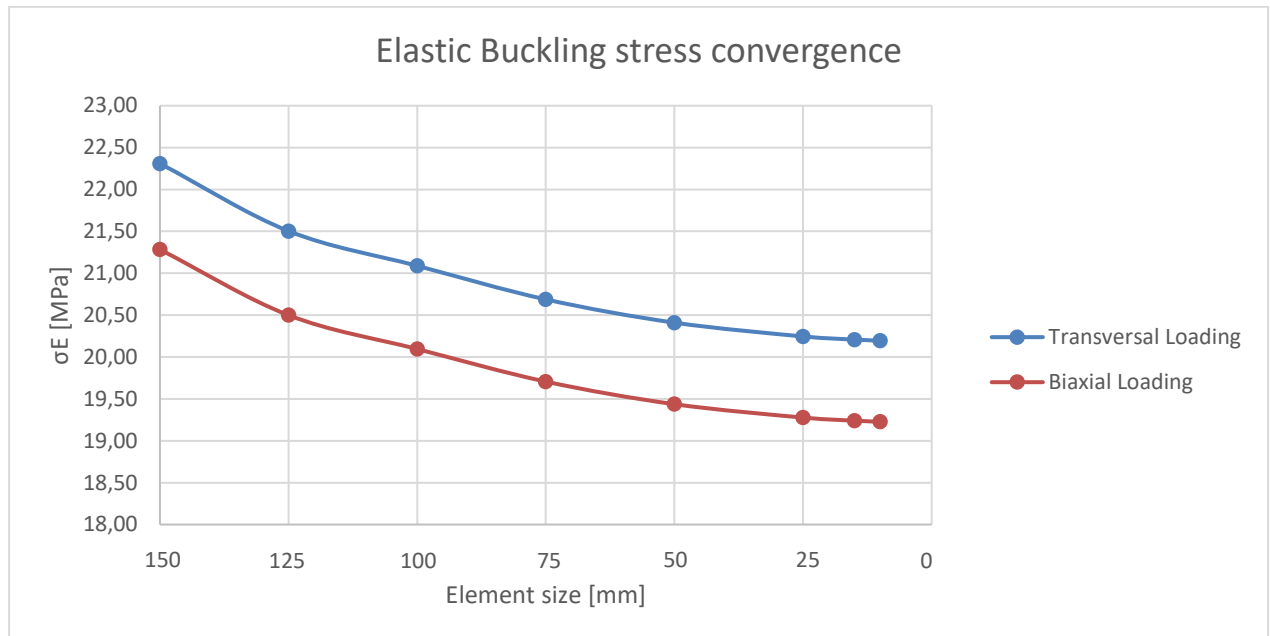


Figure 89: Elastic buckling stress convergence of 6 mm stiffened panel under transversal and biaxial loading